THE UNIVERSITY OF
SYDNEY

1-BIT PROCESSING BASED MODEL PREDICTIVE CONTROL FOR FRACTIONATED SATELLITE MISSIONS

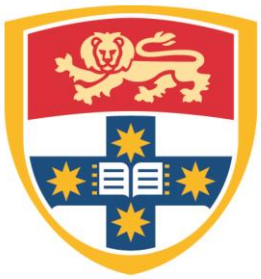

THE UNIVERSITY OF SYDNEY

A thesis submitted in fulfillment of the requirements for the degree of
Doctor of Philosophy in the School of Aerospace, Mechanical and Mechatronic Engineering at
The University of Sydney

Xueliang Bai

2015

To my long supportive wife,
and my homies…
for making this happen.

ABSTRACT

In this thesis, a 1-bit processing based Model Predictive Control (OBMPC) structure is proposed for a fractionated satellite attitude control mission. Despite the appealing advantages of the MPC algorithm towards constrained MIMO control applications, implementing the MPC algorithm onboard a small satellite is certainly challenging due to the limited onboard resources. The proposed design is based on the 1-bit processing concept, which takes advantage of the affine relation between the 1-bit state feedback and multi-bit parameters to implement a multiplier free MPC controller. As multipliers are the major power consumer in online optimization, the OBMPC structure is proven to be more efficient in comparison to the conventional MPC implementation in term of power and circuit complexity. The system is in digital control nature, affected by quantization noise introduced by $\Delta\sum$ modulators. The stability issues and practical design criteria are also discussed in this work.

Some other aspects are considered in this work to complete the control system. Firstly, the implementation of the OBMPC system relies on the 1-bit state feedbacks. Hence, 1-bit sensing components are needed to implement the OBMPC system. While the $\Delta\sum$ modulator based Microelectromechanical systems (MEMS) gyroscope is considered in this work, it is possible to implement this concept into other sensing components. Secondly, as the proposed attitude mission is based on the wireless inter-satellite link (ISL), a state estimator is required. However, conventional state estimators will once again introduce multi-bit signals, and compromise the simple, direct implementation of the OBMPC controller. Therefore, the 1-bit state estimator is also designed in this work to satisfy the requirements of the proposed fractionated attitude control mission.

The simulation for the OBMPC is based on a 2U CubeSat model in a fractionated satellite structure, in which the payload and actuators are separated from the controller and controlled via the ISL. Matlab simulations and FPGA implementation based performance analysis shows that the OBMPC is feasible for fractionated satellite missions and is advantageous over the conventional MPC controllers.

TABLE OF CONTENTS

LIST OF FIGURES

LIST OF TABLES

NOTATION AND DEFINITIONS

$\mathbb{R}^n$	Set of real vectors with *n* elements
$\mathbb{R}^{n\times m}$	Set of real vectors with *n* rows and *m* columns
$f: A\rightarrow B$	*f* is a function on the set *dom f* $\subseteq A$ into the set *B*.
dom f	Domain of function *f*.
epi f	Epigraph of function *f*.
∇f	Gradient of function *f*.
$\nabla_2 f$	Hessian of function *f*.
E	Mathematical expectation
I	Identity matrix
$\|x\|_Q$	Euclidean norm of vector $\|x\|_Q = x^T Q x$
Diag(A)	Vector with diagonal of matrix
Det(A)	Determinant of a matix
A^T	Transpose of a matrix
A^{-1}	Inverse of a matrix

ABBREVIATIONS

ADCS: Attitude determination and control system
A/D: Analog to digital
BER: Bit error rates
CIDF: Cascade Integrator with Distributed Feedback
CIDIDF: Cascade Integrator with Distributed Input and Distributed Feedback
CIDIFF: Cascade Integrator with Distributed Input and Summed Feed-Forward
CXT: Charge Exchange Thruster
EKF: Extended Kalman Filter
EMPC: Explicit Model Predictive Control
FIR: Finite-impulse-response
FPGA: Field Programmable Gate Array
IIR: Infinite-impulse-response
KKT: Karush-Kuhn-Tucker
mpQP: Multi-parametric Quadratic Programming
MEMS: Micro-electromechanical system
ISL: Inter-satellite link
LUTs: Slice Lookup Tables
MAC: Multiply-and-accumulation
MHE: Moving Horizon Estimation
MIMO: Multiple-Input-Multiple-Output
MPC: Model Predictive Control
MSE: Mean squared error
OBMPC: 1-bit processing based Model Predictive Control
OSR: Oversampling Ratio,
PDM: Pulse-Density-Modulation
POD: Proper orthogonal decomposition
PWM: Pulse-Width-Modulation
QP: Quadratic program(ming)
RHC: Receding Horizon Control,
SNR: Signal-to-noise ratio
SVD: Singular value decomposition
RMS: Root mean square value
WCS: Wireless Control System
XPE: Xilinx power estimator

SUMMARY OF PUBLICATION

JOURNAL PAPER:

(1)Bai, X, and Wu, X. "1-Bit processing based model predictive control for fractionated satellite missions." *Acta Astronautica* 95 (2014): 37-50

(2)Bai, X., Hagel, P., Wu, X., & Xiao, S. (2012, July). Improved model predictive control for virtual satellite attitude control. Journal of University of Science and Technology of China, vol.42, No.7.

(3) Bai, X, and Wu, X. "Customized Processor Architecture for Model Predictive Control in Magnetic Actuated Small Satellites." *Advanced Electrical and Electronics Engineering*. Springer Berlin Heidelberg, 2011. 71-79.

CONFERENCE PAPER:

(1)Bai, X., Wu, X., and Xiao, S. (2012, July). A design of one bit processing based Model Predict Control. In *Control Conference (CCC), 2012 31st Chinese* (pp. 5910-5914). IEEE.

(2)Bai, X., Hagel, P., Wu, X., and Xiao, S. (2012, July). Improved model predictive control for virtual satellite attitude control. In *Control Conference (CCC), 2012 31st Chinese* (pp. 4085-4090). IEEE

(3)Bai, X., Wu, X., and Xiao, S. (2012, June). Modified model predictive control in a virtual satellite. In *American Control Conference (ACC), 2012* (pp. 2497-2502). IEEE.

(4)Xiao, S., Wu, X., Bai, X., Cairns, I., Bland-Hawthorn, J., Funamoto, J., and Betters, C. (2011). i-INSPIRE Tube-Satellite Bus Design.

(5) Bai, X. and Wu, X. (2011, August). A simulation and visualization platform for fractionated spacecraft attitude control system. In *Mechatronics and Automation (ICMA), 2011 International Conference on* (pp. 2033-2038). IEEE.

(6) Wu, X. and Bai, X. (2010, December). A fractional attitude decision and control system design for a virtual satellite. In *Decision and Control (CDC), 2010 49th IEEE Conference on* (pp. 1510-1515). IEEE.

(7)Bai, X and Wu, X. (2010). A Virtual Satellite Design for the University Student Satellite. Paper presented at the 10th Australian Space Science Conference Proceedings, Atlanta, Georgia, USA.

1. INTRODUCTION

==========

1.1 Background and Motivation
1.2 Outline of the Thesis

==========

1.1 Background and Motivation

Today's space missions are tending to be more demanding and therefore require larger and more complex spacecraft. Traditional monolithic spacecraft with limited environmental adaptation capability become less efficient and are subject to larger risks. Future spacecraft are envisioned as autonomous, miniature, intelligent and massively distributed space mechatronic systems. Within the last ten years, a number of small satellites have been launched. However, such small/nano-satellites have only been successful in relatively simple space missions such as educational purposes.

Networked space missions such as formation flying and fractionated spacecraft have become popular research topics during the past few decades. In comparison to the traditional spacecraft, networked satellite structures decentralize a multi-functional monolithic satellite into a number of networked small satellites, which are cheaper to build, launch and maintain. They also provide better coverage and multiple sensing angles so that comprehensive space missions can be achieved with relatively low cost.

Amongst various types of distributed satellite systems, the formation flying system is easy to approach by simply building network protocols and algorithms in the onboard computers of the individual smaller satellites. However, formation flying is still cumbersome and expensive since the integrity of each satellite must be preserved. The development of distributed space systems, namely fractionated spacecraft systems, has also become another approach to achieve the complex space missions. In such

spacecraft systems, the controllers for each satellite subsystem are not central in location but are “fractionated” and “distributed” in space, and are controlled by the accompanying master satellite. Each fractionated component does not necessarily maintain the integrity as an autonomous satellite but only play as one of the subsystems in the concept of the monolithic spacecraft, i.e. each subsystem becomes an individual small satellite module. The individually fractionated components are then wirelessly interconnected to emulate a complete larger monolithic satellite.

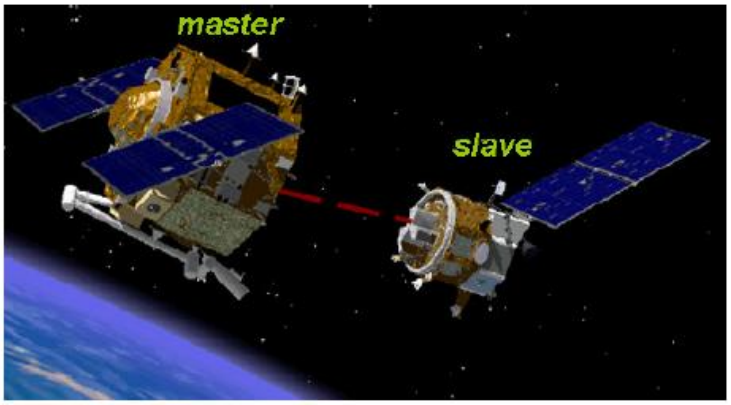

Figure 1.1 Conceptual view of a fractionated satellite

Fig.1.1 presents a conceptual view of such a fractionated satellite system. In this thesis the author proposes a fractionated satellite attitude determination and control system (ADCS) using a novel 1-bit processing based MPC (OBMPC) algorithm. The fractionated satellite subsystems are decentralized wirelessly via the inter-satellite link (ISL), forming a Wireless Control System (WCS) in orbit. The ADCS subsystem could be decentralized on two satellite modules:

1) The sensors and actuators will be located on the ‘slave’ module, in which the scientific instrument must be controlled to point to the area of interest.
2) The controller will be located on the ‘master’ module, in which most computing tasks will be processed on-board.

Although most bus subsystems are located remotely, the slave satellite requires a partial bus subsystem to perform the mission requirement. For example, it needs an

electrical power subsystem to power on payload sensors, unless wireless power transmission becomes feasible.

The challenges for the proposed fractionated satellite attitude control mission are mainly twofold. Firstly, small satellite missions generally have limited onboard resources in terms of power and circuit complexity. Hence the on board controller needs to be carefully designed if comprehensive control objectives are required. Secondly, the ISL introduces both communication noise and time delays, which may compromise the robustness of the control system.

Meanwhile, the model predictive control (MPC) algorithm is appealing to space missions due to the ability to include hard constraints directly in the control algorithm. The MPC algorithm is an optimization based control strategy. It makes explicit use of the known dynamic model, and performs optimization over a control horizon to predict the future process behavior over a prediction horizon. However, such online optimization increases the on-board computation intensity, which is not suitable for small satellite missions.

The main objective of this thesis is to develop an efficient MPC algorithm to achieve a power efficient on board controller that is suitable for fractionated satellite missions. Towards this goal, a 1-bit processing based MPC (OBMPC) for satellite attitude determination and control is developed, which is the first aerospace application for the 1-bit processing control system to the best knowledge of the author. The strategy is characterized by using the 1-bit state feedback data directly to perform the online optimization that required by the MPC algorithm. The state feedbacks are modulated into 1-bit format by bi-level Delta-Sigma ($\Delta\sum$) modulators on-board the “slave” satellite, sent and processed by the onboard computer on the “master” satellite directly without de-modulation. Due to the 1-bit nature of the feedback data, all the “multiplication” operations can be executed between the 1-bit data and the multi-bit coefficient, resulting in a simple sign change of the multi-bit coefficient. Hence, no “multiply” or “division” arithmetic blocks are required in the online optimization

process, which makes the OBMPC controller feasible for the proposed mission. Moreover, the resultant 1-bit data is stand-ready for transmission, and less sensitive to the data loss due to the nature of the modulation technique.

In the next few chapters, a novel 1-bit processing based MPC (OBMPC) is designed for a small satellite attitude control mission. The benefits and drawbacks of OBMPC systems are discussed from a design perspective, and a practical implementation method is developed to satisfy the proposed fractionated satellite attitude control mission. The stability issues are also discussed. Also, a 1-bit sensing component and a 1-bit state estimator are also developed to complete the OBMPC control loop. Simulations are performed using both Matlab and the Field Programmable Gate Array (FPGA) implementation to verify the feasibility of the proposed theory and prove that the OBMPC is advantageous in terms of speed, power and circuit complexity over the conventional MPC controllers.

1.2 Dissertation Overview

This work involves developing a novel 1-bit processing based MPC architecture for the proposed fractionated satellite mission. The reminder of the thesis is organized as follows.

Chapter 2 gives a literature review of the related fields. Firstly, the development of the distributed satellite system and the fractionated satellite structure are examined. Secondly, the history of the $\Delta\sum$ Modulation and 1-bit processing control system is introduced. The author then focuses on the MPC algorithm and implementation methods for fast MPC developed to date.

In Chapter 3, the fundamental theories behind the Delta-Sigma ($\Delta\sum$) Modulation and the 1-bit processing control system are presented and detailed. A space mission has been briefly modeled and used in simulation to verify the feasibility of 1-bit processing control algorithm for the space mission. This chapter is based on the

conference paper (Wu and Bai, 2010)

In Chapter 4, a novel 1-bit processing based MPC (OBMPC) algorithm has been examined. The author starts with the MPC problem formulation, and then propose the implementation of the OBMPC structure. The stability issue is further developed in this section. This chapter is based on the journal paper (Bai and Wu, 2013).

In Chapter 5, 1-bit sensing components are considered. The $\Delta\sum$ Modulation based micro-electromechanical system (MEMS) gyroscope is discussed as an example of implementing the sensing component under the framework of the 1-bit processing structure. An OBMPC based 1-bit MEMS sensor is developed in this chapter to adopt the proposed 1-bit processing system for the onboard ADCS.

Chapter 6 deals with issues in the OBMPC control developed for the WCS. Environmental effects such as error and data loss shall be discussed in this chapter. A 1-bit state estimator is proposed to improve the state measurement of the control system.

In Chapter 7, a nano-satellite with a fractionated satellite structure is modeled to validate the proposed OBMPC control algorithm. The simulation results of both the OBMPC and the traditional MPC are compared in Matlab. The efficiency of the OBMPC is also compared in terms of power and area with the conventional MPC using FPGA implementations. The chapter is partially based on (Bai and Wu, 2011).

Chapter 8 concludes and discusses the future work of this thesis.

2. LITERATURE REVIEW

==========

==========

2.1 Satellite Formation Flying and Fractionated Satellite Structure

As a typical implementation, the concept of formation flying is well understood and practical to approach with state-of-the-art networking techniques. As described in (Gill, et al., 2001), satellite formation flying is composed of multiple satellites, who collaborate together in a group to achieve the objective of single large monolithic satellite. In comparison to other networked satellite systems, formation flying missions are easier to accomplish by simply implementing the network protocols and control algorithms in on-board computers to coordinate a group of satellites via the ISL. The formation flying approach enables the possibility of using multiple small satellites, e.g. nano-satellite and pico-satellites, to achieve complex space missions (Barnhart, et al., 2007). Depending on the application, the formation flying can be specified into distinct kinds (Sabol, et al. 2001; Burns, et al., 2000) . These types include:

- Trailing formations which are constituted by multiple satellites orbiting on the same path.
- The satellite cluster which includes several minor satellites that fly in close formation.

- Satellite constellation which is a collection of artificial satellites working in concert.

The autonomous control systems are designed for each satellite in the formation, to reach unified goals in a space mission. The major benefits of formation-flying satellite missions are that an individual failed satellite can be easily replaced and the formation can be reconfigured.

The concept of the satellite formation flying broadens the potential solutions of the space missions. However, in the formation flying group, each individual satellite is a complete satellite system. Subsequently, one may suggest that some of these individual satellites may not have to be complete systems, but rather may act as partial systems whose operations are controlled by a master satellite. A novel architecture has been developed by the Defense Advanced Research Projects Agency (DARPA) of the United States Department of Defense and is termed as "fractionated" spacecraft. As described in (Brown and Eremenko, 2006), the word fractionation is used to describe the decomposition of a system into distinct modules which can be "assembled" on orbit to deliver the capability of the equivalent monolithic system. In this structure, the subsystems of a conventional spacecraft are implemented by the elements or nodes and connected to form a "virtual satellite" in space.

Comparing to the satellite formation flying, the fractionated satellite provides more flexibility of degradation and extension as the fractionated subsystems are generally cheaper than the formation flying controlled satellites. Fractionated satellites can bring many potential advantages, such as reducing launching costs (sending small elements instead of big spacecraft), fast response and replacement for failure elements with low recovery costs. Also, no complicated rendezvous, docking, or robotic servicing is needed. Theoretically speaking, increased fractionation levels can improve the flexibility of the satellite. However, it also brings mass and cost penalty. In 2005, a series of simulations and evaluations was done to assess the feasibility for the concept of fractionated satellites by DARPA and other research groups e.g.

(Brown, et al., 2002; Mathieu and Weigel, 2005; Mathieu and Weigel, 2006) . In the model presented by Mathieu and Weigel (2005), when a subsystem is fractionated, it is taken out of the spacecraft as it is and becomes the "payload" of a new module. For instance, when the communication subsystems are fractionated, it becomes a communication module with its own power, propulsion, attitude control, and thermal subsystems. In 2007, the DARPA initiated the System F6 (Future, Fast, Flexible, Fractionated, Free-Flying Spacecraft United by Information Exchange) project (DARPA 2007), which aims to prove the feasibility and benefits of the fractionated satellite architecture through a space demonstration. A System F6 fractionated spacecraft demonstrator program has been released to develop an open and ubiquitous space architecture and an associated set of open standards (Brown and Eremenko, 2006). Comparing with the traditional satellites, based on the model provided in (Mathieu and Weigel, 2005) and (Brown and Eremenko, 2006), the mass and cost penalty decrease if the communication, control and data handling subsystems are fractionated, and show notable increase if the fractionation involves power subsystem and collaborative separated positioning. Hence, the main focus of the fractionated satellite mission at the current stage is to replace the data bus with wireless communication protocols unless wireless power transmission becomes feasible.

2.2 Delta-Sigma ($\Delta\sum$) Modulation and 1-Bit Processing

Delta-Sigma ($\Delta\sum$) modulation was developed in the 1960s based on the delta modulation as an efficient modulation technique. Just as delta modulation is well known as Pulse-Width-Modulation (PWM), $\Delta\sum$ Modulation is also known as Pulse-Density-Modulation (PDM) because it quantizes the signal directly, rather than the signal's derivative like the delta modulation does. Thus, the maximum quantizer range is determined by the maximum signal amplitude. Essentially, $\Delta\sum$ modulation is a kind of over-sampled A/D converter. Among various $\Delta\sum$ modulation methods, the ones with bi-level quantizers draw more attractions due to their circuit simplicity and the binary nature of the quantizer outputs, which have been proven as an efficient

alternative to the multi-recording format (Johns and Lewis, 1993). Such bi-level quantizers were then used to develop the multiplier free analog to digital (A/D) converters, e.g. (Schreier, 1993), to achieve simplest digital hardware circuitry. Based on the bi-level quantizer, the concept of 1-bit processing has been widely investigated in the context of finite-impulse-response (FIR) filters (Kershaw, et al., 1996), infinite-impulse-response (IIR) filters e.g.(Johns and Lewis, 1991), and digital communication e.g.(Stewart and Pfann, 1998; Sklar, 2001). One of the many successful applications of the 1-bit processing is in audio data compression for the Compact Disc (CD) (see (Reefman and Janssen, 2004) for an overview), where the 1-bit coding scheme is used to develop high frequency (64 or 128 times 44.1kHz) encoding technology for the audio industry.

Inspired by the multiplier free A/D converters, a multiplier free control system has been proposed by Wu and Goodall (2005a), namely the 1-bit processing control system. Such control system uses $\Delta\sum$ modulators to encode either analogue or multi-bit digital signals into the 1-bit format. The work can be regarded as digital control systems with the assumption that analogue signals are converted into an equivalent digital format by the A/D converter. The resultant control signals are high-frequency digital signals, often used directly to drive electronic power amplifiers, and the effect of which is filtered by the physical system being controlled. Stability issues of such digital control systems can be analyzed during the design process using classic stability analysis tools (e.g. pole locations and Routh-Hurwitz Stability Criterion).

Unlike conventional digital control approaches, the control laws are designed to cooperate with the 1-bit signals directly. The advantages of 1-bit processing control systems are threefold. Firstly, as the signals are in the 1-bit format, multipliers can be removed by choosing a modified controller structure (Wu and Goodall, 2005b). Hence the area of silicon required to implement a 1-bit controller and wireless transceivers is potentially much less than that of a multi-bit system, which is an important consideration for embedded control systems. Secondly, sensing and control signals are

modulated into 1-bit signals, ready for transmission directly. The effects of transmission delay and data loss during the wireless transmission are less significant to the control system because of the properties of the modulation technique. Thirdly, no decoding process is required at the receiver end, i.e. the 1-bit signals being fed into controller or actuator directly. In the proposed fractionated satellite mission, since the controller is decentralized from the actuator, the $\Delta\sum$ modulation can also be employed in the WCS to compress data and to transmit the signal over the transmission channels between the controller and the controlled plant.

The main drawback, however, is that $\Delta\sum$ modulation introduces a nonlinear 1-bit quantizer into the control loop. The nonlinearity results in quantization noises, which cover a wide bandwidth including the baseband. To obtain a high signal-to-noise ratio (SNR), 1-bit processing must be carried out under a sampling frequency which is significantly higher than that would be normal for a digital controller. Therefore, 1-bit processing raises issues such as control law formulations and sampling criteria, both of which need to be well understood. For the 1-bit processing control system, it is not uncommon to over sample the control system perhaps thousands of times of the controller bandwidth to obtain a high SNR. Meanwhile, the phase lags introduced by sampling and computation delays are to remain small. This intrinsic requirement for high sampling with real-time control (which does not pre-apply for other forms of signal processing) means that modest sampling frequency increases are needed in a relative sense. Hence as the signal is necessarily fast-sampled, the system characteristics can approach those of high-quality analogue processors in terms of phase responses and distortion effects, while retaining the advantages of digital-processing techniques (Goodall and Donoghue, 1993). Consequently, a trade-off between the benefits introduced by the multiplier free structure and the drawbacks caused by the high sampling rate needs to be taken account during the design process. Moreover, despite that mature filter techniques can be applied to the 1-bit processing control systems, the non-ideal $\Delta\sum$ modulation will bring (filtered) quantization noise into the control loop, which could affect the robustness of the

control system.

The removal of the multipliers make the 1-bit processing based control system advantageous over convention control systems in terms of circuit area and power efficiency. However, most of PID control based applications are not computationally expensive as the PID algorithm is relatively simple. The 1-bit processing based algorithm is more attractive for advanced control algorithms (e.g. The MPC algorithm) as the computational load is normally quite large for the embedded control system applications. In this work, the author integrates the 1- bit processing method into the MPC algorithm, which forms an OBMPC structure, to decrease the computational effort and circuit area for the proposed satellite attitude control mission.

2.3 Model Predictive Control (MPC)

The MPC has been developed extensively during the past three decades and successfully adopted by many industrial applications (see (Garcia, et al., 1989) and (Richalet, 1993) as earlier industrial application researches and (Qin and Badgwell, 1997) as a survey of industrial MPC application through 1995). Meanwhile, the MPC for nonlinear models has also been developed into practices e.g. (Morari and H Lee, 1999; Qin and Badgwell, 2000; Young, et al., 2002). However, the main downside of the MPC is that on-line optimization is required, which results in a large computational burden for the control system. Due to the online optimization nature, most MPC applications are in the process control industries, where the sampling frequency is relatively slow. The other notable benefit accounted for the popularity of the MPC is that hard constraints can be directly formulated in the optimization problem, which facilitates the controller design and tuning. Moreover, MPC can handle Multiple-Input-Multiple-Output (MIMO) control systems directly, which means it is suitable for large scale industrial implementations. Nevertheless, the technique has also been adopted in many other fields such as automotive, medical and aerospace applications along with faster onboard computers and better quadratic programming (QP) solvers, e.g. (Rao, et al., 1998). The prosperous progress of the

algorithm was aroused after a systematic analysis of the stability issues achieved by Mayne (2000). The same methodology is also adopted to perform the state estimation, namely the Receding Horizon Estimation e.g. (Muske, et al., 1993; Scokaert, et al., 1997), (Alessandri, et al., 2003). Though less popular than the Extended Kalman Filter (EKF), the RHE inherits most of the benefits from the MPC algorithm, and mainly adopted by the applications where hard constraints are applied to the estimator.

Despite the booming development in various applications, the MPC is limited by the massive online computational demand to embedded control systems. This is especially true for fast sampled real-time control missions due to the scarcity of onboard resources. The efforts toward fast MPC schemes shall be reviewed in the next sub-section.

2.4 Fast MPC Implementation Methods

A typical MPC algorithm designed for MIMO control systems with long prediction horizon generally requires repetitive large matrix multiplications. In this sub-section, the author examines the efforts to decrease the online computational burden, including: (1) model reduction methods, (2) means of iterative solution methods (3) pre-compute the solution and bring the online calculation off line (i.e.: using look up tables). Some other hybrid control schemes are also discussed in this section.

2.4.1 Model reduction methods

The model reduction methods can be described as means to replace the system dynamic model with a lower order model that has similar model characteristics (i.e. stability and passivity) as the original model. They can effectively decrease the implementation difficulty for the MPC in terms of system storage requirements and online evaluation time, especially for optimization based control algorithm on large scaled or highly sampled control systems. Most general purpose model reduction

techniques can be classified into either singular value decomposition (SVD) or Krylov-based methods. Research work relating to such concepts can be found in (Antoulas, et al., 2001; Gugercin and Antoulas, 2004; Antoulas, 2005) as a series of recent surveys.

Due to the preserved system characteristics, most model reduction methods can be easily utilized by MPC algorithms directly or with minor modifications. The projection based methods are usually used to decrease the system order. Such a method finds a basis matrix which can be used to redefine the parameters, so that the control variable matrices can be reconstructed into a lower order form. The reduced model is required to be computationally stable and efficient, and the approximation error needs to be small enough to maintain the robustness of the control system. In MPC algorithms, the control input is computed based on the reduced state vector estimated by an observer, which is based on the output of the reduced model. Therefore, the observer should account for the approximation error in the reduced model (Hovland, et al.; 2008). The challenge, however, is that the errors that exist in the output of the reduced model could lead to constraint violations even the optimal solution can be obtained from the reduced model.

Generally speaking, the model reduction methods trade-off the accuracy of the control object model with the system order. For a large scaled MPC controller with limited onboard resources, model reduction methods can greatly decrease the online computational effort as the amount of calculation decreases exponentially when the model order decreases. Two general model reduction methods are discussed here, along with their applications to the MPC.

1) Proper orthogonal decomposition (POD)

The proper orthogonal decomposition (POD) has been proven to be a promising method for implementation in control systems. For POD, the basis vector can be conveniently solved by various numerical methods, and therefore recognized as a

straightforward application of the approximation on the SVD e.g. (Ravindran, 2000; Afanasiev and Hinze, 2001; Atwell, et al., 2001; Cohen, et al., 2006; Bui-Thanh, et al., 2007).

Along with accuracy improvement of the POD，it has been applied to the MPC to reduce system order by many researchers. For example, Hovland, et al.(2008) proposed a Goal-oriented model-constrained reduction algorithm to adopt the POD into the MPC. The goal oriented model constrained reduction algorithm is taken from (Bui-Thanh, et al., 2007), in which more information can be acquired to address the accuracy issues of the reduced model. Such a method enforces the reduced order governing equations to be constraints and the cost is targeted to minimize the output error, while the POD minimizes the error of state prediction over the entire domain (Hovland, et al., 2008). The stability of the POD based MPC has been discussed in (Hovland, et al., 2006) and (Kvasnica, et al., 2011).

To better suit the MPC, the POD can also combine with other methods to improve the quality of the model reduction. For instance, Xie, et al.(2011) and Theodoropoulos (2011) combined a finite element Galerkin Projection with the POD and then used trajectory piece-wise linearization to linearize the nonlinear model. Similarly, Den Camp, et al. (2008) proposed a subspace identification technique coupled with POD to obtain a better model reduction for systems with inherent nonlinear dependence on process parameters. Agudelo, et al. (2009) use the univariate polynomials to approximate part of the basis vectors to decrease the number of constraints applied to the model.

2) Balanced truncation

Balanced Truncation (BT) has been developed in the early 1980s, e.g.(Moore, 1981), (Pernebo and Silverman, 1982). The method provides strong guarantees on approximation error constraint, but is normally limited to linear systems as the general balancing scheme for nonlinear systems is not available. The nonlinear systems,

however, can be linearized and the BT method can then be applied at the cost of losing nonlinear behavior. Such situations can also be addressed by including the cost function of the system when solving the projection matrices, e.g. (Hahn and Edgar, 2002). More details about BT can be referred in a recent survey (Gugercin and Antoulas, 2004).

Similar to the POD, balanced truncation can also be combined with some tools for better performance with the MPC. For example, the Galerkin projections is also applied to the balanced truncation by Hahn and Edgar (2002). The balanced truncation can also be applied to the multi-parametric programming based MPC to decrease the number of parameters stored in the memory, e.g. (Narciso and Pistikopoulos, 2008), (Hovland and Gravdahl, 2008).

As a summary, the model reduction methods can greatly reduce the online computational burden of the large scale MPC algorithms. They can be combined with means of iteration methods to achieve faster MPC schemes. The method requires a trade-off between the robustness/accuracy of the control system and reality limitations due to model mismatch issues. Therefore, although it can still be a practical implementation method, the model reduction methods are hardly a “solution” to the MPC applications. However, as mentioned in the later part of this thesis, the model reduction method can be combined with our OBMPC method, to further decrease the on-board computational effort.

2.4.2 Fast MPC with online solver

The improvement of iterative method of the online solver is naturally the most straightforward research direction for the MPC algorithm. General iteration methods include the active set methods (Best, 1996) and the interior point methods (Mehrotra, 1992). Most fast MPC schemes apply various mathematical tools toward such iterative methods. For example, The Mehrotra’s predictor–corrector algorithm (Mehrotra, 1992) has been used in (Rao, et al., 1998) to decease the computational

effort, where the Riccati approach was used to solve the linear sub-problem. In (Wang, 2009), the Hildreth's QP procedure (Hildreth, 1957) is proposed to solve the dual problem. This method is also used in this work to form an explicit relationship between the state variables and the control inputs. (Axehill and Hansson, 2008) proposed a gradient projection method to improve the active set method and solve the MPC problem. It allowed the working set changes to be faster than a generic active set method. A series of studies done by Richter and his colleagues use the optimal gradient method (Nesterov, 1983) to solve MPC problems, which generalized the method to the MPC algorithm with different constraint sets (Richter, et al., 2009). Patrinos and Bemporad (2012) and Bemporad and Patrinos (2012) developed a fast dual gradient-projection algorithm for linear MPC problems with general polyhedral constraints on inputs and states. The algorithms provided are easy to program as it requires only a few steps and the computational cost increase linearly with the prediction horizon.

Also, the combination of the online iteration methods may effectively decrease the online computation effort. Wang and Boyd (2010) combined a series of existing iteration methods to increase the online optimization speed. In addition to the fast primal barrier interior point method, a warm-starting method can be used to reduce the number of Newton steps e.g.(Yildirim and Wright, 2002). It suggests that an appropriate interior point method can terminate early (typically between 3 and 5 online iterations) while a relatively accurate optimal solution is proven to exist.

However, both active set methods and interior-point methods have cumbersome matrix multiplications when dealing with large scale control systems and long control horizons. Subsequently, some researchers also considered approximation methods. It is suggested in (Zheng, 1999) that for a control horizon with N_c elements, since $u(k+N_c-1|k)$ are never implemented, calculating them approximately in order to reduce the on-line computational demand should not significantly affect the closed-loop performance. Since the constraints only applied to the first element of the control horizon, the calculation for the rest of the control horizon can be determined

offline. Moreover, (Patrinos, et al., 2011) proposed a piecewise smooth Newton method with the modified Newton approximation scheme to speed up the convergence of the online optimization problem.

Similar to the model reduction methods, most of the fast online searching methods can work with the OBMPC proposed in this thesis directly to further decrease the online computational effort. For simplicity purposes, such combination will not be discussed in this work but left as future discussions.

2.4.3 Other control schemes

Moreover, as a direct implementation of the MPC algorithm into the high-fidelity model is not feasible in time-critical systems, various model reduction methods, e.g. (Afanasiev and Hinze, 2001), have been developed to decrease the system order while maintaining the same properties of the model, such as the stability and passivity. Furthermore, if one considers the limited processing resources as constraints to the MPC system, efforts have been developed such as:

- choosing sub-optimal solutions for the MPC controller when computing resources are scarce (Henriksson, et al., 2002; Henriksson and Åkesson, 2004) (Such trade-off between successive iterations in the MPC algorithm and the computational delay mirrors the anytime algorithm proposed by Bhattacharya and Balas (2004);
- switching amongst a set of pre-designed controllers (Greco, et al., 2007);
- block MPC, a hybrid control scheme that uses two different sampling intervals when the processing resources limitation changes e.g.(Sun, et al., 2007);
- Algebraic MPC, a MPC algorithm with non-uniform prediction point distribution. The prediction points can be placed at a few critical times along the horizon based on the open loop dynamics of the system, e.g. (Gibbens and Medagoda, 2011; Lamburn, et al., 2014; Medagoda and Gibbens, 2014; Medagoda and Gibbens, 2010).

- and sequence-based anytime algorithms by Quevedo and Gupta (2013).

It is worth noting that the Block MPC and the Algebraic MPC methods have good adoptability to the OBMPC method. As the one 1-bit processing based control system requires OSR, defining the prediction window with a specific time period may require a large number of prediction points, which requires intensive online computational efforts. The Block MPC or the Algebraic MPC can help to decrease the prediction point by neglecting the non-important points or time instant. Once again, for simplicity reasons, the author leaves this part as the further work of the OBMPC study.

2.4.4 Removal of the online solver

2.4.4.1 Explicit MPC (EMPC)

Meanwhile, some researchers shifted their focus from fast online QP solvers to online computation lookup tables, where all the computations are conducted offline. The most notable work on this subject include studies of the EMPC method proposed in (Bemporad, et al., 2002) and (Tøndel and Johansen, 2002). Such a method solves all the possible solutions raised in the QP problem beforehand by solving a multi-parametric QP (mpQP) problem. All the possible solutions are calculated off-line and stored in the memory. More specifically, by finding the affine relationship between the pre-defined vector z (z is a function of the control input and the state vector) and the state vector, the optimal solution can be obtained through an affine mapping. Then the online QP solver can be replaced by a lookup table searcher. The online effort thus becomes a simple iteration of region searching (i.e. binary searching tree) and the online computation time is logarithmic in terms of the number of polyhedral in the state space partition (Tøndel, et al., 2003).

Essentially, the EMPC method is a trade-off between the onboard computational resource and the storage size. This is feasible for most fast sampled control systems with limited on board resources considering the low cost of memory chips. Such

methods are further developed by other efforts such as (Tøndel, et al., 2003; Tøndel, et al., 2003; Spjøtvold, et al., 2004) and many applications e.g. (Hegrenæs, et al., 2005). A recent survey of EMPC methods is given in (Alessio and Bemporad, 2009). The EMPC algorithm is also proposed for spacecraft attitude control in (Hegrenæs , et al., 2005) as one of the few practical studies for the spacecraft attitude control system using MPC.

The main drawback of the EMPC, however, is that the possible solutions of the QP problem will grow exponentially when the horizon, state and input dimensions and the number of constraint sets grow, which may suggest big memory storage and large searching effort (i.e. finding the correct critical region). Such issues also lead to the combination of the model reduction methods based EMPC as discussed above. The other problem is that the once the controller is customized, it is difficult to reconfigure as the offline computation (solving all the possible solutions) is hard to achieve by an onboard computer with limited time and on-board resources.

2.4.4.2 Approximate Methods Based EMPC

Beside model reduction methods and fast online searching methods, to overcome the limitations of EMPC, the approximate methods are also suitable tools to trade off the accuracy of the control result and online computation time. Under certain circumstances, the accurate region may not be available if a large scale control system is considered. The main purpose of the approximate method is to combine smaller pieces into bigger ones, therefore achieving a faster online searching process and less off-line computational effort. (Bemporad and Filippi, 2003; Johansen and Grancharova, 2003) and (Tøndel, et al., 2003) are some of the earliest works towards the development of the approximate EMPC. These researchers suggested an orthogonal searching tree with will only partially solve the QPs, which “will terminate with a continuous piecewise linear (PWL) function that is an approximation to the continuous PWL exact solution” (Johansen and Grancharova, 2003). The block MPC method as mentioned in (Tøndel and Johansen, 2002) can also be combined to further

decrease the searching effort. To further narrow down the online searching, (Pannocchia, et al., 2007) proposed a partial enumeration approach, where only relevant critical regions are calculated and stored in the memory. Ferreau, et al. (2008) proposed an online active set strategy for the EMPC. Additionally, Ferreau, et al. (2008) also added a time constraint to the controller. A "near optimal" solution will be chosen when the time constraint is violated, which somehow mirrors the anytime control method developed for controllers with limited onboard resources. Similarly, Zeilinger, et al. (2011) combined the warm-starting active set linear programming procedure with the EMPC, which utilizes the piecewise affine approximation of the optimal solution offline to warm start an active set method. The "optimal" solution also includes the consideration of online computation time frame, memory size and performance. In (Jones and Morari 2009) and (Jones and Morari 2010), direct approximations for inner and/or outer polytopic convex sets are applied to pre-specify the number of pieces in an EMPC problem. Also, an input to state stability approach is developed in Genuit, et al. (2012) so the approximation errors can be bounded to preserve the closed-loop stability of the approximation method.

2.4.4.3 Quantized MPC

Aside from the methods discussed above, if the system is determined by a finite set of possible control actions or measurements, then a fast MPC scheme can be achieved by directly mapping a set of the constraints with a control decision. Specifically, similar to the EMPC algorithm, due to the explicit relationship between the decision variable and the state variable, the quantized control variables can be mapped with certain state space partition, which greatly simplifies the online searching process. Such problems can be referred as quantized control systems, e.g. the on-off control systems. A successful approach has been developed by Quevedo, et al. (2004) towards the MPC with finite constraint sets, which leads to a series of successful applications e.g. (Cortés, et al., 2008; Kouro, et al., 2009; Cortes, et al., 2010). Such implementations took the advantage of the property of digital control systems, where the control inputs can be modulated into finite constraint sets, and use a vector quantizer to map the

optimal solutions. The stability issues for the quantized control system have been studied by many researchers, e.g. (Delchamps, 1990; Schreier, 1997; Fagnani, 2003).

The efforts made to implement the quantized EMPC can be found in (Bemporad and Filippi, 2003; Grancharova and Johansen, 2008; Grancharova and Johansen, 2011). The approximation method for the quantized EMPC has also been developed by (Grancharova and Johansen, 2009) to further decrease the online computational effort. The problem, however, is that the quantized signals may not always be regarded as continuous signals, which may cause robustness issues in the MPC algorithm. Therefore, it is necessary to consider the quantization noise induced into the control system e.g. (Picasso, 2003).

In this work, the 1-bit processing based MPC system can also be classified into the framework of the quantized MPC as a special case. It shares some of the features and drawbacks with the quantized MPC, while appears to be advantageous in term of implementation as the memory searching algorithm is not required and it is not necessary to store a number of possible solutions in the memory. As compensation, the online computation is still required, although it has been reduced to a minimum due to the removal of the multiplier.

2.5 Stability Issues for the MPC

The most widely discussed stabilization technique for the MPC is the implementation of terminal state equality constraint. It was first established by (Chen and Shaw, 1982) for unconstrained linear systems, and then extended into general constrained control systems by (Keerthi and Gilbert, 1988). Most research works toward the stability of the MPC around the time of 1990s are constructed based on these papers and rely on the equality constraints to stabilize the optimization problem. Briefly speaking, such methods establish a terminal cost and terminal constraint both equal to zero, which means the optimization process will asymptotically approach the terminal constraints and be eventually stabilized. Such an equality constraint method is quite strict and

computationally expensive. However it provides a foundation of the stability research by explicitly focusing on the terminal cost function and terminal constraint, which leads to the development of a vast variety of stabilization techniques e.g. (Bitmead , et al.,1990; Mayne and Michalska, 1990; Muske and Rawlings, 1993; Rawlings and Muske, 1993). The result was improved by Michalska and Mayne (1993) by relaxing the equality constraints with a terminal constraint set and a suboptimal solution can be found without compromising the stability of the MPC. This allows the MPC to be feasible for many applications and also inspired many researches to further develop many types of robust MPC with a modified terminal penalty (Chisci, et al., 1996; Robertson, et al., 1996; Chen and Allgöwer, 1998). The survey conducted by Mayne (2000) provided an abundant review about the stability methodologies of the MPC, which is regarded as the foundation of MPC stability research. For the stability of quantized MPC, one can refer to the analysis made in (Mayne, 2003) and (Quevedo, et al., 2004).

The stability issues discussed in this work are based on the quantized MPC. The conditions for the OBMPC is quite simple (bi-level quantizer) but hard to analyze due to its non-linearity. Hence, the "safe" design criteria are also discussed so that the proposed algorithm can be easily adopted in a practical engineering mission.

2.6 Summary

In this chapter, firstly the history of the fractionated satellite structure was briefly introduced. Then the previous work of $\Delta\sum$ modulation and 1-bit processing control system was briefly reviewed. More focus was then placed towards the MPC problem, and specifically to existing fast MPC methods.

As an optimization based algorithm, the online computational burden limited the MPC from most fast sampled applications. To decrease the online computational effort, one can improve the iteration methods by means of mathematical tools (e.g. different QP solvers). Additionally, a model reduction method can be used to reduce

the model order and hence the computational requirements. The most popular approach for the fast sampled MPC systems is the mpQP approach (also known as EMPC), where all the possible solutions are solved off-line and stored in the memory, leaving only the requirement of online searching processing in each iteration. The combination of different methods can also be utilized to trade-off between the on-line optimization time and the accuracy of the control system. Moreover, one can also decrease the online computational cost by designing customized MPC controllers if a finite number of constraint sets are explicitly known. The improvement, however, is limited by the algorithms themselves but it may feasible for special applications.

In this thesis, the author proposes a 1-bit processing based MPC (OBMPC) for the fractionated satellite mission. The proposed algorithm addresses issues introduced due to the tough wireless communication environment as well as the limited onboard resources in the fractionated satellite structure. The algorithm can fit into the framework of the quantized MPC, and the 1-bit nature of the controller allows a high sampling rate with low computational cost. It is worth noting that as an implementation method, most efforts made to decrease the online computational effort such as model reduction and fast online solvers can be combined with the OBMPC structure to further improve the system performance.

3. DELTA-SIGMA MODULATION AND 1-BIT PROCESSING

==========

==========

The 1-bit processing is a new concept proposed by Wu and Goodall (2005a). It was inspired by the development of bi-level $\Delta\sum$ modulators and single bit filters. The theory is then extended into the control theory for controller implementation. The key concept of such implementation is that the $\Delta\sum$ modulation uses Pulse Density Modulation (PDM) where each pulse contains useful information and noise introduced during the quantization process (namely quantization noise). In contrast to the Δ modulation (e.g. Pulse Width Modulation, PWM), the $\Delta\sum$ modulation gives a representation of the signal's amplitude rather than its slope. Hence, with the FIR filter technology, each pulse can be considered as independent control information with filtered noise. Additionally, although not necessary, the control input signal can be encoded by $\Delta\sum$ modulation for digital communication proposes. Such bi-level control signals can be used to drive the control object directly, which may be convenient for hardware implementation. Fig.3.1 (Wu and Goodall, 2005b) shows a comparison between conventional digital control system and a 1-bit processing control system.

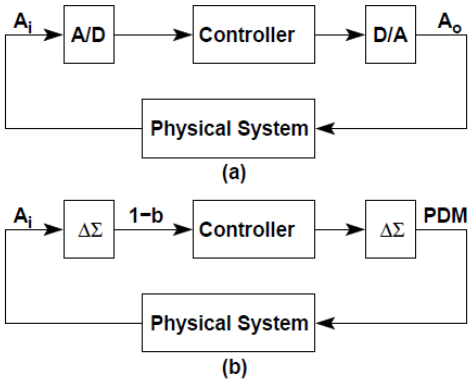

Figure 3.1 Comparation of (a) conventional digital control system and (b) 1-bit processing control system.

Note that for both digital control systems in Fig.3.1, the control law can be designed using either classic or modern control theory. In other words, one-bit processing is a way to implement rather than to design control laws. The benefit of 1-bit processing is appealing due to the explicit use of the 1-bit signal. The most attractive one is that 1-bit signals can be processed independently by the controller. All the feedback based multiplications can be simplified by changing the signs of the multi-bit coefficients. Hence, a multiplier free structure can be designed by choosing a modified controller structure. The area of silicon required to implement a 1-bit controller is potentially much smaller than that of a multi-bit system. Such implementation is especially beneficial for optimization based control algorithms for large scaled control systems, where extensive matrix multiplications may apply. Other benefits for the 1-bit processing include:

- It retains the advantages of digital-processing techniques while approaching high quality analogue processors (Wu and Goodall, 2005a).
- Only 1-bit A/D converters are needed in the control loop, and D/A converters or PWM logics are not necessary as 1-bit signals can drive physical systems directly. Thus, there is no error accumulation in the sigma-delta demodulator and the system is less sensitive to channel errors.
- The 1-bit processing control system can be beneficial to a wireless networked control system in many ways. Firstly, sensing and control signals are modulated

into 1-bit signals, ready for transmission directly. Secondly, at the receiver end there is no decoding process, i.e. the 1-bit signals being fed into controller or actuator directly. Thirdly, the control performance is not affected by data loss due to the modulation techniques (Wu and Bai, 2010).

However, comparing to the conventional digital control systems, 1-bit processing control systems bring new challenges to the designers. As a kind of A/D conversion, $\Delta\sum$ modulation requires high sampling rate (Oversampling Rate, namely OSR) to achieve good resolution and high SNR. Therefore, for 1-bit processing, the main drawback is that the OSR needs to be involved in the entire control loop rather than the A/D converter itself, so the controller needs to be heavily sampled. The interests in such control systems are the controller formulation and the trade-off between reasonable OSR and system performance. Moreover, even with proper filtering technology, the quantization process still introduces nonlinearity to the control system and therefore compromises the robustness of the control algorithm.

3.1 Delta-Sigma Modulation

3.1.1 Definition and description

The $\Delta\sum$ modulation technology was developed based on the Δ modulation, and added integrators to include the sum of the previous difference. Unlike Δ modulators, the overload characteristic of the $\Delta\sum$ modulator is independent of the frequency of the input signal. In other words, the maximum SNR is independent of the frequency of the input signal in $\Delta\sum$ modulation (Yu, 1992). The resulting signal is also known as PDM, as it uses the relative density of the pulses to represent the analog signal. For $\Delta\sum$ modulators, bi-level quantizer is the most widely adopted structures due to the circuit simplicity and robustness.

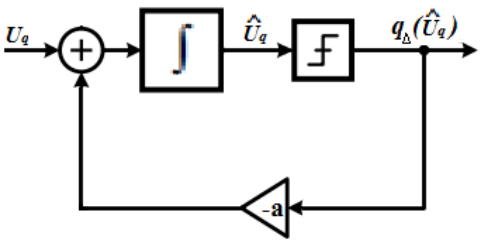

Figure 3.2 Conceptual view of bi-level ∆∑ modulation

As an effective method for building high resolution data converters, ∆∑ modulator is featured with a high dynamic range and the modulation process is not affected by the cumulative error. Among ∆∑ modulators, bi-level quantizer based ∆∑ modulation is used more than others due to the circuit simplicity and the binary nature of the quantizer output. Fig.3.2 shows a conceptual view of the bi-level ∆∑ modulation, where U_q is the modulator input, $\widehat{U}_q$ is the quantizer input and $q_\Delta(\widehat{U}_q)$ is the modulator output. The ∆∑ modulation quantizes the signal directly, rather than the signal's derivative. Hence the maximum quantizer range is determined by the maximum signal amplitude. If the input exceeds this limit, scaling needs to be applied.

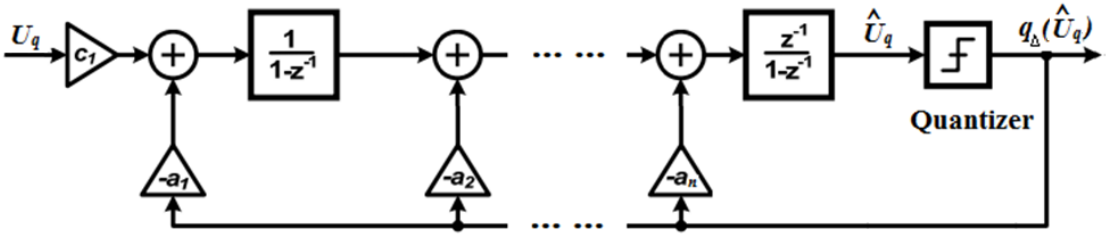

Figure 3.3 A High order ∆∑ modulator structure

Fig.3.3 illustrates the structure of a discretized high order ∆∑ modulator, where *z* denotes the *z*-transform of a shift operator. To a discrete-time sample $U_q(n)$ at time step *n*:

$$z^{-1}U_q(n) = U_q(n-1). \tag{3.1}$$

Also, the bi-level quantizer q_Δ is defined as:

$$q_\Delta(\widehat{U}_q) \triangleq \begin{cases} \Delta & if\ \widehat{U}_q \geq 0 \\ -\Delta & if\ \widehat{U}_q < 0 \end{cases}. \tag{3.2}$$

To approach high resolution performance of a bi-level ΔΣ modulator, the OSR is required for ΔΣ modulation. If the frequency of interest is from 0 to f_0, the OSR is defined to be the ratio of the sampling frequency f_s to the Nyquist frequency $2f_0$:

$$OSR \triangleq \frac{f_s}{2f_0} \tag{3.3}$$

For decoding, decimation is required. The corresponding multi-bit digital format Y_q of the input U_q is determined by taking the average value within an OSR period:

$$Y_q = \frac{1}{OSR}\sum_{i=1}^{OSR} q_\Delta(\widehat{U}_q)_i\,, \tag{3.4}$$

where $\widehat{U}_q$ is the integrator's output with respect of the input U_q, and $q_\Delta(\widehat{U}_q)$ is the output of the quantizer q_Δ. If $\widehat{U}_q$ is positive or 0, $q_\Delta(\widehat{U}_q)$ is +Δ. If $\widehat{U}_q$ is negative, then $q_\Delta(\widehat{U}_q)$ is -Δ. The output after decoding is limited to -Δ and +Δ. Eq.3.4 also suggests that the bi-level output can be decimated by simply taking the average of a group of oversampled signals, or adding a low pass filter to convert the digital signal to an analog signal. The fact that most physical dynamic systems can be regarded as low pass filters means that the ΔΣ modulation requires no additional A/D converter in the loop.

The question raises that, if the dynamic system can be driven by the PDM signals, whether the controller can process these 1-bit data individually or not. It has been proven by various literatures, e.g. (Delchamps, 1990), that in fact, the 1-bit signals generated by the ΔΣ modulation contains all the useful information of the input, but this information is obscured by the errors, in other words, the quantization noise.

3.1.2 Wavelet analysis

For ΔΣ modulations, the nonlinear nature of a quantizer introduces the quantization noise. As the author is including the ΔΣ modulator in an oversampled control loop, the quantization noise will be processed along with the useful information at each time step. Moreover, the error may accumulate fast due to the integrators existed in

the control loop and the controller may lose the track in a few time steps.

To analyse the quantization noise in detail, wavelet de-noising is applied here. Assume $(\aleph_{j,k})_{j,k} \in K$ as an orthogonal basis of wavelets on the interval I = [a; b] as described by (Cohen, et al., 1993) so that any signal $u \in L^2(I)$ can be written as the sum of a series

$$u = \sum_{j,k\in K} \langle u, \aleph_{j,k} \rangle \aleph_{j,k}, \tag{3.5}$$

where

$$< u, \aleph_{j,k} >= \int_a^b u(x)\, \aleph_{j,k}(x) dx\,. \tag{3.6}$$

Define hard threshold operator η as:

$$\eta(x) = \begin{cases} x & if|x| \geq \lambda \\ 0 & if|x| \leq \lambda \end{cases} \quad (\lambda \; is \; the \; threshold)\,. \tag{3.7}$$

Then the de-noised signal can be presented as

$$u_0 = \sum_{j,k\in K} \eta(< u, \aleph_{j,k} >)\aleph_{j,k}\,. \tag{3.8}$$

Hence, the noisy signal can be written as

$$u = \tilde{u} + \sum_i \omega_i\,. \tag{3.9}$$

where $\tilde{u}$ is the noiseless signal to be estimated, ω_i is the additive Gaussian white noise of standard deviation δ_i, and i is the number of de-noising steps. Then 1-bit signal can be linearized by a signal plus additive quantization error approximation, making it easier to design and analyze the 1-bit systems. Normally, such linearization is followed by some basic assumptions based on (Norsworthy, et al., 1996):

A.3.1: The absolute in-band quantization noise power is expected as white noise within the interval [0, f_s] of the frequency band.

A.3.2: The probability density function (PDF) of the quantization error is uniform in the interval [- Δ , Δ].

3.1.3 Quantization noise

As suggested in the wavelet analysis, the nonlinearity in the ∆∑ modulation can be linearized by modeling the 1-bit quantizer with an additive noise. The nonlinear quantizer can be replaced with a signal-dependent gain and the quantization noise, and therefore described as a quasi-linear model as suggested in (Slotine and Li, 1991). Consider the discrete counterpart of the ∆∑ modulator described in Fig 3.2, its quasi-linear ∆∑ modulator model is shown in Fig 3.4. The encoder and sampling time for the discrete model are not discussed here as they do not affect the analysis in this section.

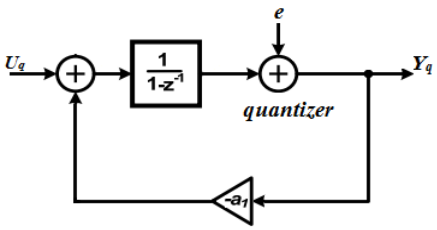

Figure 3.4 First order quasi-linear ∆∑ modulator

To decrease the in-band noise, the ∆∑ modulation also adds noise-shaping benefits by placing integrators in the main loop before the quantizer. The input to the quantizer is the integral of the difference between the input and the quantized output, which approaches zero. Hence the average value of the binary pulses tracks the input. The relationship between the input U_q, the quantization noise e and the output Y_q can be described by

$$Y_q = \overbrace{\frac{1}{z}}^{STF} U_q + \overbrace{(\frac{z-1}{z})}^{NTF} e. \qquad (3.10)$$

This equation contains a signal transfer function (STF) and a noise transfer function (NTF). The STF is a low-pass filter and the NTF is a high-pass filter. The integrator therefore forms a low-pass filter on the difference signal, providing low frequency feedback around the quantizer. This feedback results in a reduction of quantization noise at low (in-band) frequencies. The noise, however, is shaped by a high-pass filter, shaping the noise out of the low frequency area. In most digitalized control

applications, the quantization noise is neglected due to the assumption that the error is filtered by the physical system (physical systems are generally not sensitive to signals in high-frequency range). However, as mentioned before, for $\Delta\sum$ modulators, the nonlinearity introduces spectral components which cover a wide bandwidth including the baseband (Ardalan and Paulos, 1987). Therefore it is hard to adequately filter the quantization noise if the noise power in the base band is too high. In order to settle the data rate and sampling frequency for 1-bit processing, the approach taken here is to increase the SNR within the baseband.

Assuming *A1* and *A2* hold, letting $\sigma_{e-total}^2$ stand for the power density of the quantization noise *e*, it can be calculated as

$$\sigma_{e-total}^2 = \frac{1}{2\Delta}\int_{-\Delta}^{\Delta} e^2 de = \frac{\Delta^2}{3}. \tag{3.11}$$

When the sampling frequency is f_s, all of the quantized signal power folds into the frequency band $0 \le f \le f_s/2$. Assuming that the quantization noise is white noise, its spectral density is obtained as

$$E(f) = \sigma_{e-total}\sqrt{\frac{2}{f_s}}. \tag{3.12}$$

Therefore, the spectral of the quantization noise of the first order $\Delta\sum$ modulator is given by

$$N(f) = E(f)|NTF(e^{j\omega})|. \tag{3.13}$$

Hence the noise power within the signal band is

$$\sigma_e^2 = \int_0^{f_o} |N(f)|^2 df = \frac{\sigma_{e-total}^2}{2\pi}\int_{-\pi}^{\pi} |NTF(e^{j\omega})|^2 \, d\omega, \tag{3.14}$$

and its root mean square value (RMS) is

$$\sigma_n = \sigma_e \frac{\pi^2}{3}\left(2\frac{f_0}{f_s}\right)^{3/2} = \sigma_e \frac{\pi^2}{3}(OSR)^{-3/2}. \tag{3.15}$$

Eq.3.15 shows that the noise can reduce 9dB by doubling the OSR, which again suggests that in theory, the quantization noise can be lowered to an acceptable range with appropriate OSR. In other words, the $\Delta\sum$ modulator based systems allow designers to trade-off system performance with the OSR. However, extremely high

sampling frequency is not expected in the digital control system as the time interval is too small for the controller to finish the calculation at each time step and it results in very small coefficients which require long word length. To reduce the sampling frequency and maintain the quantization noise within the acceptable range, high-order ΔΣ modulation has to be considered. Similar to Eq.3.15, general RMS noise for the high order ΔΣ modulators can be obtained as:

$$\sigma_n = \sigma_e \frac{\pi^m}{\sqrt{2m+1}} (OSR)^{-(2m+1)/2} \quad , \tag{3.16}$$

where *m* is the order of the modulator. The RMS noise therefore is reduced 3(2*m* + 1) dB by doubling the OSR. Fig.3.5 represents the linearized counterpart of the high order ΔΣ modulator shown in Fig3.3.

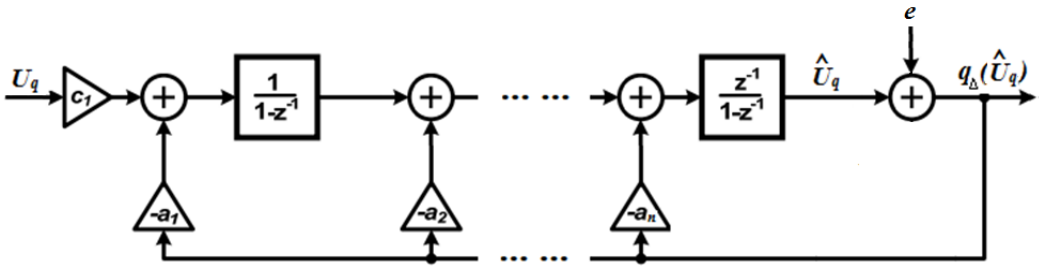

Figure 3.5 A High order linearized ΔΣ modulator

The transfer function in terms of *U* and *e* can be obtained as Eq.3.17.

$$Y_q = \overbrace{\frac{1}{z}}^{STF} U_q + \overbrace{(\frac{z-1}{z})^m}^{NTF} e \, . \tag{3.17}$$

The NTF then becomes a high order high pass filter, and the ΔΣ modulator can therefore achieve a good SNR performance, but it is also expensive to implement it with more than two integrators in circuit. In practice, the second order ΔΣ modulator is a most common application in data conversion. In this thesis, simulations are only based on the implementation of the second order ΔΣ modulator, which reduces the RMS noise by 15dB by doubling the OSR, resulting in a high dynamic range for signal processing. Fig.3.6 shows the relationship between the calculated SNR and the OSR for a second order ΔΣ modulator with sinusoidal input.

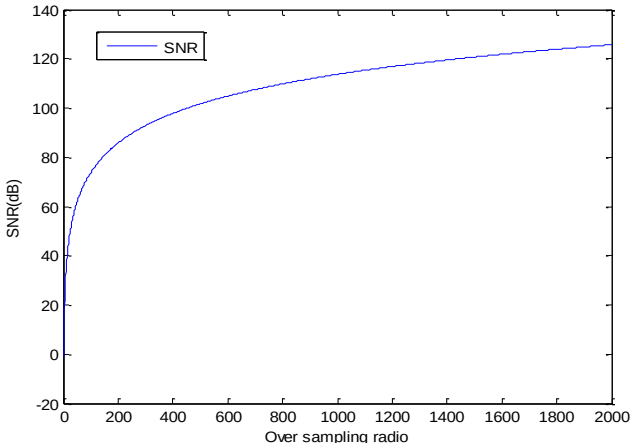

Figure 3.6 SNR for Second order ΔΣ modulator with sinusoidal input

Given a sinusoidal input with Standardized total power density of σ_u^2, based on the Eq.3.16, the SNR can be obtained:

$$SNR = \frac{\sigma_u^2}{\frac{\sigma_{e-total}^2}{2\pi}\int_{-\pi}^{\pi}\left|NTF(e^{j\omega})\right|^2 d\omega}. \tag{3.18}$$

It is shown in the Eq.3.18 that given a ΔΣ modulation structure and a known signal input, the *SNR* is a function of input power density and the *OSR*. Furthermore, the amplitude of the input signal is also critical to the SNR and the stability of the ΔΣ modulator. If the input power overloads the quantizer, the modulator will become unstable even the input amplitude drops back to small (Bourdopoulos, et al., 2003). Unlike signal processing, in terms of control theory, input signals are normally less predictable. Therefore, a good design of the quantization level is also important to the design of ΔΣ modulators. The author will continue the discussion of stability criteria and stabilization techniques of the ΔΣ modulator in Chapter 4 and Chapter 5.

3.1.4 Implementation structure

A large variety of the high order ΔΣ modulator structures exist, e.g. (Chao, et al., 1990; Troster, et al., 1993; Moussavi, 1994; Aziz and Sorensen, 1996; Brooks, et al., 1997). Three of common structures are collected here:

(1) Cascade Integrator with Distributed Feedback (CIDF).

The structure of CIDF is shown in Fig.3.7(a). The structure is the simplest

structure where the feedback coefficients a_n realize the NTF and STF poles and the NTF zeros are fixed to unity.

(2) Cascade Integrator with Distributed Input and Distributed Feedback (CIDIDF).

The structure of CIDIDF is shown in Fig.3.7(b). Similar to the CIDF, feedback coefficients a_n realize the NTF and STF poles, but the STF zeros can be determined by the feed-in coefficients b_n. State scaling coefficients c_n are used for dynamic range scaling.

(3) Cascade Integrator with Distributed Input and Summed Feed-Forward (CIDIFF).

The structure of CIDIFF structure is shown in Fig.3.7(c). It has the same input distribution but the zeroes of NTF and STF are implemented by the feed forward coefficients a_n.

Other than the above three structures, a stable resonator can be added into the structure with two delay integrators and a feedback coefficient g_1, which can be used to realize the complex zeros in NTF (i.e. $z_i = e^{\pm j\sqrt{g1}}$). For odd order structures, the resonators are normally located at the second and the third integrators to avoid noise coupling due to the feedback coefficient (Bourdopoulos, et al., 2003). A CIDIFF structure with resonator is shown in Fig.3.7(d).

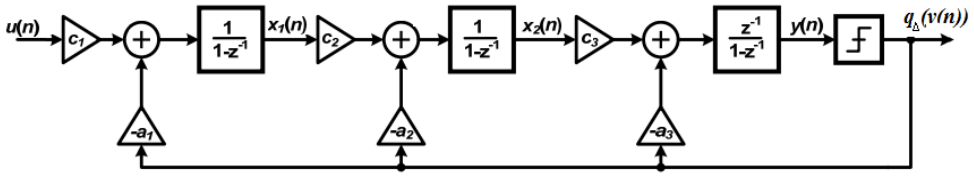

(a)

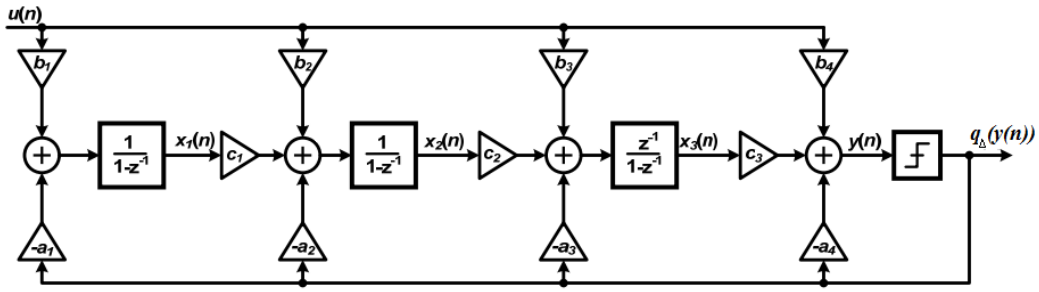

(b)

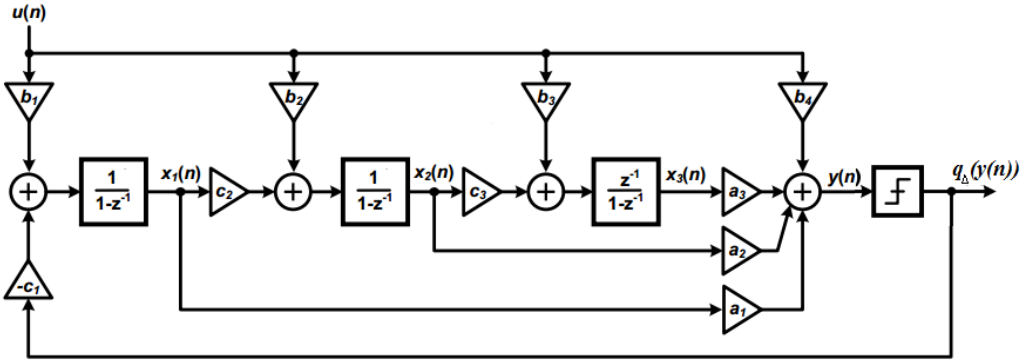

(c)

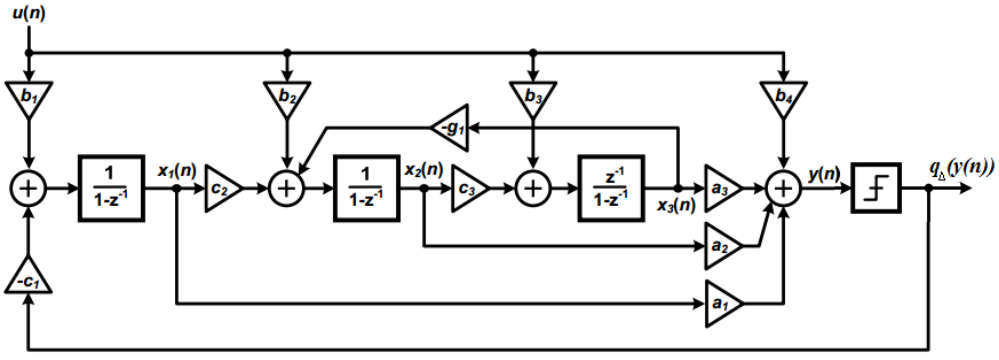

(d)

Figure 3.7 Implementation structures for the 3rd order bi-level ΔΣ modulators: (a)CIDF (b) CIDIDF (c) CIDIFF (d) CIDIFF with resonator

It is worth noting that for the bi-level $\Delta\sum$ modulators, feedback data are in 1-bit form. Therefore the operations in the filter loop can be implemented by the resource friendly combinations of shift and add. It can even be implemented without any comparison operations, and selection of the sign bit is all that is required (Janssen and van Roermund, 2011). In the work of 1-bit processing based MPC presented in the next chapter, the author considers the $\Delta\sum$ modulators as off the shelf analog components. Therefore the computational efforts made by the $\Delta\sum$ modulators themselves are not included in the control loop.

However, these structures will be used as the foundation of designing the 1-bit processing control loop and the $\Delta\sum$ modulation based sensors and estimators as discussed in Chapter 5 and Chapter 6. In addition to the above discussion, a state space approach will be further discussed in Chapter 5 and a parallel structure is used to develop an OBMPC based $\Delta\sum$ modulator.

3.2 1-Bit Processing Control Systems

To design a 1-bit processing control system, a few things need to be taken into consideration. Firstly, the control structure needs to be designed to fully utilize the "1-bit" characteristic of the signal, so that good system performance can be achieved with relatively low computational resources. Secondly, reasonable OSR need to be chosen to achieve high resolution of the modulated signal while maintain the functionality of the controller to operate in real-time. Thirdly, the stability issues need to be addressed since the quantization noise is introduced into the control loop, which will affect the robustness of the control system.

The basic idea of the 1-bit processing is to encode analogue signals into binary pulses and represent these pulses with 1-bit registers in hardware, then work on these 1-bit data to produce desired actuation in real-time. Rather than using multi-bit A/D converter, the proposed system structure uses bi-level $\Delta\sum$ modulators to encode signals, and then process these signals directly with controllers. Also, considering that most dynamic models are insensitive to high frequency signals (i.e. works as a low

pass filter), the oversampled $\Delta\sum$ modulator output can be considered to drive the dynamic model directly without demodulators.

3.2.1 Controller structure

Here, a canonic *z*-form is presented first and the control structure is shown in Fig.3.8. (Goodall, 1990; Wu and Goodall, 2005a).

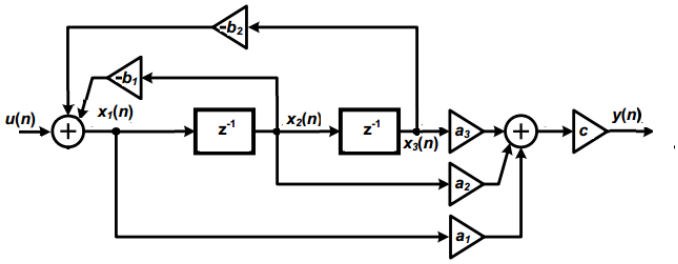

Figure 3.8 Canonic *z*-form

In Fig.3.8, the discrete transfer function can be described as:

$$H(z) = c\frac{a_1z^2+a_2z+a_3}{z^2+b_2z+b_1}, \tag{3.19}$$

where a_1, a_2, a_3 and b_1, b_2, b_3 are the coefficients of the transfer function, c is the gain outside the feedback loop. At sampling step k, define $X(k) = [x(k-2), x(k-1), x(k)]^T$, $U(k) \in \mathbb{R}$ and $Y(k) \in \mathbb{R}$ as the state vector, control input and output respectively, then its state space equation can be formulated as:

$$X(k+1) = A_zX(k) + B_zU(k),$$

$$Y(k) = C_zX(k), \tag{3.20}$$

where $A_z = \begin{bmatrix} 0 & -b_1 & -b_2 \\ 1 & 0 & 0 \\ 0 & 1 & 0 \end{bmatrix}, B_z = \begin{bmatrix} 1 \\ 0 \\ 0 \end{bmatrix}$, $C_z = [ca_1 \quad ca_2 \quad ca_3]$.

However, the required high sampling frequency (e.g. much higher than the system poles) may result in long word lengths for both coefficients and variables within the controller, primarily because as the differences between successive values of the input and output become increasingly small, the coefficients need more bits to achieve accurate control result. For example, as suggested in Eq. 3.20, $x(k)$ can be

calculated using the previous data $x(k-1)$, $x(k-2)$ and the control input:

$$x(k) = u(k) - b_1 x(k-1) - b_2 x(k-2). \tag{3.21}$$

The coefficients b_1 and b_2 are determined so that the suitable proportions of the small differences are combined to give the required output y (Goodall, 1990). For each step of the fast sampled system, the difference between $x(k-1)$ and $x(k-2)$ has to be small to ensure the dynamic response converges to the Laplace transform, or in other words, its continuous counterpart. Meanwhile, digital processors only provide a finite word length of the coefficients. Hence, the effect of coefficient round off may share a higher proportion of the overall system noise and error, especially when the coefficient value varies within a big range. Then the coefficient quantization error may be significant, especially for higher order control systems. Such error may integrate during each control action and compromise the system robustness.

To address this problem, a δ transform is proposed to implement the control law. δ transform is proposed by Middleton and Goodwin (1986, 1990). Simply define $\delta = \frac{z-1}{T}$, where T is the sampling interval, or $\delta = z - 1$ (since T in this equation only changes coefficients). The δ transform is developed along with the commencement of digital microprocessor. Considering a δ transform on Eq. 3.19, then

$$H(\delta) = \frac{n_1\delta^2 + n_2\delta + n_3}{\delta^2 + m_2\delta + m_1}. \tag{3.22}$$

Since δ and Z are linear function transform, then corresponding state space equation for this form are

$$X_{n+1} = A_\delta X_n + B_\delta U_n \tag{3.23}$$

$$Y_n = C_\delta X_n \ ,$$

where $A_\delta = \begin{bmatrix} 0 & -m_1 & -m_2 \\ 1 & 0 & 0 \\ 0 & 1 & 0 \end{bmatrix}, B_\delta = \begin{bmatrix} 1 \\ 0 \\ 0 \end{bmatrix}$, $C_\delta = [n_1 \quad n_2 \quad n_3]$, are functions of the A_z, B_z, C_z respectively. As a linear transform, δ transform shares most of the characteristics with the z transform. However, unlike the z transform, the δ transform

has low coefficient sensitivity as the accuracy of the coefficients simply needs to have the same accuracy as is required for the overall system performance (typically 5% for control; Forsythe and Goodall 1991). Again a conventional canonic structure in δ form can be considered as Fig.3.9(a).

To approach an explicit relationship between coefficients and the control variables, a modified canonic structure in δ form is demonstrated in Fig.3.9(b) (Parra, 2001). Both control structures can represent the same transfer function with

$$p_1=n_3$$

$$p_2=n_2$$

$$p_3=n_1$$

$$q_1=m_2, \text{ and}$$

$$q_2=m_1.$$

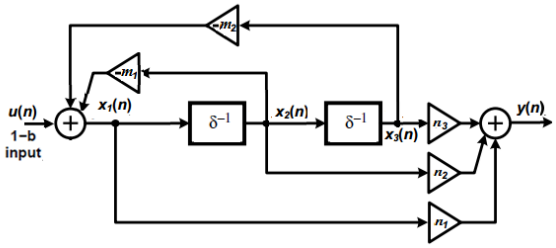

(a)

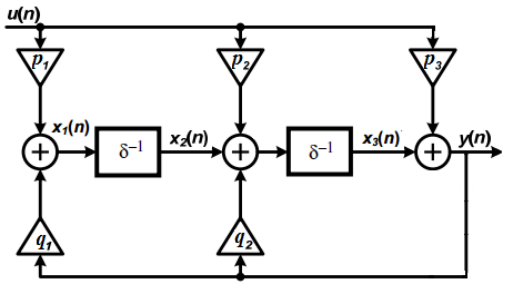

(b)

Figure 3.9 (a) canonic structure in δ form (b) modified canonic structure in δ form

3.2.2 1-bit processing in δ transform

Based on the modified canonic structure, the structure of a 1-bit processing system

can be developed as Fig.3.10 (Wu and Goodall, 2005a).

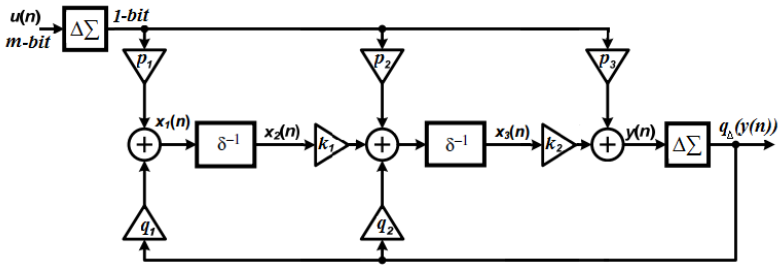

Figure 3.10 One-bit processing with modified canonic **δ** form

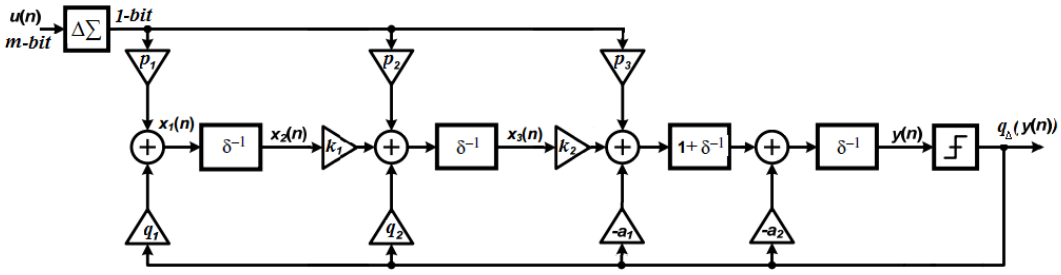

Figure 3.11 1-bit processing with modified canonic δ form with CIDF

Given a second order CIDF structure based ΔΣ modulator, the full control structure is shown in Fig.3.11. Therefore the quantization noise and sampling rate analysis can refer to the analysis of ΔΣ modulator itself. That is, given fixed ΔΣ modulation order and a known signal input, the SNR is a function of the OSR.

3.2.3 System sampling and robustness of the control system

As discussed at the beginning of this chapter, the ΔΣ data modulators require OSR with respect of Nyquist–Shannon sampling theorem to achieve good precision of modulated data. The basic idea for the OSR is to use higher sampling rate to compensate for the low resolution of the quantizer. Specifically speaking, for a first order bi-level (single bit) ΔΣ modulator, to obtain the 8-bit precision, the sample frequency needs to be at least 256 times more than the bandwidth to achieve the same precision of a multi-bit processing. Increasing the modulator order can decrease the OSR accordingly, which, however, will sacrifice the circuit simplicity and increase the number of integrators in the control loop. The author can again consider the "controller plus ΔΣ modulator" structure as a higher order ΔΣ modulator, and then

apply Eq.3.18 to analyze the SNR. To have a satisfying SNR, normally, the OSR also need to be chosen at a relatively high range. In this case, for 1-bit processing control systems, the phase delay introduced by the controller and $\Delta\sum$ modulator only has a minor effect on the robustness of the control system.

For 1-bit processing control system, the OSR is applied to the whole control system rather than just the modulators, raising issues of the trade-off between system precision and the capability of completing all the instructions within the time interval. This is the main drawback for the 1-bit processing control system. The decreased on board computational effort and circuit simplicity is necessarily compromised by the increased sampling rate. The comparison in terms of circuit occupation and energy consumption between 1-bit processing control systems and conventional control systems will be conducted in the simulation and hardware implementation. It is worth stressing here that a longer bit length not only means higher OSR to maintain system precision, but also means higher complexity of multiplications. Therefore, for most real-time control systems, the bit lengths are normally chosen as 8 to 12 bits (Wu and Goodall, 2005a). Recall Eq. 3.18, given fixed $\Delta\sum$ modulation structure and a known signal input, the SNR is a function of input power density and the OSR. For PDM control, SNR is expected to be a minimum of 50dB (Wu and Goodall, 2005a). The resultant OSR can be used as a design criterion during the simulation.

The stability analysis of the 1-bit processing control system is rather difficult due to the non-linearity introduced by the $\Delta\sum$ modulator. If the quantization noise can be linearized and all the assumptions made for the linearization hold, then the control loop can be analysed by standard signal plus white noise systems as discussed in (Delchamps, 1990). For simple SISO control systems, an alternative approach is to combine the control system with the lower order $\Delta\sum$ modulator, and treat them together as a higher order $\Delta\sum$ modulator (Johns and Lewis, 1993). Then the stability issues for the 1-bit processing systems fall into the framework of the stability of $\Delta\sum$ modulators. Practically, on the other hand, for a well-designed $\Delta\sum$ modulator, if the input is always bounded within the quantization level, the $\Delta\sum$ modulator can be

regarded as a simple A/D converter, which means the quantization noise can be ignored due to the oversampling technique. However, thorough theoretical analysis for the either 1-bit processing control system or even $\Delta\sum$ modulator itself is still hard to complete. This thesis mainly focuses on the 1-bit processing based implementation of optimal control algorithms (e.g. MPC), where such analysis is even harder as the canonical structure is not applicable to advanced control systems. Hence the author leaves this issue here and will continue the discussion in Chapter 4. Here, one can firstly use the results provided in (Johns and Lewis, 1993), that the stability of $\Delta\sum$ modulators based control system is determined by the stability of the original ones excluding the $\Delta\sum$ modulators from the loop as long as the $\Delta\sum$ modulators are stable.

3.2.4 1-bit processing based WCSs

As a bi-level $\Delta\sum$ modulation based control system, the 1-bit processing control system is naturally suitable to the wirelessly networked applications as the resulting binary numbers are ready for transmission directly. For WCS applications, the SNR is determined by an additional part: the need for low bit error rate (BER) of the wireless communication. Normally for wireless systems, the BER should be no more than 10^{-7}, which requires a SNR of at least 20dB. Hence the total SNR would be around 70dB (Wu and Goodall, 2005b). Together with the SNR requirement of the $\Delta\sum$ modulation, the OSR can be determined for the WCS.

The OSR is beneficial to the sensing information. As the sensing component is oversampled, more measurement quantities can be acquired even if the information is obstructed by the quantization noise and therefore provide better estimation than a single multi-bit measurement. However, this requires a customized design of the sensor. The $\Delta\sum$ modulator based MEMS gyroscopes are studied and a novel OBMPC based 1-bit MEMS gyroscope is introduced in Chapter 5. Moreover, the 1-bit processing control systems are also insensitive to the noise introduced during the WCS. As discussed above, each quantized data carries only partial information but can be processed in sequence. Due to the OSR, the significance of data loss is much

less than that of traditional multi-bit D/A conversion methods (Wu and Bai, 2010). This conclusion is discussed in Chapter 6 and verified in the simulation part in Chapter 7.

3.3 1-Bit Processing Control System for a Fractionated Satellite Mission

As discussed above, the 1-bit processing based control system is efficient in terms of circuit areas and power consumption, and advantageous to the wireless communication. Hence, it is attractive to the fractionated satellite missions as the onboard resources are limited and the control process is maintained by the ISL. The benefits of the 1-bit processing control system in the fractionated satellite mission will be further discussed in the later part of this thesis.

In this section, a 1-bit processing based control system is designed for the fractionated satellite mission. A numerical design example is provided to verify the feasibility of such design. The dynamic model of the satellite is built based on our QB50 mission. As the focus of this thesis is the OBMPC based fractionated satellite attitude control, the detailed mission modeling and environmental issues are omitted here and will be discussed in chapter 7. More details of the 1-bit processing control based fractionated satellite mission can refer to (Bai and Wu, 2010), which is the first aerospace application of the 1-bit processing control system to the best knowledge of the author. In Eq.3.24, a nano-satellite with rigid body is numerically presented:

$$x_s(k+1) = Ax_s(k) + Bu_s(k),$$

$$y_s(k) = Cx_s(k), \tag{3.24}$$

where:

$$A = \begin{bmatrix} 0 & 0 & 0 & 1 & 0 & 0 \\ 0 & 0 & 0 & 0 & 1 & 0 \\ 0 & 0 & 0 & 0 & 0 & 1 \\ -4.64 \times 10^{-6} & 0 & 0 & 0 & 0 & 1.28 \times 10^{-3} \\ 0 & 6.62 \times 10^{-7} & 0 & 0 & 0 & 0 \\ 0 & 0 & 0 & -1.08 \times 10^{-3} & 0 & 0 \end{bmatrix};$$

$$B = \begin{bmatrix} 0 & 0 & 0 \\ 0 & 0 & 0 \\ 0 & 0 & 0 \\ 1.46 \times 10^3 & 0 & 0 \\ 0 & 1.46 \times 10^3 & 0 \\ 0 & 0 & 1.22 \times 10^3 \end{bmatrix}; C = \begin{bmatrix} 0 & 0 & 0 & 0 & 0 & 0 \\ 0 & 0 & 0 & 0 & 0 & 0 \\ 0 & 0 & 0 & 0 & 0 & 0 \\ 0 & 0 & 0 & 1 & 0 & 0 \\ 0 & 0 & 0 & 0 & 1 & 0 \\ 0 & 0 & 0 & 0 & 0 & 1 \end{bmatrix}.$$

The state variable is chosen as $x_s = [\varphi, \theta, \psi, \omega_x, \omega_y, \omega_z]^{\mathrm{T}}$, where $\varphi, \theta, \psi, \omega_x, \omega_y, \omega_z$ are the roll, pitch and yaw angles and angular velocities respectively. Since all the state variables are measurable, no observer is necessary in the control system. The model is only suitable for small angles. A 2nd order command tracking controller is designed and located on-board the master satellite. For three axes attitude control and stabilization, it is recommended that each channel should be controlled separately. The master satellite carries out control system processing directly upon the 1-bit signals, and then encodes and transmits the control input signal as 1-bit signals to drive actuators on the slave satellite directly. The sensing components are MEMS sensors with built-in $\Delta\sum$ modulators, e.g. MEMS gyroscopes by (Kraft and Ding, 2009), and provide 1-bit feedback data to the controller. Environmental disturbances are ignored here to simplify the problem. The constraints applied on the control input are set to $\pm 1 \times 10^{-5}$ Nm. The control objective for the roll angle is set to 1°.

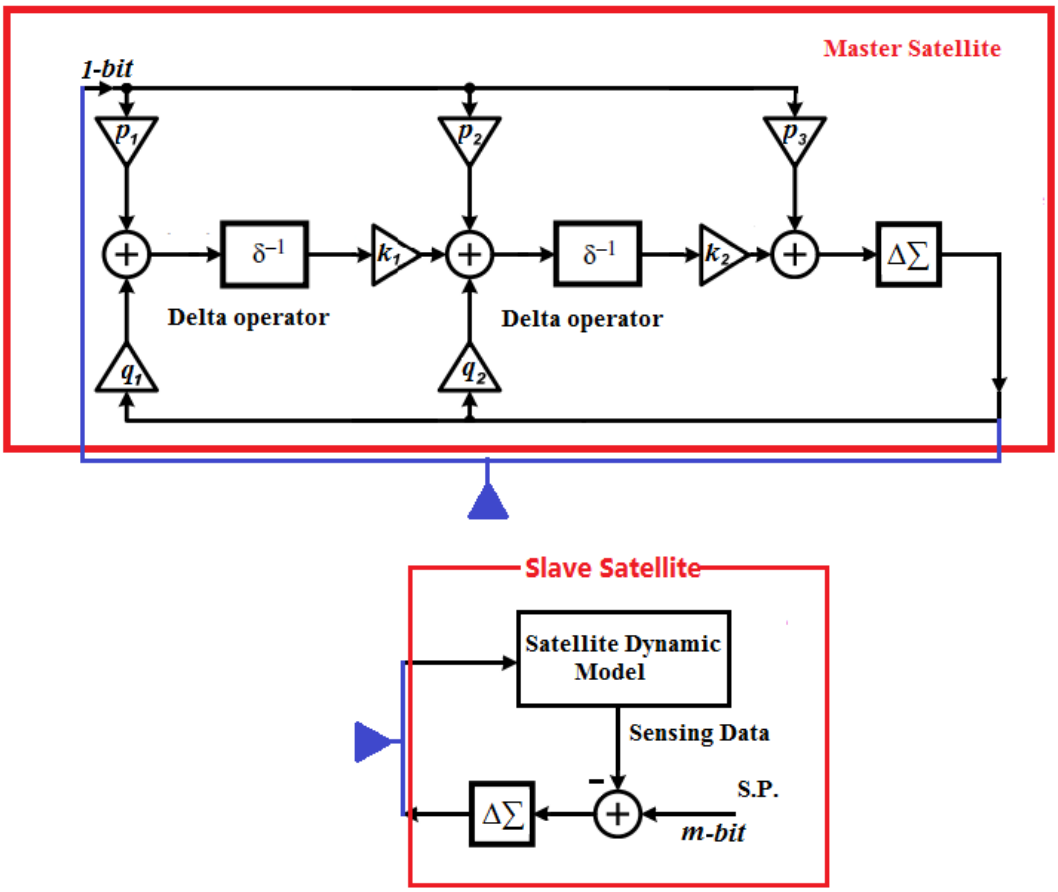

Figure 3.12 Diagram of a fractionated satellite attitude decision and control system

The control structure of a fractionated satellite attitude decision and control system is illustrated in Fig.3.12. In the proposed structure, two $\Delta\sum$ modulators are used to encode the multi-bit data into 1-bit data for the feedback signals and the control inputs respectively. The resulting 1-bit data are utilized to drive the dynamic model directly. A modified canonical structure is used so all the coefficients are related to the distributed 1-bit feedback signals and control inputs. Therefore, no multiplication is required in the control structure. The sampling frequency is set to 100 kHz. Transmission delay, data loss and the BER are considered to be negligible in this simulation and will be further discussed in Chapter 7.

For simulation, the roll angle is taken as an example of the design process. A PID controller using the canonic structure is proposed here to achieve the control objective. As discuss above, given relatively high OSR, the stability of the 1-bit processing control system is determined by the stability of the original control system excluding

the $\Delta\sum$ modulators from the loop as long as the $\Delta\sum$ modulators are stable. Hence the PID controller can be designed first to stabilize the control system with P=2.8×10^{-7}, I=1.5×10^{-10}, D=5.7×10^{-5}. The sampling rate is chosen as 1Hz and the OSR is set to 1000 (i.e.1000Hz). Then the discrete controller in *z* form can be acquired as

$$H(z) = \frac{n_1 z^2 + n_2 z + n_3}{z^2 + m_1 z + m_2}, \tag{3.25}$$

where

n_1=5.6×10^{-5};

n_2= -1.114×10^{-4};

n_3= -5.63×10^{-5};

m_1= 0;

m_2= -1.

Further transfer the *z* form discrete controller into δ form, then the coefficients in Eq.3.25 can be calculated as

$$H(\delta) = \frac{p_2 \delta^2 + p_1 \delta + p_0}{\delta^2 + q_1 \delta + q_0} \tag{3.26}$$

where

p_2 =5.6×10^{-5};

p_1 = 1.14×10^{-6};

p_0 = -5.514×10^{-5};

q_2 = 1;

q_1 = 2;

q_0 = 0.

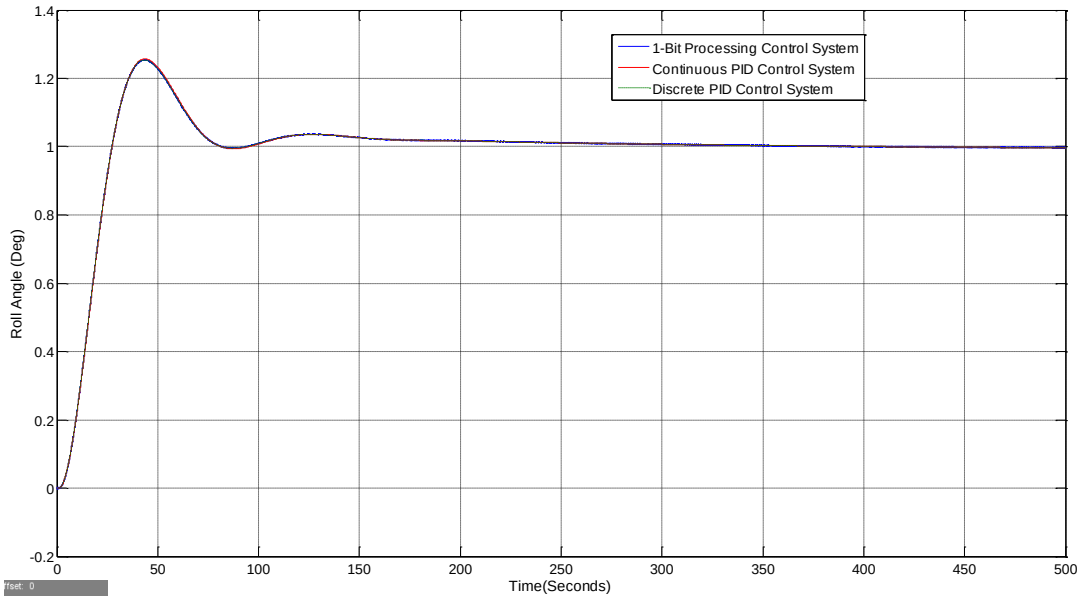
1-Bit Processing Control System
Continuous PID Control System
Discrete PID Control System
Roll Angle (Deg)
Time(Seconds)

(a)

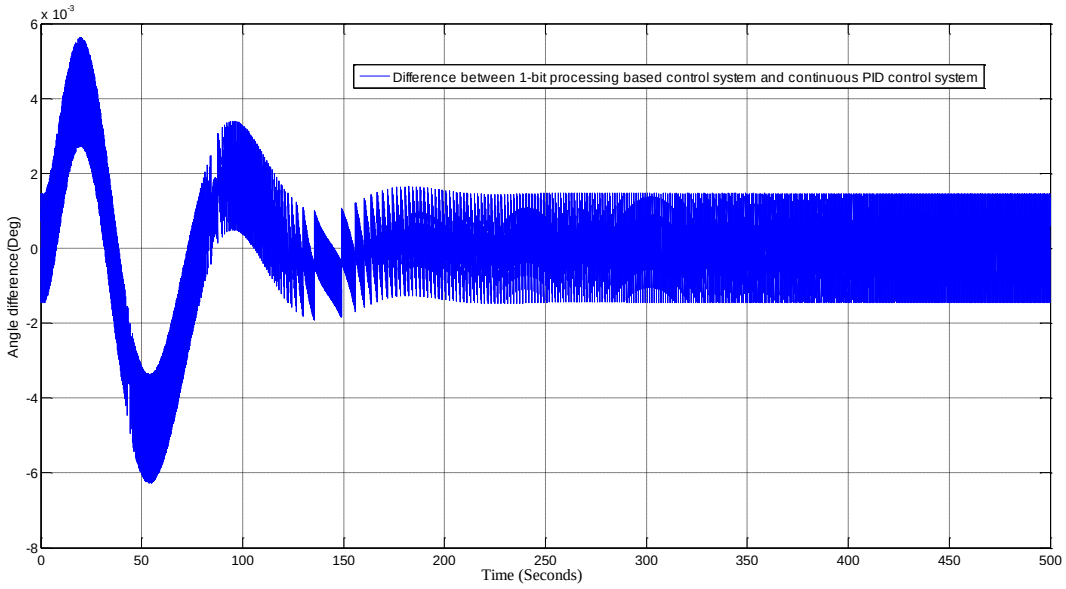
x 10^-3
Difference between 1-bit processing based control system and continuous PID control system
Angle difference(Deg)
Time (Seconds)

(b)

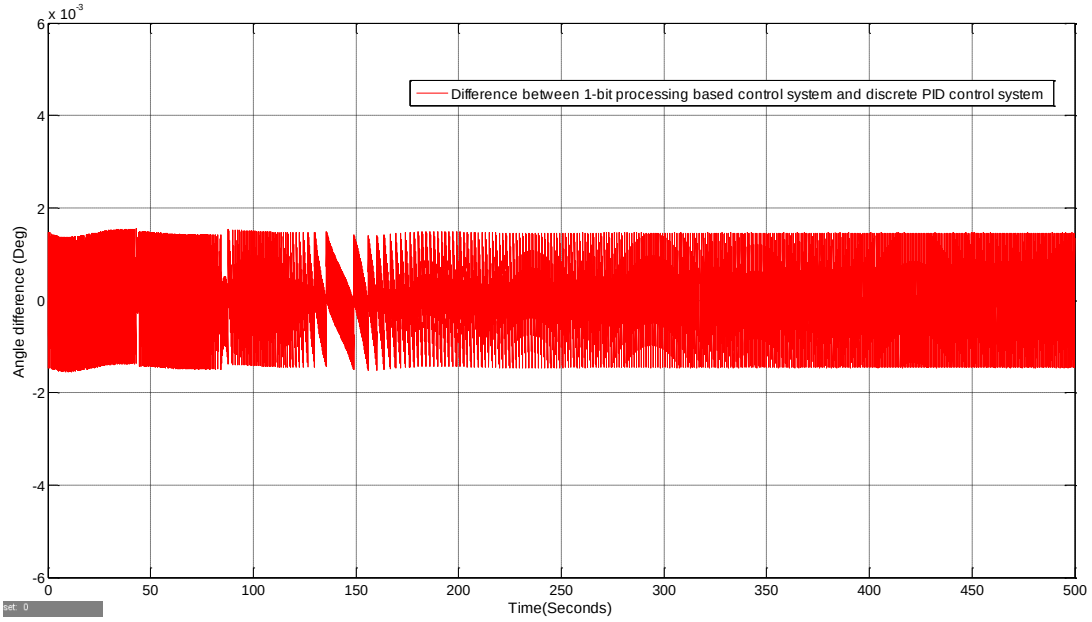

(c)

Figure 3.13 Simulation results: (a) Position response of the control systems; (b) Difference of the responses between the 1-bit processing based control system and the continuous PID control system. (c) Difference of the responses between the 1-bit processing based control system and the discrete PID control system.

The simulation results are shown respectively in Fig.3.13 and Fig.3.14. Fig.3.13(a) shows the step response of the continuous PID control system, discrete PID control system and the 1-bit processing based control system respectively. It can be seen that the 1-bit processing based control system tracks the continuous benchmark well. The difference between the 1-bit processing based control system and its continuous benchmark is shown in Fig.3.13(b). The difference between the 1-bit processing based control system and its discrete benchmark is shown in Fig.3.13(c). The peak difference in Fig.3.13(b) is about 0.006% and 0.002% in Fig.3.13(c), which is suggesting that the quantization noise remains in a reasonable level in the proposed 1-bit processing based control system under the given OSR.

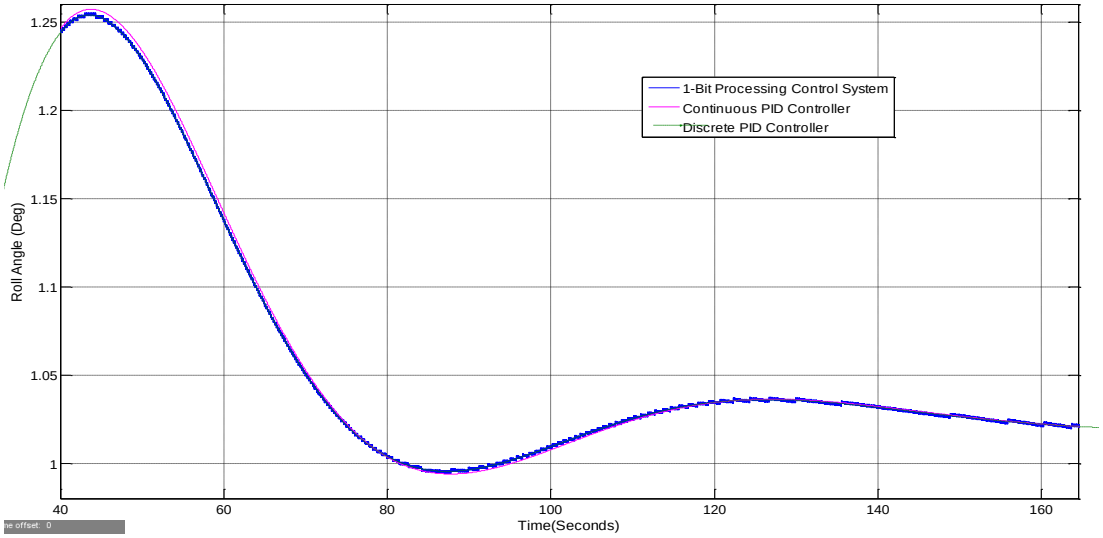

Figure 3.14 Comparison between the simulation results: the data are removed randomly by considering a 10^{-7} BER

Furthermore, transmission delay and BER are investigated for the ISL using $\Delta\sum$ modulation. The delay and BER are considered for both the sensing and control signals. During the simulation the delay is added to the loop for some sampling time; and the data are removed randomly by considering a 10^{-7} BER. The simulation results are shown respectively in Fig.3.14. The delays are introduced into the control system when the sensing signal is sent to the master satellite and when the control signal is sent to the slave satellite. The peak error for the transmission delay model is less than 0.1%. And the error for the BER model can be ignored. The results show that the ISL using $\Delta\sum$ modulation is robust and feasible.

3.4 Summary

This Chapter introduced the concept of the 1-bit processing based control system as proposed by Wu and Goodall (2005a). The benefits of such 1-bit processing based control system are discussed and the author proposed that such structure is feasible for the fractionated satellite mission.

The 1-bit processing control system is built based on the bi-level $\Delta\sum$ modulation. Normally two $\Delta\sum$ modulators are required: one is used to encode the control input to drive the dynamic model directly; and the other is used to encode the control feedback

to repeat the control loop. The resulting 1-bit data are in pulse density modulation nature and include all the useful information. They can be processed individually so it is possible to implement the control system with a multiplier free structure. However, the information is blocked with quantization noise. As a nonlinear component, the behaviour of the $\Delta\sum$ modulation can be modelled by linearizing the quantization noise into additive white noise. To maintain the robustness of the controller, such noise needs to be sufficiently filtered to decrease the noise within the bandwidth of interest. A built-in noise shaping filter is applied to address this problem, but may also require a high sampling rate (i.e. the OSR) to achieve desired precision.

The OSR is the main drawback of the 1-bit processing control system. Fast sampled control systems may trigger various problems to the control loop. Firstly, the high sampling rate normally means long word length, which makes it impractical for implementation. This problem is addressed by introducing the δ transform. Secondly, small time interval may be a challenge to the controller, especially for the embedded control systems where the on-board resources are limited. This means the controller needs to be carefully customized to suit the need of 1-bit processing control system.

Even with all the disadvantages, the 1-bit processing control system is proven to be efficient in term of circuit simplicity and online computational effort. The main improvement is to replace all the multiplications with conditional-negate (CN), add and shift operators. By using a modified canonical structure, an explicit relationship is formed between the multi-bit coefficients and 1-bit controller input and control feedbacks. Therefore, the control loop can be implemented with a multiplier free approach. Also, the 1-bit processing control is especially suitable for wireless control applications. The modulated 1-bit data are naturally ready for wireless communication, and the OSR makes both the control input data and measurement data less sensitive to the errors and communication loss. Based on such advantages, the 1-bit processing based control system is proposed for the attitude control system of the fractionated satellite missions. A numerical example is provided at the end of this chapter to verify the feasibility of such proposal.

4. 1-BIT PROCESSING BASED MODEL PREDICTIVE CONTROL

==========

==========

In this chapter, a 1-Bit Processing Based MPC (OBMPC) algorithm is proposed. The proposition is based on the fractionated satellite attitude control mission but it can be extended to the more general case of fast sampled MPCs in embedded control systems. The results of this thesis are generated based on the 1-bit processing system proposed in Chapter 3, where the bi-level $\Delta\sum$ Modulators are used and the modulation output shall be processed directly by the controller. To discuss the OBMPC, it is necessary to study the MPC algorithm and its extensions. As an optimization based algorithm, the MPC is typically based on the online QP solver. Before the discussion about the MPC algorithm, a few basic definitions and the QP problem shall first be introduced.

4.1 Quadratic Programming and Bi-level Problem:

The definitions in this section are based on (Boyd and Vandenberghe, 2009).

Definition 4.1: Convex Set and convex function:

A set *C* is a convex set if the line segment between any two points in *C* lies in *C*. A function *f*: $\mathbb{R}^n \to \mathbb{R}$ is a convex function if **dom** *f* is a convex set and if for all *x*, y ∈ **dom** *f*, the line segment between (*x, f(x)*) and (*y, f(y)*) lies above the graph of *f*.

■

Definition 4.2: Polyhedron:

A *polyhedron* is defined as the solution set of a finite number of linear equalities and inequalities:

$$P = \{x | a_j^T x \leq b_j \; j = 1, \dots, m, c_j^T x = d_j, j = 1, \dots, p\}. \quad \blacksquare \qquad (4.1)$$

Definition 4.3: The set of positive semi-definite matrix:

Define notation $\mathbb{S}^n$ to denote the set of symmetric $n \times n$ matrices, then define $\mathbb{S}_+^n$ to denote the set of symmetric positive *semi-definite matrices*.

$$\mathbb{S}^n \triangleq \{x \in \mathbb{R}^{n \times n} | x = x^T\}$$

$$\mathbb{S}_+^n \triangleq \{x \in \mathbb{S}^n | x \geq 0\}. \quad \blacksquare \qquad (4.2)$$

Definition 4.4: Convex optimization problem:

A convex optimization problem is a optimization problem where

(a) The objective function is convex,
(b) the inequality constraint functions are convex,
(c) the equality constraint functions are affine. ■

Definition 4.5: Quadratic Programming (QP) problem formulation

The convex optimization problem is called a quadratic program (QP) if the objective function is (convex) quadratic, and the constraint functions are affine. Defining $x \in \mathbb{R}^n$ and $p \in \mathbb{R}^n$, q is a symmetric matrix where $q \in \mathbb{S}^{n \times n}$, $a \in \mathbb{R}^{m \times n}$ $b \in \mathbb{R}^m$, then a QP problem can be formulated as:

$$min_x \, f(x) = \frac{1}{2} x^T q x + x^T p \qquad (4.3)$$

Subject to : $ax \leq b$ ■

Generally, if $q \in \mathbb{S}_+^n$ and all the constraints are convex, the QP can be solved by simple convex optimization. To include the inequality constraints, such QP problem can be extended into a lagrangian dual by introducing the Lagrange factor λ (also refered as Dual Problem, Bi-level Problem or Max-min Problem in some references).

Definition 4.6: Lagrangian Dual

Define the lagrangian function $L(x,\lambda)$ as

$$L(x,\lambda) = \frac{1}{2}x^T qx + x^T p + \lambda^T(ax - b) \tag{4.4}$$

Subject to : $\lambda \geq 0.$

Based on Definition 4.4, an optimal solution x^* for $L(x)$ can be solved by $\nabla_x L(x,\lambda)$=0.

$$x^* = -q^{-1}a^T\lambda - q^{-1}p. \tag{4.5}$$

Substituting x^* into Eq.4.4, then a dual function can be acquired:

$$g(\lambda) = -\frac{1}{2}\lambda^T m\lambda - \lambda^T n + \frac{1}{2}p^T q^{-1}p. \tag{4.6}$$

where $m = -aq^{-1}a^T$ and $n = b + aq^{-1}p.$ ■

To better describe the problem, the optimization can be formulated in Eq.4.7 as a Dual Problem:

$$x^* = arg\, max_{\lambda \geq 0}\, min_x\, L(x,\lambda). \tag{4.7}$$

Let the lower-level problem to be convex (i.e. $f(x)$is a convex problem with convex constraints), the problem can be treated as the Karush-Kuhn-Tucker (KKT) conditions (Kuhn and Tucker, 1951), where exists a unique $x^* \in \mathbb{R}^n$ and a vector λ^* that satisfy:

$$qx^* + a^T\lambda^* = -p; \tag{4.8}$$

$$\lambda^{*T}(ax^* - b) = 0;$$

$$ax^* - b \leq 0;$$

$$\lambda^* \geq 0.$$

However, even when the constraint sets are strictly convex, the combination of these constraints still need to be addressed to find the optimal solution. The numerical issue for the bi-level problem can be found in the survey (Colson, et al., 2005).

4.2 MPC Concept and Formulation

MPC (also known as Receding Horizon Control, RHC) is one of the most attractive and promising control theories for the past few decades. The MPC algorithm is an optimization based control strategy. Typically, a MPC system optimizes a quadratic problem, which is formulated depending on the performance criterion (i.e. minimizing the predicted error or the objective function.), over a control input sequence (control horizon). The basic concept of MPC is to perform optimization over a control horizon to predict the future process behavior over a predefined prediction horizon by explicitly using the process model. A sequence of control signals including the current and future N_c time steps is computed and only the first component of the sequence is applied as the optimized solution to obtain feedback. In the next time step, a receding horizon strategy is applied. The first component in the control sequence is discarded and the prediction horizon is moved one step forward. The optimization process is then repeated. A conceptual view of the discrete MPC is shown in Fig.4.1.

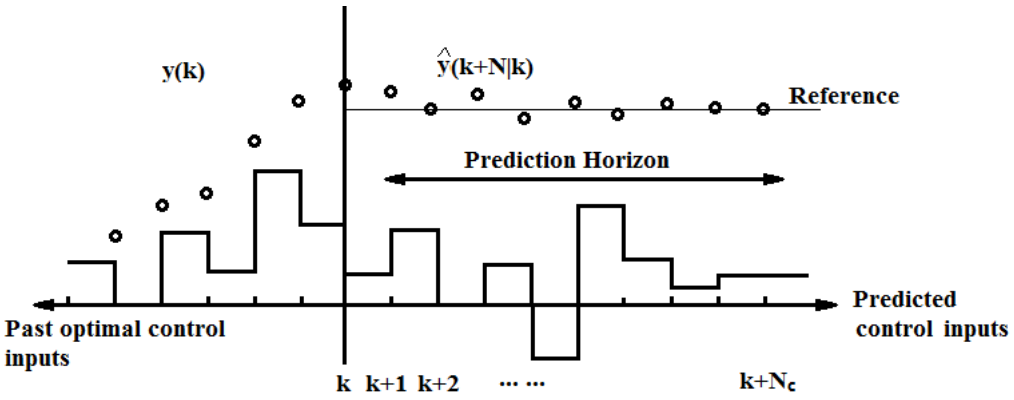

Figure 4.1 A conceptual view of the discrete MPC

Consider a MIMO system with *p* inputs, *q* outputs *(q≤p)* and *n* state variables. This system is described by the discrete time state space model with sampling interval *dt*. At time step *k*

$$x_m(k+1) = A_m x_m(k) + B_m u(k)$$

$$y_m(k) = C_m x_m(k) \tag{4.9}$$

where $k \in \mathbb{Z}$, and $x_m \in \mathbb{X}^n$, $u(k) \in \mathbb{R}^p$ and $y_m(k) \in \mathbb{R}^q$ denoting respectively the

state, input and output at time step *k*. $A_m \in \mathbb{R}^{n\times n}$, $B_m \in \mathbb{R}^{n\times p}$, $C_m \in \mathbb{R}^{q\times n}$ and (A_m, B_m) is a controllable pair. $\mathbb{X}^n \subseteq \mathbb{R}^n$, and $\mathbb{U}^p \subseteq \mathbb{R}^p$ are closed constraint sets. The control horizon and prediction horizon are denoted as N_c and N_p respectively. Define vectors *Y* and U as:

$$Y = [y_m(k|k)\ y_m(k+1|k) \dots y_m\big(k+N_p|k\big)]^T;$$

$$U = [u(k|k)\ \ u(k+1|k) \dots u(k+N_c-1|k)]^T,$$

By substituting Eq.4.9 into vector Y, the following result is obtained:

$$Y = Fx_m(k) + \vartheta U, \tag{4.10}$$

where

$$F = \begin{bmatrix} C_m \\ C_m{A_m}^1 \\ C_m{A_m}^2 \\ \vdots \\ C_m{A_m}^{N_p-1} \end{bmatrix}; \vartheta = \begin{bmatrix} C_mB_m & 0 & 0 & \cdots & 0 \\ C_mA_mB_m & C_mB_m & 0 & \cdots & 0 \\ C_m{A_m}^2B_m & C_mA_mB_m & C_mB_m & \cdots & 0 \\ \vdots & \vdots & \vdots & \ddots & \vdots \\ C_m{A_m}^{N_p-1}B_m & C_m{A_m}^{N_p-2}B_m & C_m{A_m}^{N_p-3}B_m & \cdots & C_m{A_m}^{N_p-N_c}B_m \end{bmatrix}.$$

The cost function in Eq.4.10 can be formulated with respect to the state variable x_m(k) and the control input *u(k).* The problem can then be described as a standard QP problem with constraint sets:

$$J\big(x_m(k),u(k)\big) = \min_{U(k)}\left\{||x_m\big(k+N_p|k\big)||_P^2 + \sum_{i=0}^{N_p-1}\big(||x_m(k+i|k)||_Q^2 + ||u((k+i)||_{R_L}^2\big)\right\} \tag{4.11}$$

Subject to

$$u_{min} \le u(k+i) \le u_{max}, i = 0, \dots, N_c - 1;$$

$$y_{min} \le y_m(k+i|k) \le y_{max}\ , i = 1, \dots, N_p;$$

$$u(k+i) = u(k+i-1); N_c \le\ i \le N_p;$$

$$x_m(k|k) = x_m(k);$$

$$x_m(k+i+1|k)\ = A_m x_m(k+i|k)\ + B_m u(k+i)\ , i \ge 0;$$

$$y_m(k+1|k) = C_m x_m(k+i|k)\ , i \ge 0;$$

where $Q \in \mathbb{S}_+^n$, $P \in \mathbb{S}_+^n$ and $R_L \in \mathbb{S}_+^n$ are weighting matrices and where

$||x_m||_P^2$ denotes the quadratic form ${x_m}^T P x_m$. $x_m(k+i|k)$ is the prediction of $x_m(k+i)$ at time step *k*. At further step *i*, define:

$$\Omega \triangleq \Sigma_{i=1}^{N_p}\left(\sum_{j=0}^{i-1} {A_m}^{i-j-1} B_m\right) \boldsymbol{Q} {A_m}^{i} \in \mathbb{R}^{N_p \times n}$$

$$\Phi \triangleq \Sigma_{i=1}^{N_p}\left(\sum_{j=0}^{i-1} {A_m}^{i-j-1} B_m\right) \boldsymbol{Q} \left(\sum_{j=0}^{i-1} {A_m}^{i-j-1} B_m\right)^T + \boldsymbol{R_L} \in \mathbb{R}^{N_p \times N_p},$$

where $\boldsymbol{Q} \triangleq diag(Q, Q \ldots . P) \in R^{N_p n \times N_p n}, \boldsymbol{R_L} = diag(R_L, R_L \ldots . R_L) \in R^{N_p \times N_p}$. If the constraints in the QP problem stated in Eq.4.11 are not taken into consideration, then the global optimal solution can be found as:

$$U(k) = -\Phi^{-1} \Omega x_m(k). \tag{4.12}$$

If the constraints are taken back into consideration, with the problem formulation presented above, the MPC problem becomes a constrained QP problem. Hence, Eq.4.11 can be rewritten with respect of *U(k)* as

$$J(x_m(k)) = \min_{u(k)} \left\{ \frac{1}{2} U^T(k) \Phi U(k) + U^T(k) \Omega x_m(k) \right\} \tag{4.13}$$

$$\text{Subject to} \quad GU(k) \leq \gamma.$$

where G, γ are functions of the bounds u_{min}, u_{max}, y_{min}, and y_{max}. Assuming the dual problem is strictly convex and regular. $U(k) \in \mathbb{U}^{N_c} \triangleq \{u: GU(k) \leq \gamma\}$. Then introducing the Lagrange factor λ can help to further format the problem into a Lagrangian dual problem.

$$J(x_m(k), U(k), \lambda) = \max_{\lambda} \min_{U_k} \left\{ \frac{1}{2} U(k)^T \Phi U(k) + U(k)^T \Omega x_m(k) + \lambda^T (GU(k) - \gamma) \right\} \tag{4.14}$$

$$\text{Subject to} \qquad \lambda \geq 0.$$

If the constraint sets are convex, then the typical *KKT* is the necessary and sufficient condition for optimality. If the constraint sets are non-convex, then a near optimal solution can be solved by various numerical methods, e.g. (Garcia, et al., 1989; Bemporad and Morari, 1999; Qin and Badgwell, 2003; Colson, et al., 2005).

4.3 Design of 1-Bit Processing based MPC

This section proposes a novel approach to design an embedded MPC controller for the satellite attitude control mission. Based on the 1-bit processing control system discussed in Chapter 3, the author developed a 1-bit processing based MPC system, namely OBMPC. Such OBMPC system embeds bi-level $\Delta\sum$ modulators in the control loop, transforming the control inputs and feedbacks into 1-bit format. The work can be briefly described as:

1) The control feedback is acquired in 1-bit format via the bi-level $\Delta\sum$ Modulation based sensors.

2) The 1-bit state feedback is processed in the OBMPC controller. The iterative process shall be based on the explicit relationship between the 1-bit state feedback and the 1-bit control input.

3) An optimal solution is determined and sent to the dynamic model to perform control action.

As the state vectors are encoded into 1-bit signals, by pre-calculating the coefficients, all the multiplication operations are performed only between 1-bit signal and multi-bit coefficients. Therefore, multiplication operations in the arithmetic block of the controller can be replaced by conditional-negates (CN) and bit shifters (i.e. appropriate standardization and sign changing), so that each iteration can be processed in a small time frame. The small circuit scale and high power efficiency of such implementation makes the OBMPC algorithm feasible for large scale real-time control applications. Moreover, the OBMPC system inherits the benefits of the 1-bit processing control system, which renders it beneficial for the proposed WCS application. Moreover, if the sensing devices can be embedded into $\Delta\sum$ Modulator control loops, e.g. MEMS gyroscopes (see (Kraft and Ding, 2009) for a recent survey), no D/A converter is necessary as 1-bit signals can be processed directly by the controller.

The main drawback, however, is that an OSR is necessarily required to achieve a high resolution. As discussed before, unlike the conventional A/D conversion based digital control systems, for the 1-bit processing control system, the OSR is applied to the entire control system rather than the A/D convertor itself, which may cause relatively high energy consumption for the controller. A low OSR, on the other hand, will cause high quantization noise power in the base band. Hence, a moderate OSR shall be considered between a reasonable OSR and the system performance.

Moreover, unlike the simple, direct implementation of a PID controller based 1-bit processing control system, the MPC algorithm needs to be modified to achieve an explicit relationship between the 1-bit state feedback and the multi-bit parameter during each of iteration process.

To address the above problems, the interest of this work is focused on how to implement the $\Delta\sum$ modulator in MPC (i.e. how to take advantage of the 1-bit signal to decrease the online computation), and the stability issues caused by the quantized signals given moderate OSR.

4.3.1 1-Bit processing based MPC

As discussed in Chapter 3, $\Delta\sum$ modulator based control system requires a high sampling frequency, which may result in long word lengths for both coefficients and variables within the controller. The δ transform based control system can be used to replace the common *z* transform to overcome such issue by performing a simple linear transform. It is proven that the design of the δ-operator based predictive control is very similar to the traditional ones based on the shift operator, but computationally advantageous at high sampling rates (see e.g. (Lauritsen and Rostgaard, 1997) and (Ebert, 2001)).

Delta operator methods introduced in (Middleton and Goodwin, 1986) require smaller word length when implemented in fixed-point digital control processors than shift operator models (Goodwin, et al. 1986). In δ transform, a δ operator is more like a

derivative by resembling the continuous operator d/dt with $\delta = (z-1)/T$ or $\delta = z-1$ (the mathematical model in the delta operator form has different coefficients only changes the coefficient magnitudes). Since δ and z are linear transformations, then Eq.4.9 can be rewritten as

$$x_m(k+1) = A_\delta x_m(k) + B_\delta u(k)$$

$$y_m(k) = C_\delta x_m(k) \tag{4.15}$$

where $A_\delta = \frac{A_m - I_m}{T}$, $B_\delta = \frac{B}{T}$, $C_\delta = C$. To get rid of the observer bias problem, the author adopts the augmented model here, as described in Eq. 4.16:

$$\begin{bmatrix} \Delta x_m(k+1) \\ y_m(k+1) \end{bmatrix} = \begin{bmatrix} A_\delta & 0_{q\times m}{}^T \\ C_\delta A_\delta & I_{q\times q} \end{bmatrix} \begin{bmatrix} \Delta x_m(k) \\ y_m(k) \end{bmatrix} + \begin{bmatrix} B_\delta \\ C_\delta B_\delta \end{bmatrix} \Delta u(k)$$

$$y(k) = [0_{q\times q} \quad I_{q\times q}] \begin{bmatrix} \Delta x_m(k) \\ y_m(k) \end{bmatrix}. \tag{4.16}$$

Comparing to the state space model stated in Eq. 4.6, the augmented model does not require steady-state information in the control system implementation. For many linearized control systems, the linearization will introduce non-zero constant terms to the control output unless the system is at equilibrium point. These constant terms will cause steady state error or observer bias if they are not modelled. However, when using the augmented model, the difference of the constants becomes zero.

A new state variable vector is chosen to be $x(k) = [\Delta x_m(k)^T,\ y_m(k)]^T$. For notational simplicity, denoting Eq.4.17 by

$$x(k+1) = Ax(k) + B\Delta u(k)$$

$$y(k) = Cx(k)\,, \tag{4.17}$$

where A, B and C are matrices corresponding to the forms given in Eq.4.15. Define $\Delta U = [\Delta u(k|k)\ \Delta u(k+1|k) \ldots \Delta u(k+N_c-1|k)]^T$, then Eq.4.11 can be reformulated as:

$$J(x(k),\Delta U(k)) = \underset{\Delta U(k)}{min}\left\{\left|\left|x(k+N_p|k)\right|\right|_P^2 + \sum_{i=0}^{N_p-1}\left(||x(k+i|k)||_Q^2 + ||\Delta u((k+i)||_{R_L}^2\right)\right\} \quad (4.18)$$

Subject to:

$$\Delta u_{min} \le \Delta u(k+i) \le \Delta u_{max}, i = 0, \dots, N_c - 1$$

$$y_{min} \le y(k+i|k) \le y_{max}\,, i = 1, \dots, N_p$$

$$\Delta u(k+i) = \Delta u(k+i-1); N_c \le\ i \le N_p$$

$$x(k|k) = x(k);$$

$$x(k+i+1|k)\ = Ax(k+i|k)\ + B\Delta u(k+i)\,, i \ge 0$$

$$y(k+1|k) = Cx(k+i|k)\,, i \ge 0$$

Define $r(k) = [r_1(k), r_2(k) \dots r_{N_p}(k)]$ as a sequence of set-point signals where$r_1(k) = r_2(\mathrm{k}) = \cdots = r_{N_p}(k)$, i.e. the set-point remains constant with in the prediction horizon. In this case, the augmented state variable Δx_m remains unchanged when the set-point is introduced into the system. Hence, the state variable $x(k)$ can be redefined as $x(k+i+1|k)\ = [\Delta x_m(k+i+1|k)^T,\ y_m(k+i+1|k) - r_i(k)]^T$, where the sequence of the set-point is treated as constant feedback errors. If no constraint is applied to the control system, then the QP remains the same and can be solved as Eq.4.19 by taking the first *p* elements of the state variable.

$$\Delta u^*(k) = K_y r(k) - K_{mpc} x(k); \quad (4.19)$$

where $K_y = \overbrace{[I_m\ o_m\ o_m\ o_m]}^{N_c}\,\Phi^{-1}\,\Psi$ and $K_{mpc} = \overbrace{[I_m\ o_m\ o_m\ o_m]}^{N_c}\,\Phi^{-1}\Omega$ and Ψ equals to the last *n* columns of Ω. I_m is a $p \times p$ identity matrix and o_m zero is a $p \times p$ zero matrix. In this case, the MPC problem is degraded into a simple proportional control. The 1-bit processing control system can be implemented directly as described in Fig.4.2.

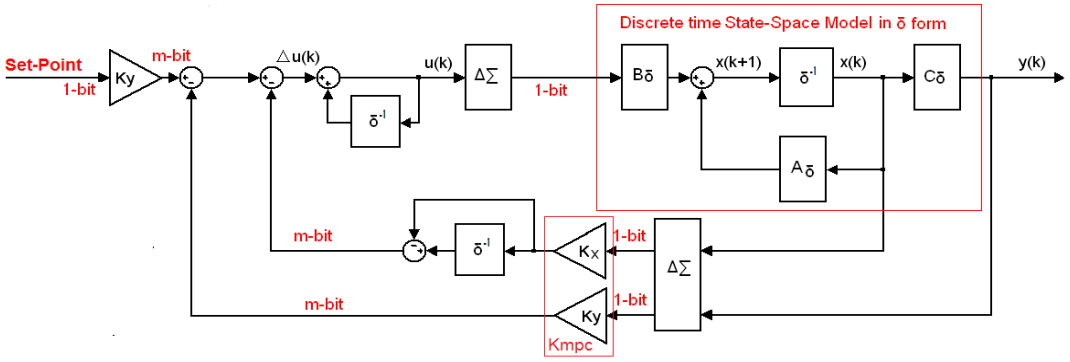

Figure 4.2 δ form based MPC control structure ΔΣ modulation.

Fig.4.2 illustrates a δ form based MPC control structure implemented with ΔΣ modulation, where δ^{-1} denotes a shift operation. In the control loop, the ΔΣ modulator is used to encode signal from a physical system into binary pulses. Then, these 1-bit data are used to solve the optimal actuation in real-time. Finally, another ΔΣ modulator encodes the control input into binary pulses to drive physical systems. As the ΔΣ modulators are included, the quantization noises shall be introduced to the control loop. For a ΔΣ modulator, define time-invariant filter *L(z)* as the loop filter, *S(z)* and *N(z)* for the *STF* and *NTF* respectively. The assumptions *A1* and *A2* in Chapter 3 will hold during the discussion below. $\tilde{x}(k)$ is the quantized state feedback. Then the control input can be determined as

$$\bar{U}^*(k) = K_y r(k) - K_{mpc}\tilde{x}(k). \tag{4.20}$$

For a bi-level ΔΣ modulator, the state feedbacks are restricted to the quantization levels, i.e. $\mathbb{X} = \{\Delta, -\Delta\}$. The filtered conversion distortion (i.e. quantization noise) can be defined as $e(k) \triangleq N(z)^{-1}(S(z)x(k) - \tilde{x}(k))$. The author leaves the analysis of the quantization error effect to the next section and assume it is small enough so that $\mathrm{E}\{\tilde{x}(k)\} = \mathrm{E}\{x(k)\}$. Therefore

$$E\{\bar{U}^*(k)\} = \mathrm{E}\{U^*(k)\}. \tag{4.21}$$

It can be seen from Eq.4.20 that if the quantization levels are standardized into ± 1, all multiplications in this structure are between a 1-bit signal and a multi-bit controller coefficient. This operation, in fact, just changes the sign of the multi-bit coefficient, which removes the multiplier from the controller. It is worth noting that encoding the

control input is not necessary to maintain the benefit of the 1-bit processing control system, but only to modulate the signal for driving the plant.

When constraints are applied, a QP solver is required to compute the optimization process. Again considering the QP problem described in Eq.4.11, a closed-form solution can be found in Theorem 4.1.

Theorem 4.1 (Closed Form Solution): Consider a combination of a finite number of active constraints is applied to the control objective and all the active constraints are linearly independent, then $u(k) = \mathcal{G}\big(\tilde{x}(k)\big)$ is a uniquely defined affine function over $\mathbb{X}^n$.

Proof: Recall Ω and ϕ defined in Section 4.22, the KKT condition can be used here for optimality, which can be solved as a Lagrangian dual problem by introducing the Lagrange factor λ, (see e.g. (Manum and Skogestad, 2010)), the cost function can be rewritten with respect of ΔU and λ as

$$J(x(k)) = \max_{\lambda} \min_{\Delta u(k)} \left\{ \frac{1}{2} \Delta U^T(k) \Phi \Delta U(k) + \Delta U^T(k) \Omega \tilde{x}(k) + \lambda^{\mathrm{T}} (\mathrm{G} \Delta U(k) - \gamma) \right\} \tag{4.22}$$

$$\text{Subject to } \mathrm{G}\Delta U(k) \leq \gamma$$

$$\lambda \geq 0$$

where G, γ are functions of the bounds u_{min}, u_{max}, y_{min}, and y_{max}, and assume the dual problem is strictly convex and regular. $\Delta U(k) \in \mathbb{U}^{N_c} \triangleq \{u: G\Delta U(k) \leq \gamma\}$. Applying the active set method, the $U(k)$ can be solved with respect to the state variable $x(k)$ and Lagrange factor $\in \mathbb{R}^n$, one can have:

$$\Delta U(k) = -\Phi^{-1} \Omega \tilde{x}(k) \; - \Phi^{-1} G^T \lambda. \tag{4.23}$$

When there is no constraint applied to the model, (e.g. $\lambda = 0$), applying the receding horizon principle, a well-known global optimal solution can be denoted as:

$$U^*(k) \; = -\overbrace{[I_m \; o_m \; o_m \; o_m]}^{N_c} \phi^{-1} \; \Omega \tilde{x}(k) \tag{4.24}$$

If there exists a finite number of active constraints and all the active constraints are linearly independent, λ can be expressed as λ_{act}:

$$\lambda_{act} = -(G\Phi^{-1}G^T)^{-1}(\gamma + G\Phi^{-1}\Omega\tilde{x}(k)). \quad (4.25)$$

For notational simplicity, one can rewrite λ_{act} as

$$\lambda_{act} = S + W\tilde{x}(k) \quad (4.26)$$

where S and W are corresponding matrices which can be pre-calculated before implementation. We can substitute λ_{act} from Eq.4.26 into Eq.4.23 to obtain:

$$u(k) = \overbrace{[I_m\ o_m\ o_m\ o_m]}^{N_c}\ U(k)$$

$$\text{where} \quad U(k) = (\Phi^{-1}G^TW - \Phi^{-1}\Omega)\tilde{x}(k) \ - \Phi^{-1}G^TS. \quad (4.27)$$

Let $\rho = (\Phi^{-1}G^TW - \Phi^{-1}\Omega)$ and $\sigma = \Phi^{-1}G^TS$, then

$$u(k) \ = \ \mathbb{G}\big(\tilde{x}(k)\big) = \overbrace{[I_m\ o_m\ o_m\ o_m]}^{N_c}(\rho\tilde{x}(k) - \sigma) \quad \square(4.28)$$

Lemma 4.1: If there is a limited number of constraint sets, then the control input is restricted to a finite set, e.g. $\mathbb{U} = \{s_1, s_2, \dots s_{2^{n_u+1}}\}$, where n_u is the number of active constraint sets.

Proof:

Since $\mathrm{G}\big(\tilde{x}(k)\big)$ is a uniquely defined affine function over $\mathbb{X}^n$. Then the real-time optimization for the dual problem can be mapped with respect of two state constraints. If no constraint exists, then

$$u^*(k) \ = \begin{cases} -\overbrace{[I_m\ o_m\ o_m\ o_m]}^{N_c}\phi^{-1}\,\Omega\Delta\,; & if\ Hx(k) \geq 0 \\ \overbrace{[I_m\ o_m\ o_m\ o_m]}^{N_c}\phi^{-1}\,\Omega\Delta\,. & if\ Hx(k) < 0 \end{cases} \quad (4.29)$$

If there are more than one set of constraints, then the sizes of matrices ρ and σ are dependent on the size of matrix G. Each combination of these constraint sets will result in a different set of ρ and σ, and therefore include two more control input components in $\mathbb{X}$. □

Remark 4.1: Such a result mirrors the work of finite constraint set receding horizon quadratic control method (Quevedo, et al., 2004) and the EMPC (Bemporad, et al., 2002) method. Similar to the EMPC, the proposed OBMPC is also taking the advantage of the affine relationship between the state vector and the control input. However, instead of solving the optimal solution offline, the 1-bit signals are processed online directly with the "multiplication" free structure as proposed in Chapter 3. In comparison to the EMPC approach, the 1-bit processing based online optimization overcomes the limitation that the offline computation results are hard to trace for large scaled control systems with long control horizons (Pannocchia and Rawlings et al., 2007) while it maintains the parametric nature of the EMPC.

Remark 4.2: For implementation, according to Theorem 4.1, if the parameters ρ and σ can be pre-calculated, then all the necessary multiplications for the control are only between ρ and $\pm\Delta$, which can be pre-calculated and stored in the memory. Alternatively, we can standardize $\pm\Delta$ into ± 1 by simply applying bit shifts to parameters ρ and σ. Then all the necessary multiplications processed by controller in real time are simply changes the sign of the parameters, which removes all the multipliers from the controllers. Such method mirrors our previous work for 1-bit processing control systems, e.g. (Wu and Goodall, 2005a).

4.3.2 OBMPC with modified Lagrange factor

So far, we have assumed that all the constraints are linearly independent, i.e. the rows of G are linearly independent. However, more than one set of active constraints may apply, where the Lagrange factor may not be uniquely defined by the non-convexities. In this work, we choose the Hildreth's QP procedure to deal with this situation, which has been adopted in (Wang, 2009) as an iteration method for the MPC algorithm.

Theorem 4.2: Consider a combination of a finite number of active constraints is applied to the control objective but not all the active constraints are linearly independent. If the *a priori* active constraint set can be identified, then *a near optimal solution* $u(k)$ within a finite number of iteration is still a uniquely defined affine

function over $\mathbb{X}^n$.

Proof:

If more than one set of active constraints apply, then the Lagrange factor λ may not be uniquely defined as non-convexities will be introduced into the dual problem. In this work, we choose the Hildreth's QP procedure to deal with this situation, which has been adopted in (Wang, 2009) to solve a MPC problem with model reduction. Before the proof, it is convenient to define $\bar{\lambda} \triangleq \Phi^{-1}G^T\lambda$. Then

$$U(k) = -\Omega^{-1}\Phi\,\tilde{x}(k) - \bar{\lambda}\,. \tag{4.30}$$

where $\bar{\lambda} \in \mathbb{R}^p$ and $\bar{\lambda}_i = \bar{S}_i + \bar{W}_{(i,:)}\tilde{x}(k)$, $\bar{S}$ and $\bar{W}$ are the corresponding matrices solved during the iteration process.

Hildreth's QP algorithm is based on an element-by-element search and it does not require any matrix inversion. Therefore, the program will continue without interruption even the rows of G are not linearly independent (e.g. more than one constraints is active). And the λ will always exist as a near-optimal solution in a finite iteration loop. The iteration expression of Hildreth's QP Procedure is given in following equation:

$$\bar{\lambda}_i^{m+1} = max(0, \omega_i^{m+1}) \tag{4.31}$$

where

$$\omega_i^{m+1} = -\frac{1}{h_{ii}}[k_i + \sum\nolimits_{j=1}^{i-1} h_{ij}\bar{\lambda}_j^{m+1} + \sum\nolimits_{j=i+1}^{n} h_{ij}\bar{\lambda}_j^{m}]$$

and m means the m^{th} iteration, the scalar h_{ii} is the ii^{th} element in the matrix $H = G\Phi^{-1}G^T$ and k_i is the i^{th} element in the vector $K = \gamma + G\Phi^{-1}\Omega\tilde{x}(k)$. $\bar{\lambda}(k)$ is calculated according to the previous one, $\bar{\lambda}(k-1)$, which can either be 0 or an affine function of the quantized measurement $\tilde{x}(k-1)$. Given a finite number of iteration, $\bar{\lambda}$ can be solved as a near optimal solution even if two or more constraints are active at the same time. Therefore, even if $\bar{\lambda}(k)$ cannot be solved explicitly, a set

of near optimal control input $U(k)$ can still be found as an affine function over the state feedback $\tilde{x}(k)$. □

Remark 4.3: For implementation, in the optimal solution presented in Eq. 4.30, the component $\bar{\lambda}$ and $-\Omega^{-1}\Phi\,\tilde{x}(k)$ can be implemented separately. More specifically, the global optimal solution $U(k) = -\Omega^{-1}\Phi\,\tilde{x}(k)$ can be calculated at each iteration process while the Hildreth's QP Procedure will be used to decide when it is necessary to calculate $\bar{\lambda}$. Both components can be implemented under the framework of a 1-bit processing control system. The optimal solution can be determined by adding the two components together.

Remark 4.4: The iteration can be performed by storing the previous measurement $\tilde{x}(k-1)$ into a register. Similar to Remark 4.2, the implementation can be achieved in a multiplier free controller due to the affine relationship between the quantized state feedbacks and parameters. Also, the method discussed in Theorem 4.2 allows the designer to trade-off the online computation effort with the accuracy of the optimal solution. Typically, a small number of iteration loops is designed for the proposed satellite attitude control mission.

For the specific iteration method proposed above, at each sampling time, the optimization will be performed according to the 1-bit state feedback. Theoretically speaking, the OBMPC method is an implementation method rather than a control algorithm. Therefore, most of the methods to decrease the online computational effort discussed in Chapter 2 can be combined to improve the OBMPC directly or with minor modifications. For example, the model reduction methods can be combined with the OBMPC to decrease the order of the model and therefore decrease the computational effort, while the active set method mentioned above needs to be modified to satisfy the explicit relationship between the multi-bit coefficients and the 1-bit state feedback.

4.4 Stability Analysis

The stability analysis for the OBMPC includes a few aspects. From the

implementation point of view, the easiest way to design a stable OBMPC system is to design a stable MPC controller, and include a stable $\Delta\sum$ modulator into the control loop. An efficient OSR is then chosen to ensure that the quantization noise can be well shaped so that high resolution can be achieved. In essence, the design problem is treated as a MPC controller design with an efficient digital A/D converter. However, for a 1-bit processing control system, the OSR is normally limited due to the scarcity of onboard resources and coefficient bit length. In this case, the quantization noise could become significant enough to affect the robustness of the MPC controller. To quantify the effect caused by the quantization noise, the problem can be studied under the framework of MPC with quantized state feedback.

Another problem for the quantized MPC is that the quantizer input can overload the quantizer. In such circumstances, the quantization error is large and the $\Delta\sum$ modulator will soon lose track of the input signal. Stabilization techniques such as resetting the integrators in the $\Delta\sum$ modulator or adding clippers can help to restore the functionality of the modulator but will sacrifice the SNR of the control system. Therefore, the quantization level need to be carefully designed to ensure the overload does not happen frequently.

4.4.1 Stability for the MPC

Before we study the stability of the OBMPC, it is necessary to include some fundamental assumptions and conclusions for the MPC algorithm itself. Mayne (2000) provided an abundant review about the stability methodologies of the MPC, which is regarded as the foundation of the stability research for many works. It specified three useful "ingredients" to stabilize a MPC problem including a terminal cost *F()*, a terminal constraint set X_f, and a local control law κ_f. Under the context of (Mayne, 2000), the stability can be obtained by ensuring

$$J_N^0(f(x(k),\kappa_N(k)),\kappa_N(k)) - J_{N-1}^0\big(x(k),\kappa_N(k)\big) + l(x,\kappa_N(x)) \le 0. \qquad (4.32)$$

Toward these "ingredients", four assumptions are developed as sufficient conditions

to ensure closed-loop asymptotic stability.

A.4.1: $X_f \subset \mathbb{X}$, X_f closed, $0 \in X_f$;

A.4.2: $\kappa_f(x) \in \mathbb{U}$, $\forall x \in X_f$;

A.4.3: $f\left(x, \kappa_f(x)\right) \in X_f, \forall x \in X_f$;

A.4.4: $F\big(f(x(k), \kappa_N(k))\big) - F\big(x(k)\big) + l\left(x, \kappa_f(x)\right) \leq 0.$

In this thesis, the assumption A.4.1 and A.4.2 are assumed to be true. Consider a constrained linear control system. If the system is stable, or in other words, is (strictly) Hurwitz, then the MPC problem can be proven to be stable if the weighting matrices P and Q defined by Eq.4.3 are adopted by solving the Lyapunov equation $APA+Q=P$ (Rawlings and Muske, 1993). A simple proof is collected in Theorem 4.3.

Theorem 4.3: If assumption A.4.1 and A.4.2 hold, and the system is (strictly) Hurwitz, and $Q \in \mathbb{S}_+^n$, $P \in \mathbb{S}_+^n$ are satisfying the Lyapunov equation $A^T PA+Q=P$ and $R_L \in \mathbb{S}_+^n$. Then closed-loop system for Eq.4.18 with the quantized state feedback is asymptotically stable.

Proof:

According to Eq.4.11, and Eq.4.27, an optimal solution at time step *k* can be found as $\Delta U(k)^* = [\Delta u^T(k)^* \ \Delta u^T(k+1)^* \ldots \Delta u^T(k+N_c-1)^*]$ and its cost function is $J\big(x(k)\big)$. Define a new control sequence $\bar{U}(k+1)^*$ which shifts the elements in $U(k)^*$and replaces the last element by zero and name the cost function as $\bar{J}\big(x(k+1)\big)$. Due to optimality, $J\big(x(k+1)\big) \leq \bar{J}\big(x(k+1)\big)$. Hence:

$$J\big(x(k+1)\big) - J\big(x(k)\big) \leq \bar{J}\big(x(k+1)\big) - J\big(x(k)\big)$$

$$= \Big(Ax\big(k+N_p|k\big)\Big)^T P\Big(Ax\big(k+N_p|k\big)\Big) - x\big(k+N_p|k\big)^T Px\big(k+N_p|k\big)$$

$$+x\big(k+N_p|k\big)^T Qx\big(k+N_p|k\big) - x(k)^T Qx(k) - \Delta U(k)^T R_L \Delta U(k)$$

$$= x\left(k+N_p|k\right)^T (APA+Q-P)x\left(k+N_p|k\right) - x(k)^T Qx(k) - \Delta U(k)^T R_L \Delta U(k). \quad (4.33)$$

As $APA+Q-P=0$, then $J\left(x(k+1)\right)-J\left(x(k)\right)\leq 0$. It is worth to emphasize that give $\mathrm{E}\{\tilde{x}(k)\}=\mathrm{E}\{x(k)\}$, if one replace the state feedback $x(k)$ with the quantized state feedback $\tilde{x}(k)$, the asymptotically stability of the Eq.4.18 still valid according to Eq. 4.33, which completes the proof. □

If the system is unstable, then A.4.3 and A.4.4 are required to establish the asymptotic stability of the closed-loop system. Various theories were developed during the 1990s, e.g. (Mayne and Michalska, 1990).

4.4.2 Stability for the ΔΣ modulator and the OBMPC

4.4.2.1 Quantization level design and stability criteria for the ΔΣ modulator

The stability issues for the ΔΣ modulation based control system are difficult to analyze, especially for high order ΔΣ modulators due to the non-linear nature of the quantizer and the integrators existed in the ΔΣ modulator. The noises introduced by the ΔΣ modulator are dependent on the OSR and the amplitude of the input signals to the modulators. Instability occurs in a higher-order ΔΣ modulator when the amplitude of the input signal approaches the full-scale of the quantization level. When this happens, the limit cycle (high amplitude low frequency oscillations) is excited and the quantizer is overloaded. Because of the integrators in the ΔΣ modulators, the error in the modulation loop will only become larger and soon reach extreme values. In this case, the input to the quantizer increases rapidly even if the input signal is withdrawn (Norsworthy, et al., 1996), which locks the modulator in the unstable limit cycle. The limit cycle is hard to eliminate once it is excited as the modulator loses track of the input signal quickly. It is possible to stabilize the modulator using the stabilization techniques such as resetting the integrators (Norsworthy, et al., 1996) and clipping the integrators (Dunn and Sandler, 1994). However, most of these stabilization techniques sacrifice the SNR in order to remove the limit cycles, i.e. increase the noise floor. The

stabilization techniques will be further discussed in the next chapter.

From a designer's point of view, when designing higher-order ΔΣ modulators, it is better to ensure the modulator input is always bounded. Or alternatively, one can choose the quantization level under "safe" criteria, and test the system with different control input sequences in the simulation to ensure the modulators themselves will always remain stable. A variable gain method was proposed in (Baird and Fiez, 1994) to find the appropriate maximum quantization level. Given a n^{th} order bi-level quantizer with quantization level $[+\Delta, -\Delta]$ and defining the quantizer input as u, the variable gain method substitutes the quantizer with a variable gain K where

$$K = \frac{\Delta}{u}. \tag{4.34}$$

For discrete systems, a stable ΔΣ modulator can be achieved by keeping the poles of the transfer function within the unit circle. For example, given a second order ΔΣ modulator as showed in Fig.4.3, a quantizer is substituted by a variable K.

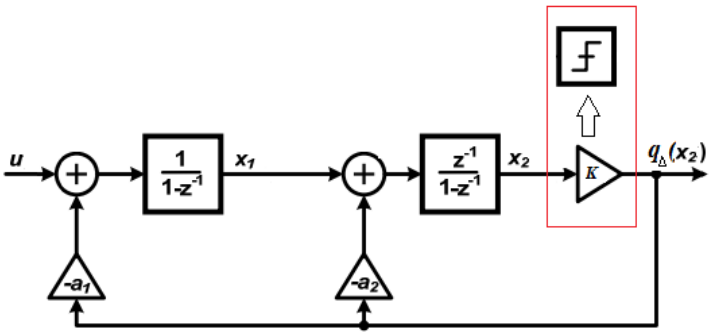

Figure 4.3 ΔΣ modulator with variable gain

Based on this, the transfer function can be derived as:

$$H(z) = \frac{K}{z^2+(a_2K-2)z+(a_1-a_2)K+1}. \tag{4.35}$$

By using this transfer function, one can plot the root loci for $K \in (0, +\infty]$ and find the K range within the limit circuit. Find the minimum K_{min} and the substitute it into Eq.4.35, then the quantization level can be found as:

$$\Delta = K_{min} x_{max}. \tag{4.36}$$

Note that the x_{max} in Eq.4.33 can also be considered as a guideline to design the clipping technique, which will be further discussed in the next chapter.

For high order ΔΣ modulators, however, the quantizer input is not explicitly known. To provide a guideline of designing a stable ΔΣ modulator, three stability criteria for the ΔΣ modulator design taken from (Norsworthy, et al., 1996) are discussed and summarized here:

(1) The sum of the absolute value of the terms in the impulse response of the NTF is bounded. Mathematically:

$$S_{|h|} \equiv \sum_{i=0}^{\infty} |h_i| = 3 - u_{\max}, \tag{4.37}$$

where u_{max} is the maximum signal amplitude for which the modulator remains stable and h_i is the impulse response of the NTF.

(2) The mean-squared value of the magnitude response of the NTF $\bar{A}_N$ (noise amplification factor) must be smaller than c ≅2.5. Mathematically:

$$\bar{A}_N \equiv \frac{1}{2\pi}\sum_{-\pi}^{\pi} |NTF(e^{j\theta})|^2 d\theta < c, \tag{4.38}$$

(3) The maximum value of the frequency response of the *NTF* must be smaller than $d \cong 2$. Mathematically:

$$M \equiv \max\{|NTF(z)|\} < d\,. \tag{4.39}$$

In theory, the NTF should be designed under the above criteria, which have been derived from extensive simulations. Unfortunately, so far the estimation of the maximum input to the quantizer is only accurate for the first order ΔΣ modulator. For other types, the above criteria can be very strict and the maximum quantizer input is normally underestimated (Bourdopoulos, et al., 2003). In the simulation presented in this thesis, the maximum input into ΔΣ modulator is set to be 75% of the quantization level (e.g. $||x(k)|| \leq 0.75\Delta$) to satisfy both stability and SNR performance.

4.4.2.2 Linearization analysis for the OBMPC and positively invariant set

For the stability analysis in this subsection, with carefully designed quantization

levels and extensive simulations, we mainly consider that the modulator $\Delta\sum$ is stable for all modulator inputs, and focus on the effect of the filtered quantization error to the robustness of the control loop. The most commonly adopted method is to linearize the $\Delta\sum$ modulated signal as a signal-plus-white-noise structure as we discussed in the previous chapter. For the OBMPC, if no constraint is applied to the input and the assumptions *A1* and *A2* hold, the globe optimal solution of Eq.4.18 can be found according to Eq. 4.24 as $\Delta u^*(k) = [1,0,0 \dots 0]K_{MPC}\tilde{x}(k)$. Recall the quantized state variable $\tilde{x}(k) = L(z)\,x(k) + e(k)$, hence

$$x(k+1) = Ax(k) + B[1,0,0 \dots 0]K_{MPC}\tilde{x}(k)$$

$$= (A - B[1,0,0 \dots 0]K_{MPC}L(z))x(k) + B[1,0,0 \dots 0]K_{MPC}e(k). \quad (4.40)$$

Let $\alpha = [1,0,0 \dots 0]K_{MPC}L(z)$, given a relatively long N_P and proper choices of P and Q, α can be designed to ensure $(A - B\alpha L(z))$ is stable. If the assumptions *A1* and *A2* hold, then the closed-loop system is a stable system which is driven by additive white noise $e(k)$. Then standard signal plus additive white noise analysis is sufficient for the OBMPC.

In fact, in most applications, $\Delta\sum$ modulators can be treated as A/D converters, which have little effect to the control system under noise shaping techniques and the OSR design. If the quantization noise is not deterministic, the stability analysis of the OBMPC fall to the framework of quantized MPC. The asymptotic stability of the MPC with an eventually quantized state feedback can be achieved if the following assumptions are satisfied.

A.4.5: A relatively large prediction horizon N_p (comparing to the system rising time) is chosen;

A.4.6: State matrix A in Eq.4.9 is Hurwitz.

Based on the assumptions above, the asymptotic stability of the MPC with quantized state feedback can be guaranteed by Theorem 4.3, which has been addressed in many literatures, e.g. (Quevedo, et al., 2004).

If *A* is not Hurwitz, the fixed points and control sequence may not be admissible. Also, the asymptotic stability may be relaxed into "practical" asymptotic stability, (such "practical" asymptotic stability is in the same context of (Picasso, 2003, Zampieri, 2003) and (Mayne, 2000)). The stability of an OBMPC can be proven if a set in state-space can be found with the property that all subsequent states lie in the original set (Schreier, 1997) or are trapped in this set for a sufficiently long time. For the case of N_c =1, it is simple to obtain a positively invariant set for the OBMPC system.

Theorem 4.4: For N_c *=1*, given the quantized feedback $\tilde{x} \in \mathbb{X}$, where $\mathbb{X}$ $=\{\Delta, -\Delta\}$. $h=\sum_{i=0}^{\infty} ||(A - B\alpha)B||$ and suppose that $(A - B\alpha)$ is Hurwitz. ||.|| stands for the Euclidean norm on $\mathbb{R}^n$. For every i *=0,1,2….,* the quantization error e satisfies $|e(k-i)| \leq L$, where L$\geq \Delta$. Then $h \leq 1 + \Delta/L$ is a sufficient condition for the set $\mathcal{D}$

$$\mathcal{D} = \{x \epsilon R: ||x|| \leq Lh\} \tag{4.41}$$

to be a positively invariant set for the system presented in Eq.4.17.

Proof:

At time step *k,*

$$|\mathrm{e}(\mathrm{k}+1)| = ||\, q_{\Delta}(x(k+1)) - x(k+1)|| = \min_{\Delta \in \mathbb{X}} |\, \Delta - x(k+1)|; \tag{4.42}$$

Since $x(k+1) = \sum_{\mathrm{i}=0}^{\infty}(A - B\alpha)^{i}\mathrm{B}e(k-i)$, inequality Eq.4.43 can be derived by using the triangular inequality:

$$||x(k+1)|| = \sum_{\mathrm{i}=0}^{\infty} \left|\left|(A - B\alpha)^{i}\mathrm{B}e(k-i)\right|\right|$$

$$\leq max_{i=0,1\ldots.}\{e(k-i)\}\sum_{\mathrm{i}=0}^{\infty} \left|\left|(A - B\alpha)^{i}B\right|\right| \leq Lh; \tag{4.43}$$

Substitute $h \leq 1 + \Delta/L$ into Eq. 4.43:

$$||x(k+1)|| \leq L + \Delta. \tag{4.44}$$

According to Eq.4.42, the quantization error *e(k+1)* satisfies the bound

$$|e(k+1)|=\min_{\Delta\in\mathbb{X}}|\Delta - x(k+1)| \le L. \quad (4.45)$$

Also, for any further time step $j \ge 1$, due to Eq.4.43, one can obtain $||x(k+j)|| \le Lh$, which completes the proof. □

Such an invariance set method for the quantized MPC problem mirrors the method proposed in (Quevedo, et al., 2004), in which only the control inputs are quantized. A systemic analysis of quantized state feedback stabilization can be found in (Fagnani, 2003) and (Delchamps, 1990). Unfortunately, for N_c >1, $||x(k+1)|| \le L + \Delta$ can only vaguely suggest that $e(k+1)$ is bounded. Reference (Schreier, 1997) also addressed another method to find positively invariant set, which provide a more general case with the constraint set applied to more than one component (e.g. N_c>1) in the control horizon. For many MIMO systems, N_c =1 is considered for practical reasons as the online computational burden will increase rapidly for larger N_c. The stability issue for this particular case has also been studied in (Müller, et al., 2011).

4.5 Numerical Example

Consider a practical 1-bit control system using a DC motor to control the angular position of a rotating load. The objective is to control the position of the rotating load with flexibility in the drive shaft. A simplified second order DC motor transfer function (Dorf, 1995) is used as shown in Fig.4.4:

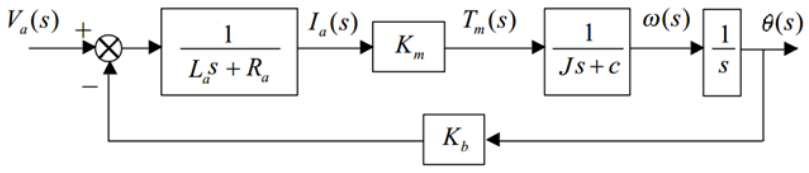

Figure 4.4 Block diagram of the closed-loop control system using the DC motor as the actuator.

In the Fig.4.4, L_a and R_a are the resistances and inductances of the armature sides of the motor. K_m is considered as the motor constant, which is the transfer function from the input armature current to the motor torque. K_b is the counter electromotive force constant to convert the feedback position θ the into voltage (assuming the feedback voltage is proportional to the position θ, i.e. $V_b(s)=K_b\theta(s)$). J is the Rotor moment of

inertia and c is the friction which is assumed to be zero in the simulation. Disturbance torque is considered to be negligible in the structure. Then the motor transfer function is shown as Eq. 4.46

$$G(s) = \frac{K_m}{s(L_aJs^2+R_aJs+K_mK_b)}. \tag{4.46}$$

Suppose we attempt to control the speed by driving the motor with a constant voltage. Given the motor parameters: R_a=5Ω, L_a=0.106, K_m=58, J=40kg.m^2, K_b=12.5, then the transfer function becomes:

$$G(s) = \frac{13.68}{s^3+47.17s^2+171s}. \tag{4.47}$$

Thus, the overall control scheme can be illustrated as Fig.4.5. The controller bandwidth f_0 is about 2Hz. For a second order ΔΣ modulator based OBMPC, to get satisfying SNR, the OSR for the OBMPC is set to 1000, i.e.4000Hz, which can achieve a SNR above 60dB according to Fig.3.6 presented in Chapter 3. The OBMPC controller is represented by the modified canonic δ-form.

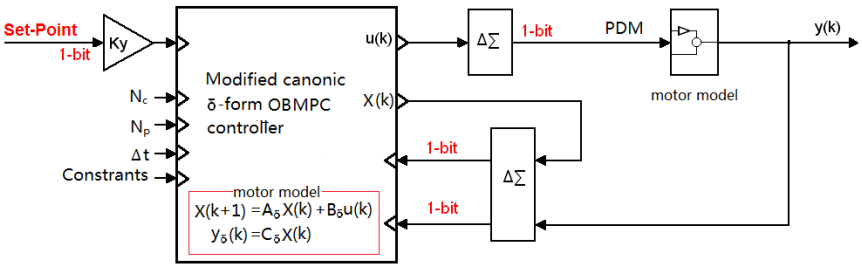

Figure 4.5 OBMPC implemention for the DC Motor control system.

The full 1-bit control system also contains a 1-bit A/D converter in the loop. In the simulation, The input voltage (control variable constraint) is 24V. To numerically standardize the voltage which is required for satisfying the quantizer, the input voltage signal is divided by 2^5 before it is sent into the $\Delta\sum$ modulator so that the signal is standardized (i.e. within 75% of quantization level) to fit within the quantization level, (i.e. ± 1). The quantized signal is amplified by 2^5 after the modulator to restore the original signal level. Such standardization can be easily operated in the controller by a simple bit shift. Similar scales are also applied to the feedback signal before and after

the $\Delta\sum$ modulator. R_w is set to be 0.01, N_p=50 and N_c=10. The operational sampling frequency for the benchmark controller, i.e. a conventional MPC controller, is set to 400Hz. The simulation structure is shown in Fig.4.5. The procedure of the control system processing can be described as follows. Firstly, the analogue signals (command and actual motor position) are sampled by a bi-level $\Delta\Sigma$ modulator, and hence produces a bit stream. Then the signals are fed into the digital controller and the state variables are updated so that they are ready for the next sample. The control input signal is modulated into the1-bit format, which can be directly used to drive the motor, i.e. pulse-density-modulation. The simulation results are shown in Fig.4.6 and Fig.4.7.

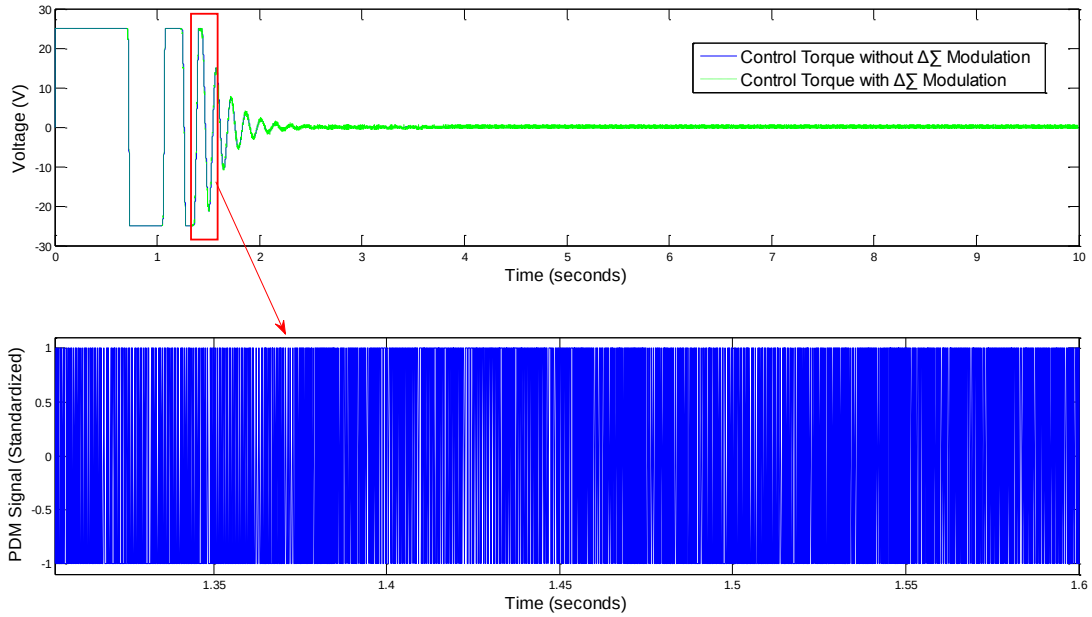

Figure 4.6 Control torque and $\Delta\sum$ modulated 1 bit signal

Fig.4.6 shows the control torques of the conventional MPC and the OBMPC (decimated). It can be seen that the decimated OBMPC control torque tracks the conventional MPC well although appears to be noisy. Such high frequency low level noise is not sensitive to the dynamic model. This will be shown in Fig.4.7. The modulated 1-bit signals are standardized into ± 1 as control signals. The signal density shown in Fig 4.6 is higher at 1 when the control torque reaches peak and higher at -1 when the control torque hits the bottom.

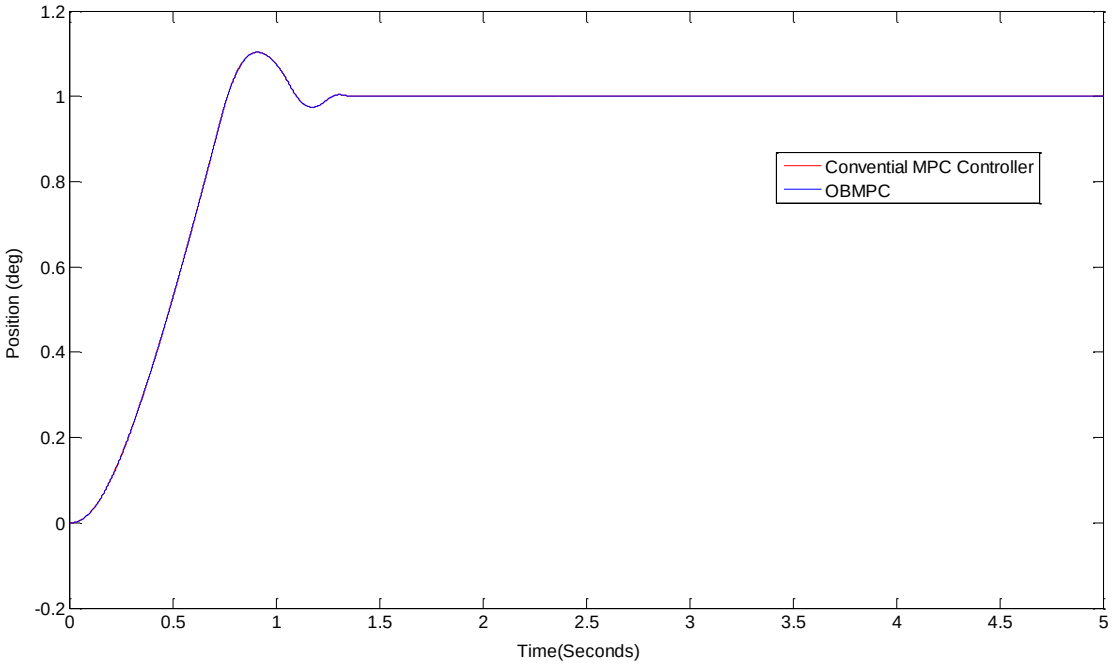
Convential MPC Controller
OBMPC
Position (deg)
Time(Seconds)
1.2
1
0.8
0.6
0.4
0.2
0
-0.2
0
0.5
1
1.5
2
2.5
3
3.5
4
4.5
5

(a)

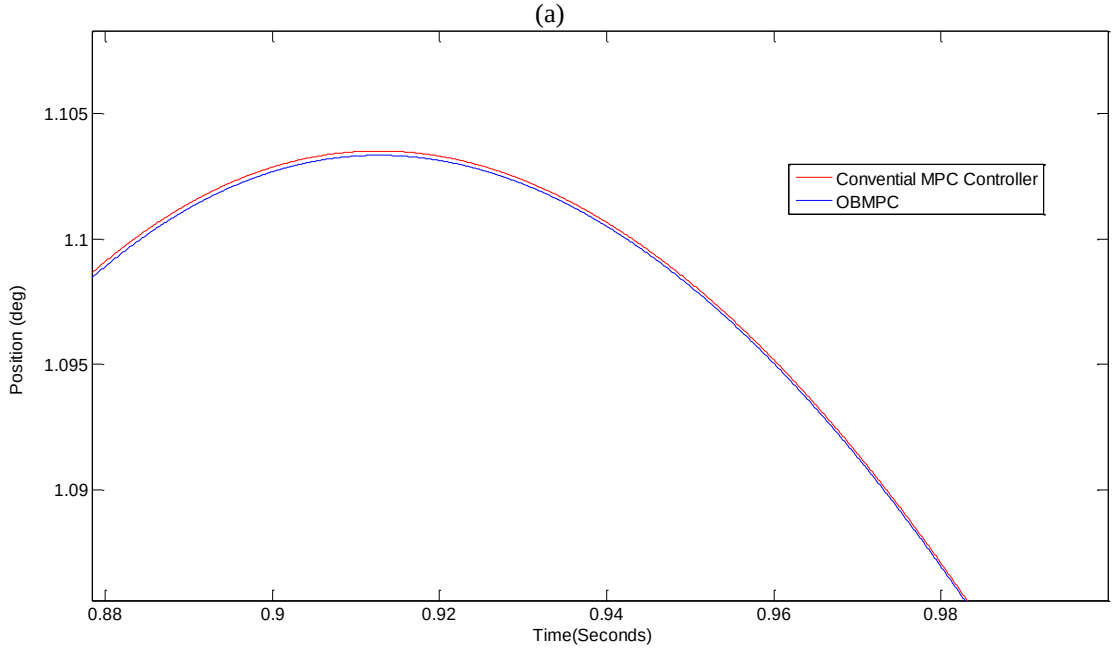
Convential MPC Controller
OBMPC
Position (deg)
Time(Seconds)
1.105
1.1
1.095
1.09
0.88
0.9
0.92
0.94
0.96
0.98

(b)

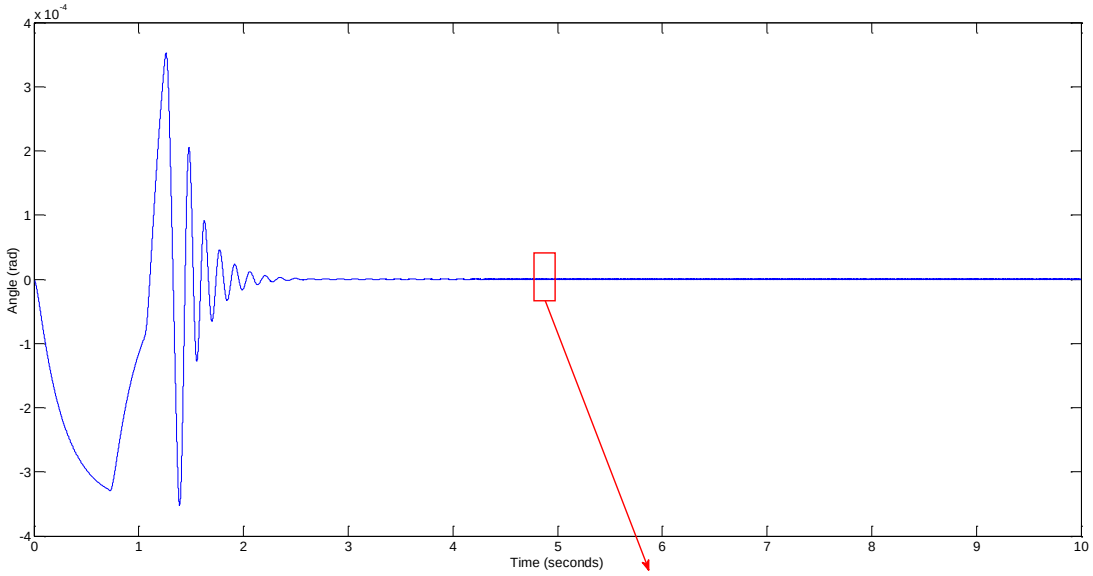

(c)

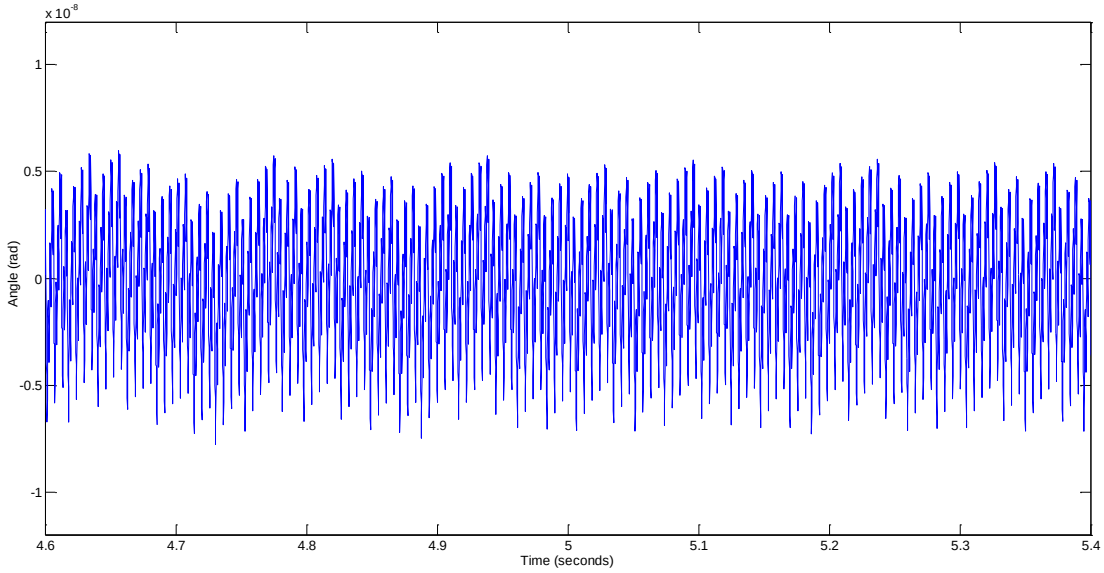

(d)

Figure 4.6 Simulation results for the 1-bit processing control system: (a) Position response and output control signal of the OBMPC control system and normal MPC control system; (b) Comparison between the simulation results (Close examination) (c) Response difference between the OBMPC and normal MPC. (d) The quantization noise

As shown in Fig.4.7, due to the high OSR, the control trajectory tracks the conventional MPC controller well. The maximum difference between the responses of OBMPC and MPC is less than 0.0003 *rad*. The peak error is mainly due to the different sampling frequency. The effect of the quantization can be seen when the control trajectory is settle. The difference is around $0.5 \times 10^{-8} rad$ when settled, which is mainly due to the quantization noise. These results show the feasibility of the OBMPC system. The quantization noise is retained in a relatively low level and can

be treated as adhesive noise with zero mean.

4.6 Summary

In this Chapter, an OBMPC structure is proposed. The design is inspired by the 1-bit processing technology, and takes advantage of the affine relationship between the 1-bit state feedback and parameters to implement a multiplier free MPC system. The proposed OBMPC encodes the sensing and control signals into a binary format, and processes such binary signals directly to obtain online optimal solutions. Because of the properties of the 1-bit data, the online optimization can be implemented with a multiplier free structure. As multipliers are the major power consumer for hardware implementation, such OBMPC structure can be very efficient in term of power and circuit complexity. The system is in digital control nature, affected by quantization noise introduced by $\Delta\sum$ Modulators.

The main issue for the OBMPC system, however, is that a higher sampling frequency needs to be employed for the entire control system rather than just the modulator. This means that a trade-off between system performance and the OSR is required. Also, the power consumption under the OSR needs to be verified to prove the efficiency and feasibility of the proposed controller.

The other important aspect for the OBMPC system is the system stability issues. The system stability relies on a stable MPC controller design and a stable $\Delta\sum$ modulator design. A general stability analysis for the OBMPC is very difficult to achieve although designing one is not. A well designed stable $\Delta\sum$ modulator has very few effects on the control system as the filtered quantization noise is small, so that the system stability can be achieve by designing a stable $\Delta\sum$ modulator and the stable MPC respectively. Otherwise, the quantization noise can be analyzed by the signal plus white noise structure. The OBMPC problem then falls into the framework of the quantized MPC.

Moreover, the OBMPC also has advantages toward the WCS as the 1-bit signals are “stand ready” to transmit, and the noises and data loss are less sensitive due to the

modulation techniques. The OBMPC for the WCS and the 1-bit state estimator design will be discussed in Chapter 6.

5. DESIGN OF 1-BIT MEMS GYROSCOPE SENSOR FOR 1-BIT PROCESSING CONTROL SYSTEMS

==========

==========

To achieve a simple and direct implementation of the 1-bit processing structure, it is necessary to acquire all the sensing data in 1-bit format. Hence, the 1-bit sensing components are required to complete the OBMPC control system for the proposed fractionated satellite mission. Specifically, all the sensing data need to be encoded by the ΔΣ modulator in order to generate the PDM signals. As an efficient A/D conversion method, the ΔΣ modulator can be embedded into almost all types of sensing components, i.e. gyroscopes, accelerometers etc. In fact, along with development of the MEMS, the ΔΣ modulator based gyroscopes and accelerometers are rather popular in many applications. For instance, it is feasible to choose MEMS gyroscopes as the sensing devices for small satellite missions, e.g. (De Rooij, et al., 2009). In this work, the author provides a design of a 1-bit MEMS gyroscope and discusses the potential issues of implementing the ΔΣ modulator based sensing components for the OBMPC system. To further minimize the quantization noise, an implementation of a novel OBMPC based 1-bit MEMS sensor shall also be developed.

5.1 ΔΣ Modulator based MEMS Gyroscope

The high-performance micro-machined MEMS gyroscope is appealing to many researchers as they are advantageous in terms of power, cost and flexibility over the bulky and expensive macroscopic gyroscopes. Incorporating the ΔΣ modulator to the

gyroscope sensing element is one of the most promising approaches to implement the MEMS gyroscope due to the circuit simplicity and the benefits of incorporating the sensing component in a feedback control loop (Kraft and Ding, 2009). The $\Delta\sum$ modulation embedded MEMS gyroscope was first introduced in (Jiang, et al., 2000), and ever since became a popular research topic in literature (Petkov and Boser, 2006; Dong, et al., 2007; Raman, et al., 2009; Antonello and Oboe, 2012).

A typical approach to design a $\Delta\sum$ modulator based MEMS gyroscope is to treat the MEMS gyroscope as a $\Delta\sum$ modulation based control loop. For most MEMS gyroscopes, the angular motion is determined by measuring the vibration of the proof mass, which is excited due to the Coriolis force. The sense mode (The mass is set up to oscillate along the axis at the resonant frequency for that axis, which is synonymously referred to as the drive mode. The axis that orthogonal to the drive mode and is called the sense mode, where Coriolis accelerations are sensed along the that axis (Wu, 2009)) of the MEMS gyroscope can then be regarded as a spring damper dynamic system responding to the Coriolis force, and hence can be modeled by two integrators in series. Fig.5.1 shows a system level diagram of a mechanical sensor.

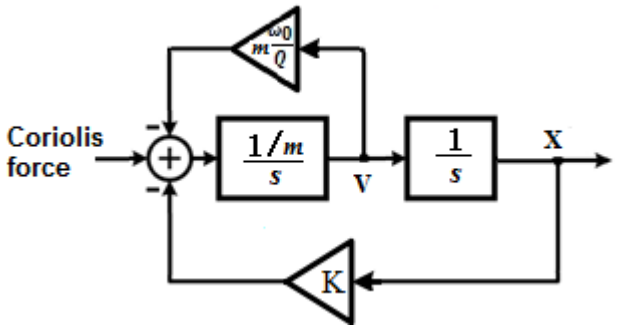

Figure 5.1 System level diagram of the dynamic system of a mechanical sensor.

where K is the spring stiffness. $\frac{\omega_0}{2\pi}$ is resonant frequency of the dynamic system and $\omega_0 = \sqrt{\frac{K}{m}}$ (Dong, et al., 2007). For the sensing mode of the gyroscope, the control loop design problem can also be treated as the $\Delta\sum$ modulator based accelerometer under Coriolis force, e.g.(Smith, et al., 1994). The continuous-time transfer function of the mechanical sensor can be denoted as:

$$H_m(\mathrm{s}) = \frac{1/m}{s^2+\frac{\omega_0}{Q}s+{\omega_0}^2}, \tag{5.1}$$

where m is the mass of the sensing element, ω_0 is the resonant frequency and Q is the quality factor. High quality factors are generally required to achieve high sensitivity of the sensor (200-250 for the sense mode and 35000-45000 for the drive mode (Dong, et al., 2008)). Due to the phase shift introduced by the mechanical sensing element, a simple lead compensator needs to be included to stabilize the control loop. Other sensor fusion technologies are also available, e.g. (Einicke, 2012), but are outside of the scope of this work. The output of the compensator can be regarded as the input of the ΔΣ modulator, which serves as an interface to digitalize the sensor signal. The resultant bi-level bit stream can be translated into an electrostatic force as the feedback to the control loop of the sensor.

To further analyze the stability and performance of the ΔΣ modulator based MEMS gyroscope, one can treat the sensing component and the compensator as two second order loop filters, and then analyze the entire control loop as a high order ΔΣ modulator. The structure of the ΔΣ modulator based MEMS gyroscope is shown in Fig.5.2.

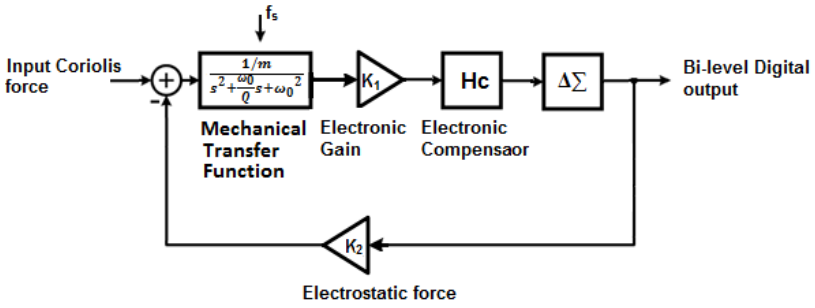

Figure 5.2 Structure of a typical ΔΣ modulator based MEMS gyroscope

Like any other A/D conversion method, the ΔΣ Modulation introduces quantization noise into the MEMS control loop. Such quantization noise, coupled with the mechanical noise and the electrical noise, may cause large gyroscope bias or instability of the control loop. Filtering techniques are therefore required to decrease the in band noise. Other filtering techniques can be embedded in the control loop before the A/D conversion as the ΔΣ modulator operates under high sampling rate

(OSR) and can be constrained in a narrow frequency band. Also, the bandwidth requirements of the electronic components needed for implementation in the integrated circuit are relatively demanding as a high OSR is eventually required to achieve a good SNR.

Similar to all $\Delta\sum$ modulators, one way to minimize the quantization noise is to increase the order of the $\Delta\sum$ modulator in the control loop at a cost of circuit complexity. A well designed high order $\Delta\sum$ modulator based MEMS gyroscope can filter most of the noise from the $\Delta\sum$ modulator loop. For instance, the results obtained in (Petkov and Boser, 2005) proved that one can achieve a SNR of 93dB with a relatively low OSR of 500, including realistic values for electronic noise introduced.

As an A/D converter, the output of the $\Delta\sum$ modulator is stand-ready for transmission. For the proposed OBMPC system as discussed in the previous chapters, it is essential to acquire the sensing data through the bi-level $\Delta\sum$ modulation. Each quantized measurement is regarded only as an entity containing partial information about the state feedback *x(k)* and can be processed independently. In other words, no decimation is required (Wu and Goodall, 2005a). The 1-bit feature enables the possibility of implementing fast QP solvers, thus achieving an OBMPC system operating under a small time interval. Moreover, according to proposition 2.2 in (Delchamps, 1990; Datta, et al., 2000), each single quantity of the oversampled measurements contains as much useful sensing information as the entire measurement history. Therefore, even if the sensor accuracies are severely limited, causing the measurements to become very rough, a long record of such measurements can result in a better estimation than the otherwise single multi-bit measurement. Since the oversampled 1-bit data is processed individually by the controller rather than by using decimation, each sampling instant can be considered as an effective measurement. In other words, at the cost of an oversampled control loop, the quantized state measurements can provide better state trajectory than slow sampled measurements.

The analysis provided in Chapter 3 for $\Delta\sum$ modulator based control system can also be used here to analyze the $\mathbf{\Delta}\sum$ modulator based MEMS gyroscope. The MEMS

gyroscope itself can be treated as a second order transfer function. Due to the non-linear nature of the quantizer, the extra integrators in the gyroscope transfer function may cause stability issues in the control loop. Moreover, the compensator will also introduce extra poles in the control loop and consequently affect the noise-shaping performance of the system (Raman, et al., 2009). Additional integrators, serving as usual noise shaping solutions, will be adopted in the feedback loop to attenuate the magnitude of the impulse response of the NTF at low frequencies (see e.g.(Miller and Petrie, 2003) for different ΔΣ modulator based MEMS gyroscope structures). This methodology is analogous to a PID (Proportional-Integral-Derivative) control system, in which the performance of the designed system depends on the experience of the designer (Datta, et al., 2000). The implementation structure can be referred to the ΔΣ modulator structures as discussed before. For example, Michael Kraft and his research team replaced the integrators with resonators, e.g. (Dong, et al., 2007; Dong, et al., 2008), to form a band-pass ΔΣ modulator, which mirrors the CIDIFF structure with resonators as discussed in Chapter 3. A third order ΔΣ modulator based MEMS gyroscope with CIDIFF structure with resonator is shown in Fig.5.3

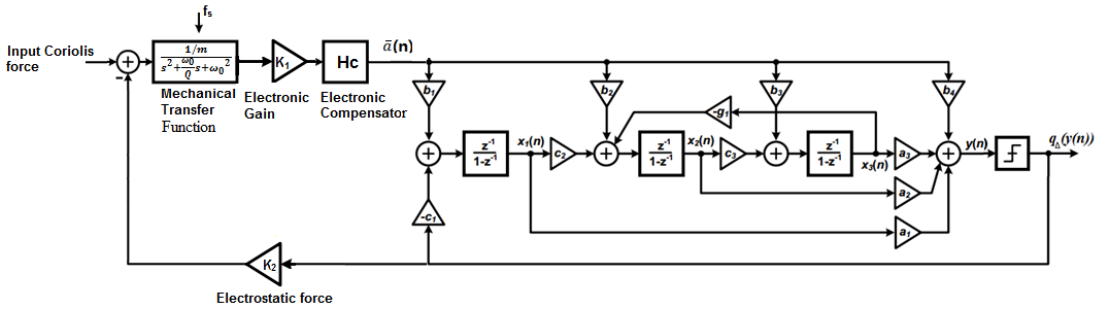

Figure 5.3 A third order ΔΣ modulator based MEMS gyroscope using CIDIFF structure with resonator

More ΔΣ modulator based MEMS gyroscope implementations can be found in a review paper (Kraft and Ding, 2009).

In such MEMS gyroscope applications, two main concerns need to be addressed other than directly combining the MEMS gyroscope with the ΔΣ modulator structure.

Firstly, as a sensing component, the input of the gyroscope is less predictable than the typical AC/DC input (i.e. audio applications). Even though one can calculate a reasonable dynamic range of the sensing component, external disturbances could still cause unexpected input amplitude which will overload the $\Delta\sum$ modulator. Therefore, it is necessary to choose an optimal scale factor for the modulator input so that it does not frequently violate the constraints in the modulator while maintaining a good SNR. Secondly, the integration of the $\Delta\sum$ modulator based MEMS gyroscope will necessarily introduce internal electrical noise. As mentioned before, such electrical noise could couple with the quantization noise, causing instantaneous high noise amplitude at a certain integrator output. Hence, stabilization techniques are necessarily required for the $\Delta\sum$ modulator based MEMS gyroscope.

5.2 Stabilization Techniques

In Chapter 3, designing a stable $\Delta\sum$ modulator control loop has been discussed. Here, we assume a stable $\Delta\sum$ modulator is engaged and a lead compensator is used to deal with the phase shift introduced by the $\Delta\sum$ modulator. As discussed before, the stability of the $\Delta\sum$ modulator relies on the amplitude of the modulator input signal. This is especially true for higher order $\Delta\sum$ Modulators as the quantization error will be accumulated by the integrators in the main loop, which can quickly steer the modulator output diverging from the input signal. For most control missions, the constraints on control inputs are known by studying the actuator of the dynamic system. The sensing range can then be predicted in the preliminary design stage and subsequently, the quantization level can be designed according to the sensing range to ensure the $\Delta\sum$ modulator is stable subject to all inputs. However, there are two integrations in the gyroscope and the speed of the proof mass is not directly available in most cases. Additional integrators are also necessary to achieve a good SNR for the $\Delta\sum$ modulators (i.e. high order $\Delta\sum$ modulators). Moreover, the electrical noise may interact with the quantization noise in the closed-loop system, especially with many integrators in the control loop. Therefore, even if the control loop is designed to be stable, there is still a chance that the modulator input will temporarily overload the

quantizer. When this occurs, the ΔΣ modulator output will enter the status of the "limited cycle" (low frequency binary signals), and will remain unstable even the modulator input restored within the quantization range (Bourdopoulos, et al., 2003). To increase the robustness of the sensing system, stabilization techniques need to be introduced to enhance the stability of the ΔΣ Modulator. It is worth noting that stabilization techniques will sacrifice the SNR of the ΔΣ modulator as the stabilization actions will change the behavior of the modulator. Therefore these techniques are using temporary loss of SNR to restrain the possibility of overloading due to the input signal or one of the integrators, and only active in the worst case scenarios (i.e. when instability is detected).

In this section, we only discuss the input scaling method and the clipping techniques. A systematic comparison of the stabilization techniques for the ΔΣ Modulator can be found in (Bourdopoulos, et al., 2003).

5.2.1 Scaling the input signal

As discussed in the previous chapters, a well-designed quantization level with respect to the input signal is crucial to the stability of the ΔΣ Modulator. For higher order ΔΣ Modulators, a more general approach is to scale the coefficients in the modulators so that overloading rarely happens. The direct scaling method (or equivalent scaling method in some references) is used to linearly scale both the feedback signal and the modulator input by $1/K_s$. In other words, all the local coefficients are scaled by the same scale factor K_s at each integrator node, i.e. $c_1, c_2 \ldots c_n$ in the CIDF, CIDIDF or CIDIFF structures in Fig.5.3. Such a method does not change the functionality of the ΔΣ Modulator, so that the stability of the ΔΣ Modulator can be preserved e.g. (Yazkurt, et al., 2006).

Such a direct scaling method is easy to design and can efficiently decrease the input signal level. However, it is limited due to the fact that the scaling factors before each integrator can be very big or very small as each integrator input in higher order ΔΣ Modulators varies within a large dynamic range. Such a limitation makes the direct

scaling method hard to implement in some cases. Alternatively, one can scale the input signal and all the feedback and forward signals by designing appropriate gains, i.e. a_1, $a_2 \ldots a_n$ and $b_1, b_2 \ldots b_n$ in the CIDF, CIDIDF or CIDIFF structures in Fig.5.3, under the pre-condition that the system stability will be preserved, e.g. (Zorn, et al., 2013). Such a modification can be referred as the functional scaling method, which does not necessarily maintain the characteristics of the system, but provides trade-off between the SNR performance and stability (Hein and Zakhor, 1993). The functional scaling method is easier to implement than the direct scaling method. However, finding the optimal scaling gains is normally a case by case study rather than a general analysis due to different topologies of $\Delta\sum$ Modulators, especially for higher order ones.

An alternative way to avoid the overloading is the adaptive approach based techniques e.g. (Yu, et al., 1992; Zierhofer, 2000; Prosalentis and Tombras, 2007; Gore and Chakrabartty, 2010). Such a method scales the quantization level based on a rough estimate of the instantaneous amplitude of the input signal (predicted input signal) so that quantizer overload rarely happens. Meanwhile, a correction bit is generated and included in the output signal so that the output signal with adaptive quantization level can be demodulated properly. However, such a method will remove the 1-bit characteristic of the bi-level $\Delta\sum$ Modulator and therefore is not suitable for the proposed OBMPC system.

5.2.2 Clipping in a $\Delta\sum$ Modulator

Among the various stabilization techniques, clipping the integrators to a certain level (Dunn and Sandler, 1994; Norsworth, et al., 1996) has been proven to be an efficient method to avoid overloading for higher order single-bit $\Delta\sum$ Modulators. Typically, the saturating clipper is implemented by clipping the supply voltage of the operational amplifiers that are used to build integrators, so that its unstable regions may not be entered (Adams, 1984). The benefit of this method is that the modulator can be designed to adapt the overloaded signal so that the system will retain the

characteristics of the input signal and relatively high SNR comparing to the setting-to-zero method. A second order ∆∑ modulator structure (CIDF) with clippers at each integrator output is presented in Fig.5.4.

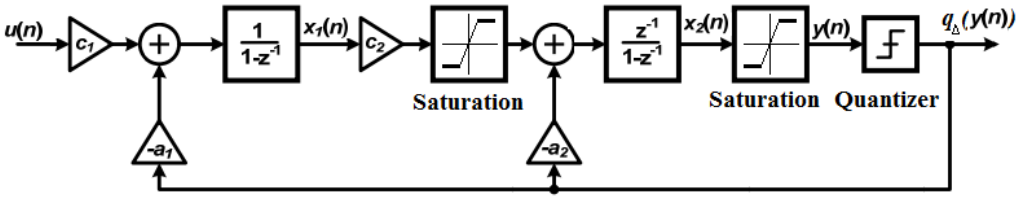

Figure 5.4 A second order ∆∑ modulator with clippers at each integrator output

Specifically speaking, as presented in (Hein and Zakhor, 1991), for a second order ∆∑ Modulator, for the CIDF structure presented in Fig.3.8(a) with unit feedback gain, the state bound can be presented as

$$|x_1|_{max} = |u_{in}| + 2;$$

$$|x_2|_{max} = \frac{(5-|u_{in}|)^2}{8(1-|u_{in}|)}. \tag{5.2}$$

where u_{in} is the modulator input, x_1 and x_2 are respectively the states for the first and second integrators. The result is further generalized in (Hein and Zakhor, 1993) with different feedback gains. (Wang, 1993) provided state bounds analysis for the third order ∆∑ Modulators. Although the main results discussed above are designed for the DC inputs, they are fairly tight from the design point of view and can be considered as a sufficient condition for most designs (Bourdopoulos, et al., 2003). To further simplify the problem, as suggested in (Dunn and Sandler, 1994) and (Bourdopoulos, et al., 2003), the clipping threshold can only be set to the last integrator. The variable gain method used in Section 4.5 can also be used as the design guide of the hard constraints of the last integrator in the control loop. In practical cases, one can find out a "safe" threshold by studying the impulse response of a stable modulator.

Designing and implementing a clipper is one of the easiest ways to stabilize a ∆∑ modulator. The main challenge, however, lies in how to choose a reasonable chipping

level while retaining the high SNR when the input does not overload the quantizer. In practical missions, if the non-ideal integrators and noises are taken into consideration, rigorous clipper level (typically much higher than the input signal for higher order ΔΣ Modulators, e.g. 90 times of the input signal for a third order ΔΣ Modulator) may result in low SNR at the noisy instants, even when the stability of the control loop can be guaranteed. Moreover, as a non-linear approach, the clipping technique will bring additional non-linearity to the ΔΣ Modulator, which is also a non-linear system itself, so that the stability analysis is even harder to perform.

5.3 OBMPC structure for the ΔΣ Modulator based MEMS Gyroscope

As discussed above, despite that the stabilization techniques can help to stabilize the system, it is not easy to design a ΔΣ modulator based MEMS gyroscope with guaranteed stability while maintaining a reasonable SNR. Toward this aspect, in this section, the author adopts the OBMPC structure as proposed in the previous chapter to implement the MEMS gyroscope.

5.3.1 Problem formulation

The control objective is to find the optimal integrator output to minimize the filtered quantization error. We first consider a digital signal (e.g. a sampled continuous-time signal) a(k) as the output of the MEMS gyroscope system and the input to a high order ΔΣ modulator. Consider an nth order ΔΣ modulator CIDIFF structure as shown in Fig.5.5.

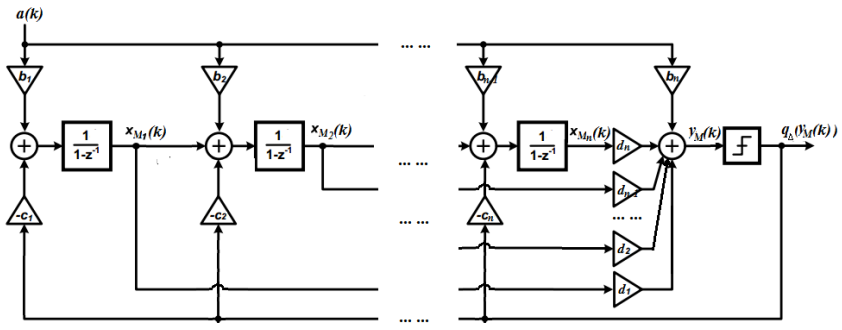

Figure 5.5 CIDIFF structure of an n^{th} order bi-level ΔΣ modulator

To discuss the problem under the context of the OBMPC, we suggest the state space approach to analyze the characteristic of the $\Delta\sum$ modulators. The state equations of the proposed structure can be written as

$$\vec{x}_M(k+1) = \vec{A}_M\vec{x}_M(k) + \vec{B}_M\vec{a}_M(k) - \vec{C}_M\vec{l}_M(k), \tag{5.3}$$

$$\vec{y}_M(k) = D_M\begin{bmatrix} x_{M_1} \\ x_{M_2} \\ \vdots \\ x_{M_n} \end{bmatrix},$$

where $x_M\ (k) \in \mathbb{R}^n$ is the state vector, $\vec{A}_M = \begin{bmatrix} 1 & 0 & 0 & \dots & 0 \\ 1 & 1 & 0 & \dots & 0 \\ 0 & 1 & 1 & \dots & 0 \\ \vdots & \ddots & \ddots & \ddots & \vdots \\ 0 & \cdots & 0 & 1 & 1 \end{bmatrix}$, $\vec{B}_M = \begin{bmatrix} b_1 \\ b_2 \\ b_3 \\ \vdots \\ b_n \end{bmatrix}$,

$\vec{C}_M = \begin{bmatrix} c_1 \\ c_2 \\ c_3 \\ \vdots \\ c_n \end{bmatrix}, D_M = [d_1, d_2, \dots d_n], \vec{x}_M \in \mathbb{R}, \vec{y}_M(k) \in \mathbb{R},\ k \in \mathbb{N}.\ l_M(k) \triangleq q_\Delta\big(y_M(k)\big)$ is the quantizer output. $a(k) \in \mathbb{R}$ is the modulator input. The asymptotical stability of such $\Delta\sum$ modulator can be designed by moving all the eigenvalues of A_M inside the unit circle. The modulator is oversampled so that $a(k)$ can be considered as constant within n time steps where $n \ll OSR$, i.e. $a(k) = a(k+1) \dots = a(k+n)$. $x_1(k)$, $x_2(k) \dots x_n(k)$ are the state variables for the n^{th} integrator. l_M is weighted by a bi-level quantizer, where $l_M \in \{\Delta, -\Delta\}$. The quantization level Δ is standardized as 1 and $\vec{l}_M$(k) is scaled by $c_1, c_2, \dots c_n$ according to the quantization level. In this particular case, the state matrix $\vec{A}_M$ can be transformed into the Jordan canonical form by replacing $\vec{x}_M$ with ${P_T}^{-1}x_M$, e.g. (Steiner and Yang, 1997), where $P_T = \begin{pmatrix} \vdots & \vdots & \vdots & \vdots \\ \rho_1 & \rho_2 & \cdots & \rho_n \\ \vdots & \vdots & \vdots & \vdots \end{pmatrix}$ and ρ_1, $\rho_2 \dots \rho_n$ are the eigenvectors of $\vec{A}_M$. Eq.5.3 then becomes:

$$x_M(k+1) = A_M x_M(k) + B_M a_M(k) - C_M l_M(k), \tag{5.4}$$

$$y_M(k) = D_M x_M(k),$$

where $A_M = {P_T}^{-1}\vec{A}_M P_T, B_M = {P_T}^{-1}\vec{B}_M, B_M = \vec{C}_M.\ x_M \in \mathbb{R}, y_M(k) \in \mathbb{R}.$

Remark 5.1: In terms of implementation, the structure proposed in Eq.5.4 is less popular than the ones discussed in Chapter 3 as the vectors B_M and C_M, i.e. the gains used to implement the $\Delta\sum$ modulator, may vary within a large range if some of the eigenvalue values in A_M is very close to zero. This will cause issues in terms of implementation as certain accuracy is hard to achieve using analog components if the gain is very small. In this work, as we prepare to use the OBMPC controller in the modulation, as discussed in Chapter 4, a δ form can be introduced to ameliorate this problem. For applications that are not suitable to include a digital controller, such structure can still be used for analysis purposes. This point will be further discussed in Remark 5.3.

The main benefit for the proposed structure is that the state variables are now decoupled. To further simplify the problem, define $D_M \triangleq [1,1,\cdots,1]$. The structure of the $\Delta\sum$ modulator with parallel state variables can then be reconstructed as shown in Fig.5.6

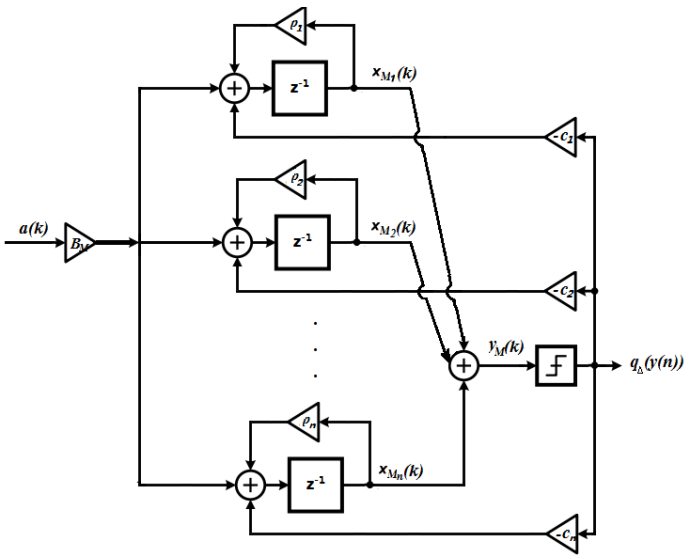

Figure. 5.6 N^{th} order $\Delta\sum$ modulator with parallel state variables (Thick lines denote vector routing)

In Fig.5.6, ρ_1, $\rho_2 \ldots \rho_n$ are the eigenvalues of A_M. It is worth noting that the inclusion of linear feedback paths other than the resonators results in a diagonal canonical form of A_M. It is possible to extend such parallel structures to many $\Delta\sum$ modulator structures if the state matrix A_M is similar to a diagonal matrix. In the following subsection, we shall assume that a simple diagonal state matrix is used. An OBMPC controller can then be applied to such $\Delta\sum$ modulator with the ability to handle the constraints (i.e. the clipping thresholds) on all the state variables. Also, the order reduction is discussed in (Steiner and Yang, 1997) for some particular $\Delta\sum$ modulators, which may help to decrease the online computation effort (if required) of the proposed method.

In some other cases, however, the use of resonators will result in a non-diagonal A_M. These cases are studied in (Steiner and Yang, 1997) and can be analyzed on a system-by-system basis. Generally, not all the state variables can be decoupled for the $\Delta\sum$ modulator structure with resonators. They can, however, be written as a parallel state structure with a certain level of decoupling. In other words, it is still possible to decouple some of the state variables in most non-diagonal structures. For example, consider a third order $\Delta\sum$ modulator with a resonator on the second and the third integrator. Hence only the first integrator can be decoupled, which can be restructured in parallel with the other two integrators. In such a structure, the first and the third state variable can be explicitly known. However, this will only require the study of the impulse response of a first order NTF and a second order NTF respectively, which is easier than studying the third order one directly in terms of determining reasonable a clipper level. The worst case is that none of the state variables can be decoupled. Hence only the last state variable can be directly constrained. It is still possible to stabilize the modulator as suggested in (Dunn and Sandler, 1994). However, the clipping action will result in a relatively low SNR in comparison to the individually clipped $\Delta\sum$ modulator. In the following section, we assume that the state matrix of the $\Delta\sum$ modulator in the proposed mission is designed to be diagonal. If otherwise, a case-by-case study needs to be performed for the proposed method.

5.3.2 OBMPC based MEMS gyroscope using 1-bit processing

5.3.2.1 Unconstrained OBMPC implementation with linearization assumption

As discussed above, if the state variables can be decoupled, so that the constraints applied on the state variable are linearly independent, the OBMPC can be implemented with relatively small circuit scale under the framework of 1-bit processing control system, i.e. a KKT condition is sufficient to address the problem. Based on the same linearization assumptions made in Chapter 3, Fig 5.6 can also be presented as seen in Fig.5.7.

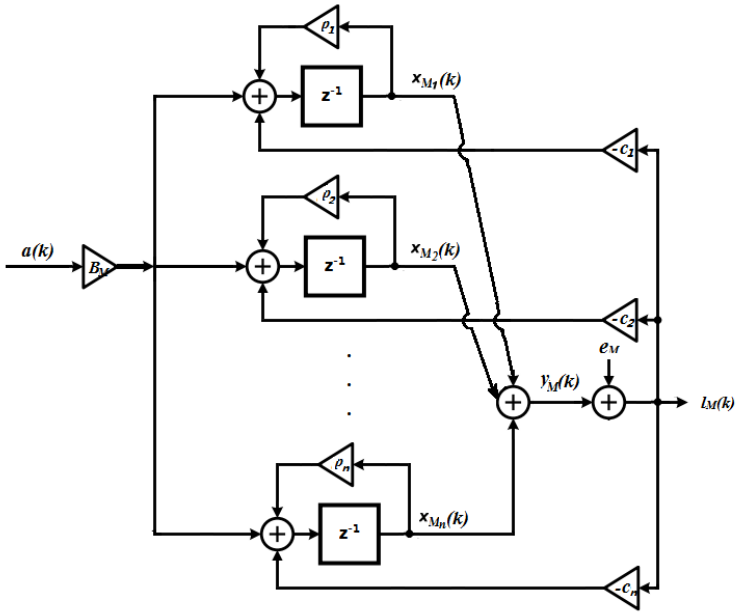

Figure. 5.7 Linearized n^{th} order $\Delta\sum$ modulator with parallel state (Thick lines denote vector routing).

In Fig.5.7, $e_M(k)$ is the filtered quantization noise. According to Fig.5.7

$$l_M(k) = y_M(k) + e_M(k). \tag{5.5}$$

Define $N(z)$ and $S(z)$ as discrete linear time invariant filter representing respectively the NTF and the STF. *S(z)* can be presented in a state space form as

$$x_M(k+1) = A_P x_M(k) + B_S a_M(k) \tag{5.6}$$

$$y_M(k) = C_S x_M(k),$$

where $A_P = A_M - C_M D_M$, $B_S = B_M$, $C_S = D_M$. Similarly, let $a_M(k) = 0$, the $N(z)$ of the proposed $\Delta\sum$ modulator structure in the state space equation form can be derived as:

$$x_M(k+1) = A_P x_M(k) + B_N e_M(k) \tag{5.7}$$

$$l_M(k) = C_N x_M(k) + e_M(k),$$

where $B_N = C_M$, $C_N = D_M$. Additionally, define $E(k)$ is unfiltered quantization noise, where

$$E(k) = (l_M(k) - S(z)a_M(k)). \tag{5.8}$$

Therefore,

$$e_M(k) = N(z)^{-1}(l_M(k) - S(z)a_M(k)). \tag{5.9}$$

The state space function for $N(z)^{-1}$ can be presented as

$$x_f(k+1) = A_F x_f(k) + B_F E(k) \tag{5.10}$$

$$e_M(k) = C_F x_f(k) + E(k),$$

where $A_F = A_M$, $B_F = C_M$, $C_F = -D_M$, and $x_f \in \mathbb{R}$ is the state variable of $N(z)^{-1}$. The goal here is to implement a control structure to minimize the filtered quantization noise $e_M(k)$. A conceptual view of an OBMPC based $\Delta\sum$ modulator is shown in Fig.5.8:

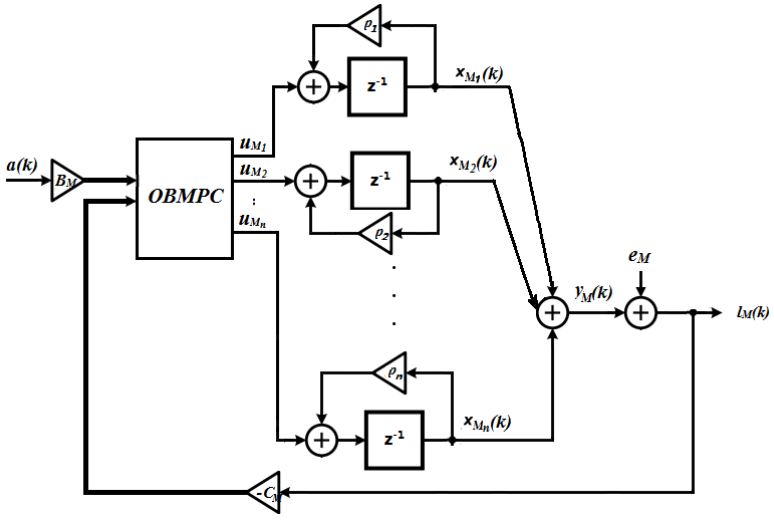

Figure 5.8 The OBMPC design for an n^{th} order $\Delta\sum$ modulator (Thick lines denote vector routing).

In Fig.5.8, $u_M = [u_{M_1}, u_{M_2} \ldots u_{M_n}]^T$ is the control input to minimize the filtered quantization noise in Eq.5.11. Similar to the statement made in the previous section, it is possible to directly process the 1-bit $\Delta\sum$ modulator output. The 1-bit processing control system structure results in simple circuits and short operation time so that it is practical to include the OBMPC in the oversampled modulation loop. Based on this perspective, the OBMPC is used in the modulation loop. The benefits of doing this are two-fold: Firstly, hard constraints can be easily included under the framework of the OBMPC structure. Therefore, the stability criteria can be easily acquired. Secondly, future predictions can be included in the control structure. Theoretically speaking, if the prediction horizon is long enough, then the quantization noise should tend towards zero.

Based on Fig.5.6 and the results discussed in the previous section, a structure of $\Delta\sum$ modulator based MEMS gyroscope using the OBMPC can be designed as shown in Fig.5.9.

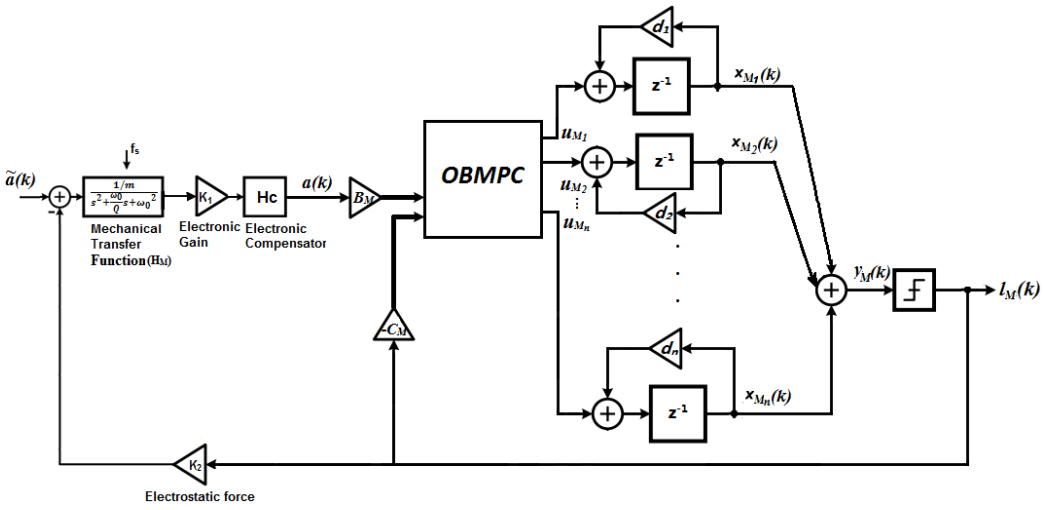

Figure 5.9 MEMS gyroscope using the OBMPC based $\Delta\sum$ modulator (Thick lines denote vector routing).

In Fig.5.9, $\tilde{a}(\mathrm{k})$ is the signal applied to the MEMS gyroscope, $a(\mathrm{k})$ is the sensing signal picked up by the MEMS gyroscope which is the narrow band of interest around the gyroscope resonant frequency and $l_M(k)$ is the quantizer output under the OSR. The optimal solution $u_M{}^*(k)$ has an affine relationship between the quantized output

and multi-bit coefficients and therefore forms a 1-bit processing structure. Specifically, define $H_{\mathrm{M}}(z)$ and $H_{\mathrm{C}}(\mathrm{z})$ as the transfer function of the discretized gyroscope dynamic model and the compensator respectively. For the OBMPC controller presented above, define the prediction horizon N and vectors:

$$\vec{e}_M(k) \triangleq [e(k|k)\ e(k+1|k) \dots e(k+N|k)]^T;$$

$$\vec{u}_M(k) \triangleq [u_M(k|k)\ u_M(k+1|k) \dots u_M(k+N-1|k)]^T;$$

$$\vec{E}(k) \triangleq [E(k|k)\ E(k+1|k) \dots E(k+N-1|k)]^T.$$

According to Eq.5.9 and Eq.5.10:

$$\vec{e}_M(k) = F_M x_M(k) + \vartheta_M \vec{E}(k), \tag{5.11}$$

$$\vec{E}(k) = \vec{l}_M(k) - S(z)\vec{a}(k),$$

where

$$F_M = \begin{bmatrix} C_F \\ C_F A_F \\ C_F {A_F}^2 \\ \vdots \\ C_F {A_F}^N \end{bmatrix}; \vartheta_M = \begin{bmatrix} D_F & 0 & 0 & \cdots & 0 \\ C_F B_F & D_F & 0 & \cdots & 0 \\ C_F A_F B_F & C_F B_F & D_F & \cdots & 0 \\ \vdots & \vdots & \vdots & \ddots & \vdots \\ C_F {A_F}^{N-1} B_F & C_F {A_F}^{N-2} B_F & C {A_F}^{N-3} B_F & \cdots & D_F \end{bmatrix}.$$

$\vec{l}_M \in \mathbb{R}^N$ and $\vec{a}(k) \in \mathbb{R}^N$ are the predicted modulator input and output respectively along the prediction horizon. The cost function of Eq.5.11 can be built to minimize the filtered quantization noise:

$$J\big(x_M, \vec{u}_M(k)\big) = min_{\vec{u}_M(k)}\big\{||x_f(k+N|k)||^2_{\mathrm{P}_M} + \sum_{i=0}^{N-1}\big(||x_f(k+i|k)||^2_{\mathrm{Q}_M} + ||u_M((k+i)||^2_{R_L}\big)\big\} \tag{5.12}$$

where P_M and Q_M are positively defined weighting matrices. Hence the optimal control input ${u_M}^*$ can be found as in Theorem 5.1.

Theorem 5.1, Define the main loop filter $L(z) \triangleq (zI - A_M)^{-1}$and a control input $u_M = [u_{M_1}, u_{M_2} \dots u_{M_n}]^T$ as shown in Fig.5.7. If no constraint is applied, then the

optimal $u_M{}^*$ can be solved as:

$$u_M{}^*(k) = [1,0 \dots .,0]\left(\vec{L}_0 H_A(z)\tilde{a}(k) - \left(\vec{L}_1 + \vec{L}_0 H_A(z)K_2\right)l_M(k)\right), \quad (5.13)$$

where $\vec{L}_0 = L(z)^{-1}(([1, z \dots z^{n-1}] + K_M(zI - A_F)^{-1}B_F)S(z);$

$$\vec{L}_1 = L(z)^{-1}K_M(zI - A_F)^{-1}B_F.$$

Proof:

Under the context of the MPC algorithm, if no constraint is applied, the global optimal solution of Eq.5.12 can be found as:

$$\vec{E}^*(k) = -K_M x_f(k), \quad (5.14)$$

where K_M is the MPC gain obtained by solving Eq.5.12. Based on Eq. 5.11, the state variable of $N(z)^{-1}$ can be derived as:

$$x_f(k) = (zI - A_F)^{-1}B_F\big(S(z)a(k) - l_M(k)\big). \quad (5.15)$$

Substituting Eq.5.15 into Eq.5.14, the following is obtained:

$$\vec{E}^*(k) = -K_M(zI - A_F)^{-1}B_F\big(S(z)a(k) - l_M(k)\big)). \quad (5.16)$$

Now substitute Eq. 5.11 into Eq.5.16 and apply the receding horizon principle. Hence the optimal modulator output $l^*(k)$ can be found as:

$$l_M{}^*(k) = q\left([1,0 \dots .,0]\left(S(z)\vec{a}(k) + K_M(zI - A_F)^{-1}B_F\big(S(z)a(k) - l_M(k)\big)\right)\right). \quad (5.17)$$

Let the quantizer input be:

$$y_M(k) = [1,0 \dots .,0]\left(S(z)\vec{a}(k) + K_M(zI - A_F)^{-1}B_F\big(S(z)a(k) - l_M(k)\big)\right). \quad (5.18)$$

According to Eq.5.18, given the main loop filter $L(z)$, the control input $u_M(k)$ can be determined as:

$$u_M{}^*(k) = [1,0 \dots .,0]L(z)^{-1}([1, z \dots z^{n-1}]S(z)a(k) +$$

$$K_M(zI - A_F)^{-1}B_F\big(S(z)a(k) - l_M(k)\big). \quad (5.19)$$

By reformatting Eq. 5.19, we obtain:

$$u_M{}^*(k) = [1,0 \dots .,0]L(z)^{-1}(([1, z \dots z^{n-1}] + K_M(zI - A_F)^{-1}B_F)S(z)a(k) - K_M(zI - A_F)^{-1}B_F l_M(k)) \quad (5.20)$$

By assigning $\vec{L}_0 = L(z)^{-1}(([1, z \dots z^{n-1}] + K_M(zI - A_F)^{-1}B_F)S(z);$

$\vec{L}_1 = L(z)^{-1}K_M(zI - A_F)^{-1}B_F,$

Hence $$u_M{}^*(k) = [1,0 \dots .,0](\vec{L}_0 a(k) - \vec{L}_1 l_M(k)) \quad (5.21)$$

Furthermore define $H_A(z) \triangleq K_1 H_{\mathrm{M}}(z)\, H_{\mathrm{C}}(\mathrm{z})$, then according to Fig. 5.8

$$a(k) \triangleq H_A(z)(\tilde{a}(k) - K_2 l_M(k)) \quad (5.22)$$

Substitute Eq.5.22 into Eq.5.21, then the optimal control input can be obtained, which completes the proof. □

Remark 5.2: Part of the above proof mirrors the work achieved in (Quevedo and Goodwin, 2005). In addition to (Quevedo and Goodwin, 2005), in the proposed structure, one can directly include the hard constraints onto each of decoupled state variables according to the impulse response of each integrator, which can greatly simplify the design process.

It is worth noting that Eq.5.13 is not strictly compliant to the 1-bit processing structure since $\tilde{a}(k)$ is the multi-bit counterpart of the analog signal. Modulating $\tilde{a}(k)$ into 1-bit signal is not appropriate as this may increase the circuit complexity and once again bring the quantization noise into the control loop. However, as the system is oversampled, $\tilde{a}(k)$ is relatively slow in comparison to the sampling rate. Hence, the computation burden is mainly caused by the second component in Eq.5.13, i.e. $\big(\vec{L}_1 + \vec{L}_0 H_A(z)K_2\big)l_M(k)$. If the bi-level quantizer is adopted, then the explicit relationship between the multi-bit parameters and the bi-level quantized signal can provide a multiplier free structure. Hence the circuit simplicity of the 1-bit $\Delta\sum$

modulator is still preserved.

Essentially, the proposed OBMPC changes the zeros of the NTF by finding the optimal solution to minimize the filtered quantization noise, and therefore improve the performance of the system. The method can also be regarded as an implementation guideline for the design of the ΔΣ modulator as will be discussed in Remark 5.3.

Remark 5.3: For applications where the ΔΣ modulator has to be built using analog components (i.e. controllers are not feasible in the modulation loop), Theorem 5.1 can still be treated as a design guideline to design a high order ΔΣ modulator. Essentially, the K_M solved by the MPC can change the zeros of the NTF and therefore affect the noise shaping characteristic of the modulator. According to Theorem 5.1, define $H_a(z) = [\frac{\vec{L}_{0_1}}{b_1}, \frac{\vec{L}_{0_2}}{b_2} \ldots \frac{\vec{L}_{0_n}}{b_n}]^T$ and $H_l(z) = [-\frac{\vec{L}_{1_1}}{c_1}, -\frac{\vec{L}_{1_2}}{c_2} \ldots -\frac{\vec{L}_{1_n}}{c_n}]^T$, then Fig.5.9 can be simplified as Fig 5.10.

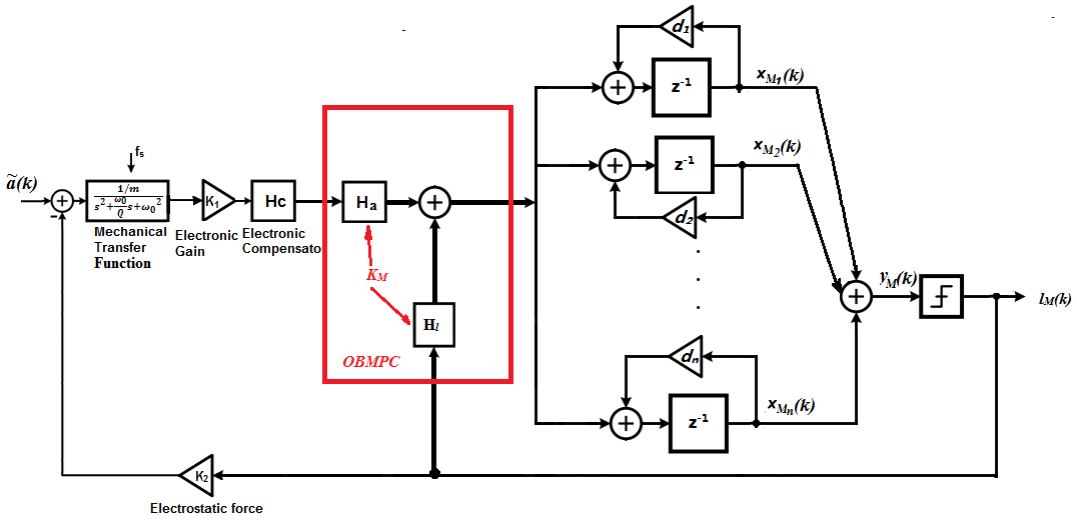

Figure 5.10 Design of high order ΔΣ modulator based gyroscope using the OBMPC

The K_M in Fig.5.10 can be regarded as the functional scaling factor on each integrator to achieve certain $\vec{L}_0$ and $\vec{L}_1$. By designing the appropriate values for P_M and Q_M (i.e. to satisfy ${A_M}^T P_M A_M + Q_M = P_M$), the modulator can be safely scaled while the stability of the control loop is guaranteed. The downside of doing this, however, is that the constraints cannot be directly included, so that the chipping or other stabilization technique needs to be once again used in the modulator.

5.3.3 Hard constraints on ΔΣ Modulator based MEMS gyroscope

Given a set of constraints applied to the state variables:

$$G_M x_M(k) \leq \gamma_M, \tag{5.23}$$

where G_M and γ_M are acquired based on the state bound for each integrator which can guarantee the stability of the modulator . The constraint levels can be determined by studying the impulse response of each integrator or simply according to Eq.5.2. In the proposed parallel state structure, even if the state variable cannot be fully decoupled, the structure in each branch will still be a relative simple one (typically second order ones if the coupling is merely caused by the resonator). Hence, it is relatively easy to determine a reasonable constraint level to the state variable. Similar to Eq.4.7, when a set of active constraints is applied to the quantizer input *a(k)*, the optimal solution can be solved iteratively by introducing the modified Lagrange factor $\bar{\lambda}$:

$$u_M{}^*(k) = \vec{L}_0 \tilde{a}(k) - \vec{L}_1 l_M(k) - \bar{\lambda}\,. \tag{5.24}$$

where $\bar{\lambda} \in \mathbb{R}^p$ and $\bar{\lambda}_i = \bar{S}_i + \bar{W}_{(i,:)}(zI - A_F)^{-1}B_F\big(S(z)a(k) - l_M(k)\big)$ and $\bar{S}$ and $\bar{W}$ are the corresponding matrices solved during the dual level iteration process. If one or several of the constraints are violated, the $\bar{\lambda}_i$ will be calculated accordingly. Note that both $\bar{\lambda}_i$ and the global optimal solution presented in Eq.5.24 have an affine relationship with the 1-bit feedback $l_M(k)$ (again $a(k)$ will be considered as constant within several time steps), the arithmetic block of the proposed OBMPC controller can process all the fast sampled operations with simple conditional-negates (CN) and bit shifters, and therefore achieve a 1-bit processing structure. In the proposed parallel structure, since the state variables are linearly independent, a simple active set method can efficiently find the optimal K_M and then in turn, find H_a and H_l. Hence the proposed OBMPC controller for the ΔΣ modulator structure has an even simpler implementation structure than the one proposed in the previous chapter. The state stability analysis for the OBMPC based ΔΣ modulator can be referred as the

standard MPC stability analysis in subsection 4.4.1.

5.4 Numerical Example

In the interest of justifying the OBMPC controller in the MEMS gyroscope design, the simulation in this section focuses on the sense mode of the gyroscope. The input signal is acted upon by the proof mass of a second order spring and damping mechanical system as stated in Eq.5.1. The proof mass of the sense mode is $m = 1.96 \times 10^{-9} kg$. The quality factor is set as $Q_f = 100$ *and* the resonance frequency of the mechanical system is *4000Hz*. The quantization level is standardized into binary alphabet $\pm$1v, and translated into electrostatic feedback force by the gain of the voltage to force conversion $K_2 = 3.35 \times 10^{-9} V/N$. The input signal is firstly defined as a periodic input signal operating at $64\, rad/sec$ with amplitude 0.6 deg. The structure of the MEMS gyroscope is shown in Fig.5.11a. The sampling time is set to 1.625×10^{-9}s (OSR=200). A lead compensator is used to deal with the phase shift introduced by the mechanical sensing element. A simple second order $\Delta\sum$ modulator is presented here as $A_M = \begin{bmatrix} 1 & 0 \\ 0 & 0.2 \end{bmatrix}$, $B_M = \begin{bmatrix} 0.2 \\ 0.2 \end{bmatrix}$, $C_M = \begin{bmatrix} 0.2 \\ 0.2 \end{bmatrix}$, $D_M = [1 \quad 1]$. The state space realization is shown in Eq.5.25

$$x_M(k+1) = \begin{bmatrix} 1 & 0 \\ 0 & 0.2 \end{bmatrix} x_M(k) + \begin{bmatrix} 0.2 \\ 0.2 \end{bmatrix} a_M(k) - \begin{bmatrix} 0.2 \\ 0.2 \end{bmatrix} l_M(k) \tag{5.25}$$

$$y_M(k) = [1 \quad 1] \begin{bmatrix} x_{M_1} \\ x_{M_2} \end{bmatrix}.$$

The filter $\mathrm{N(z)}^{-1}$ can then be denoted as:

$$x_f(k+1) = \begin{bmatrix} 1 & 0 \\ 0 & 0.2 \end{bmatrix} x_f(k) - \begin{bmatrix} 0.2 \\ 0.2 \end{bmatrix} E(k) \tag{5.26}$$

$$e(k) = [-1 \quad -1] x_f(k) + E(k).$$

If no constraint is applied and *N=4*, then K_M can be found as

$$K_M = \begin{bmatrix} -0.1584 & -0.0240 \\ -0.1411 & -0.0040 \\ -0.1245 & -0.0002 \\ -0.1064 & -0.0005 \end{bmatrix};$$

Consequently, $\vec{L}_0$ and $\vec{L}_1$ can be found as:

$$\vec{L}_0 = \frac{z^2-1.2365z+0.2111}{z^2-0.8z-0.04};\ \vec{L}_1 = \frac{0.0365z-0.0111}{0.4z-0.24}$$

Based on all of this, the control structure is shown in Fig.5.11b

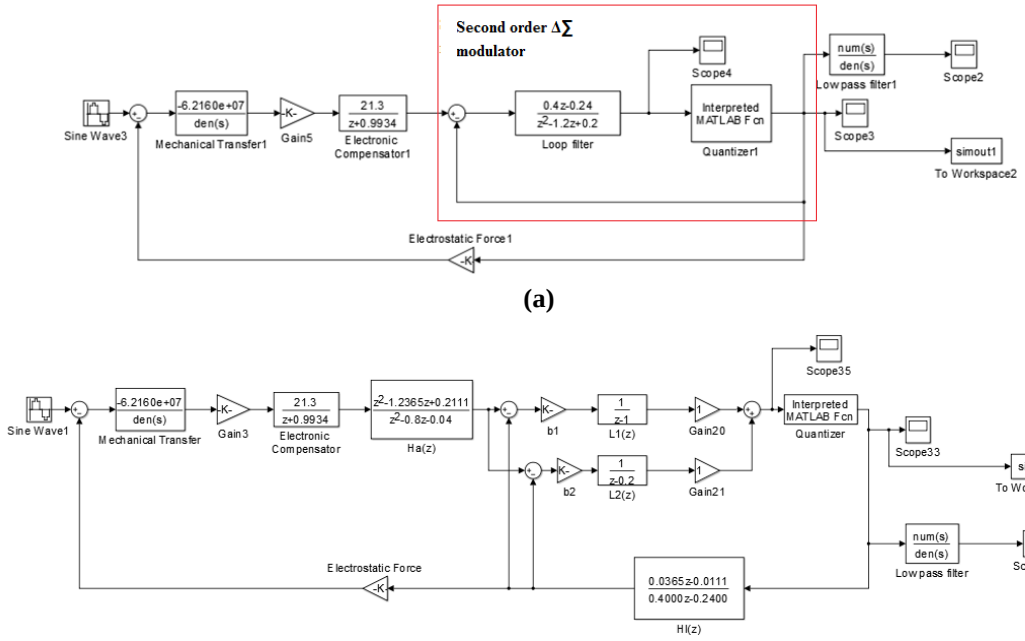

(a)

(b)

Figure 5.11 (a)Simulation structure of the ΔΣ modulator based MEMS gyroscope;(b) Simulation structure of the RHC based 1-bit MEMS gyroscope

We firstly assume the system is ideal (e.g. no electrical noises and internal distortion exist). Then the angular system input is a sinusoidal input. The delay caused by the filter is compensated in the displayed result. A second order ΔΣ modulator based gyroscope is designed as comparison group.

The tracking trajectory and the spectra of both systems are plotted in Fig. 5.12. As shown in Fig. 5.12a and Fig. 5.12c, both systems show good tracking results to the input signal. The amplitude of the quantizer input shows some difference but none of them reaches the constraint (as shown in Fig.5.12b). It can be seen from Fig.5.12d that the spectra are not much different (as expected) since no constraints are applied to the system. However, the OBMPC tends to be slightly better than its benchmark when higher frequency is applied. This is due to the fact that the low pass filter in the designed system is less sufficient in the benchmark than the one in the OBMPC

structure. This point will be further verified in the following simulations.

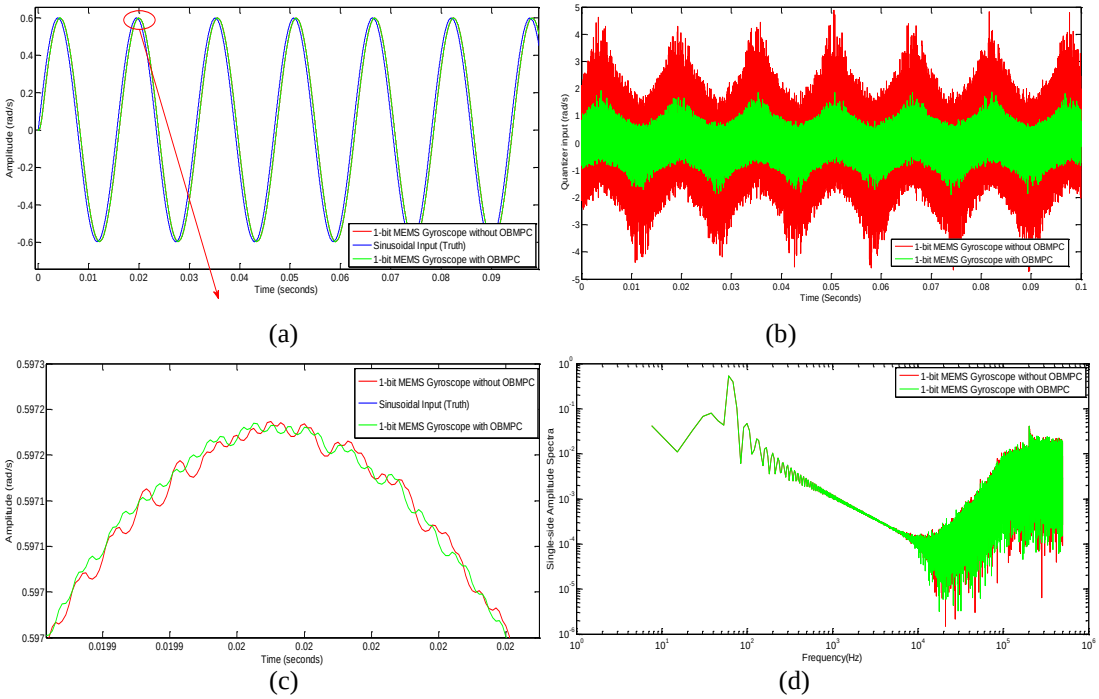

Figure 5.12 Results for the Δ∑ modulator based MEMS gyroscope with Amplitude=0.6. (a)MEMS gyroscope with sinusoidal input. (b) Comparison of the quantizer input (c) Close comparison in time domain. (d) Spectra comparison.

Now we increase the amplitude of the input signal to 1.1 *deg/sec*, so that the quantizer will be overloaded. Constraints and clippers are set to both systems respectively according to Eq.5.2. The tracking trajectory and the spectra of both systems are plotted in Fig.5.13. This time the OBMPC based MEMS gyroscope shows notable improvement comparing to its benchmark. The trajectory of the amplitude is closer to the input signal around the overloading area (as shown in Fig.5.13a and Fig.5.13c) and the quantizer input is nicely shaped (as shown in Fig.5.13e) as the hard constraints are handled better by the OBMPC than clipper. The spectra also show that the OBMPC based MEMS gyroscope performs better at both the peak (as shown in Fig.5.13d) and at higher input frequency (as shown in Fig.5.13b). The OBMPC based Δ∑ modulator shows less noise leakage at the higher frequency as the OBMPC controller improves the original low pass filter in the loop.

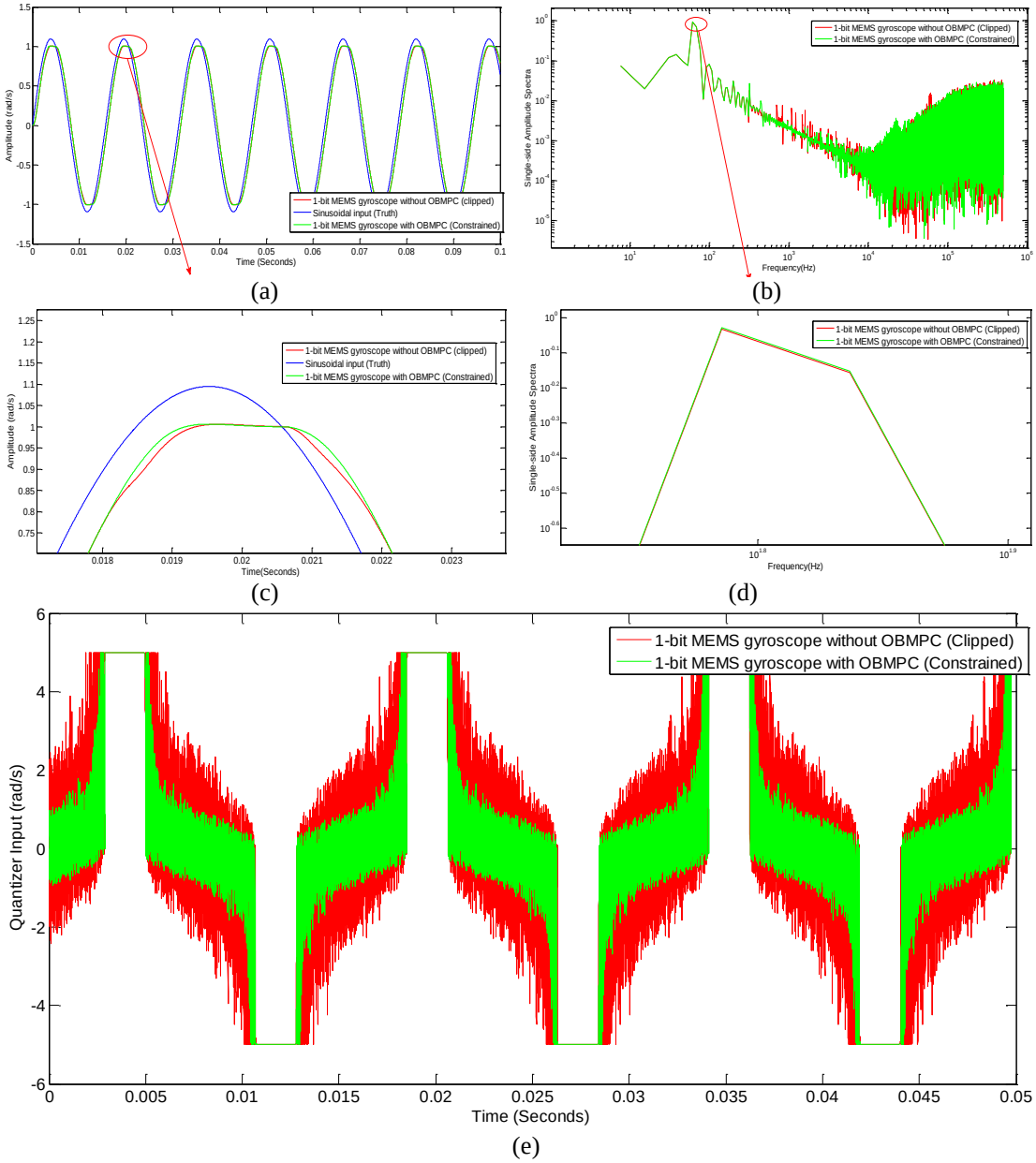

Figure 5.13 Results for the OBMPC based MEMS gyroscope with Amplitude=1.1 (a)MEMS gyroscope with sinusoidal input. (b) Spectra comparison (c) Close comparison in frequency domain (d) Close comparison in time domain. (e) Comparison of the quantizer input.

Then the proposed MEMS gyroscope under different sampling frequency is studied. The SNR and the MSE of the quantization noise are plotted in Fig.5.14.

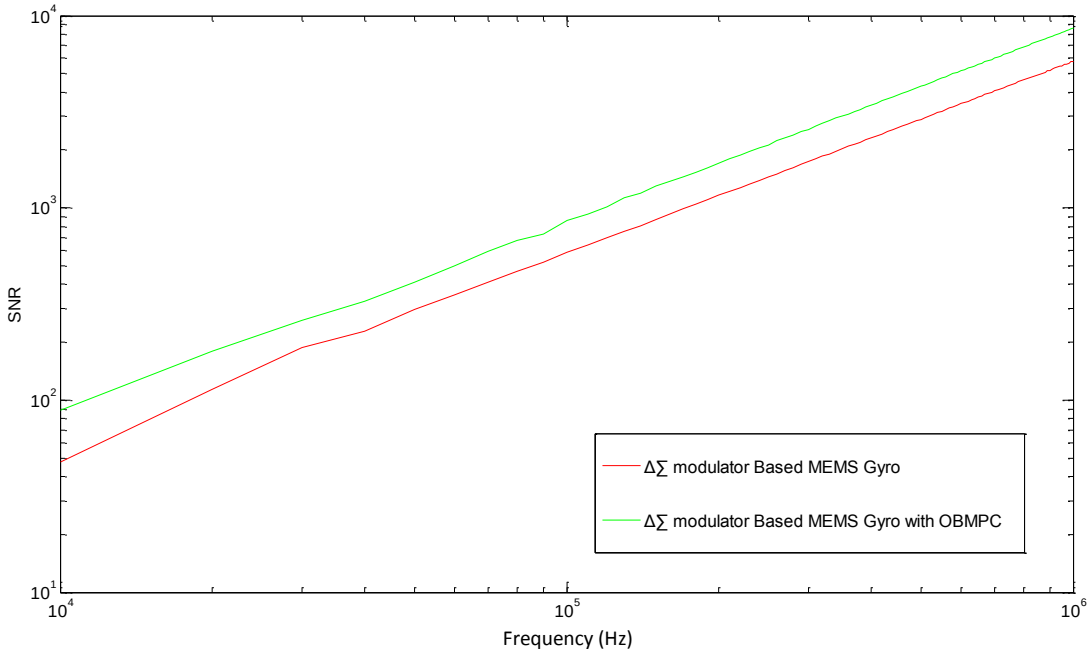

(a)

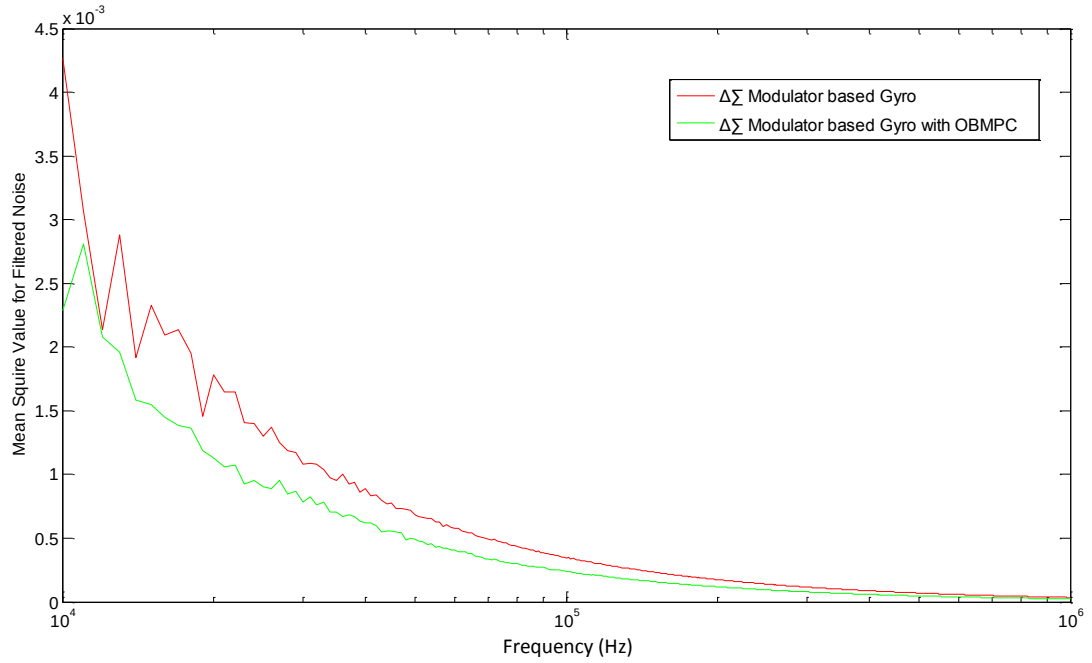

(b)

Figure 5.14 (a) SNR and (b) MSE of the quantization noise with different sampling frequency

It is can be seen that under high sampling frequency ($> 10^4$), the OBMPC based MEMS gyroscope provide better SNR and lower noise level than its benchmark due to the use of MPC controller. Moreover, since the amplitude of the modulator input signal is important to the performance of the $\Delta\sum$ modulator based system, the SNR and MSE of the quantization noise under different input amplitude are obtained as shown in Fig. 5.15.

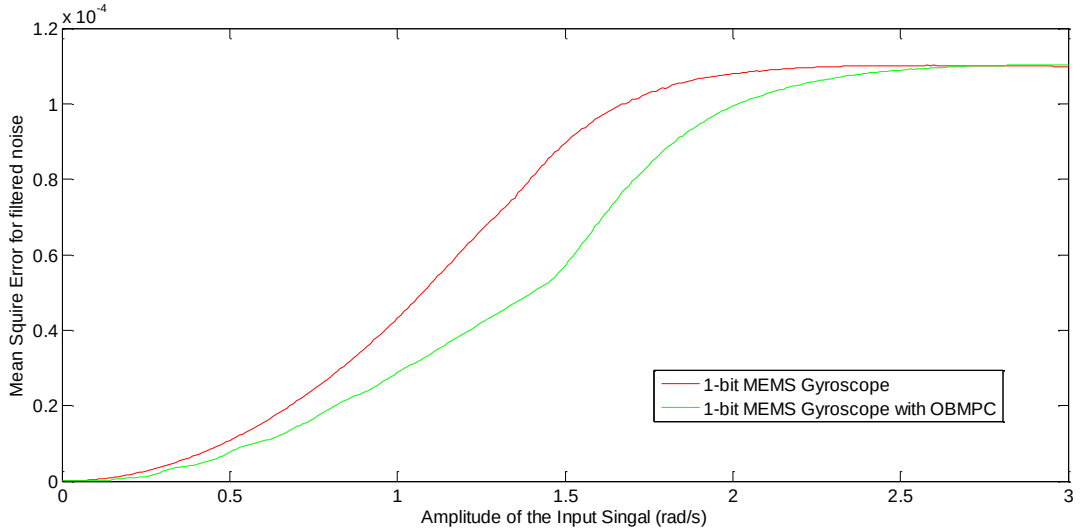

(a)

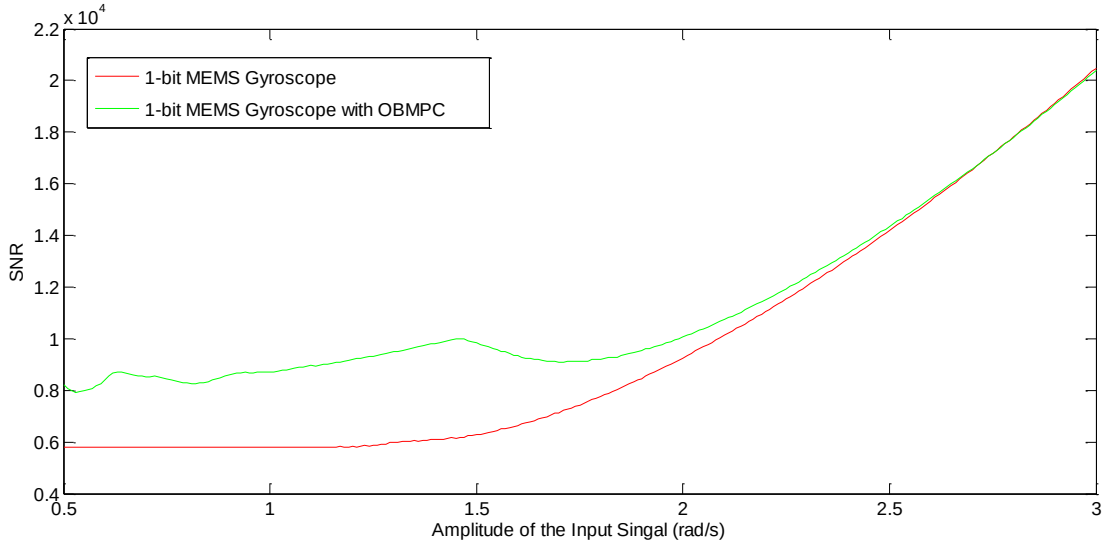

(b)

Figure 5.15 (a) MSE and (b) SNR of the quantization noise with different input amplitude

Fig5.15 again shows that the OBMPC based MEMS gyroscope provide better SNR and lower noise level than its benchmark due to the use of MPC controller. When the input amplitude gets close to the quantization level the integrators in the loop can go even higher due to the integrators in the loop and may trigger clippers or constraints in the design circuits. In this case, the clipper only chops the amplitude of the quantizer input rather than calculate the optimal value toward the cost function of the noise transfer function. Hence, the OBMPC based MEMS gyroscope provide better SNR over the conventional $\Delta\sum$ modulator based MEMS gyroscope. It is worth noting that if the amplitude of the input signal is much higher than then quantization level, then the system will no longer track the input signal and both systems need to be

redesigned (e.g. change the quantization level or the loop gain).

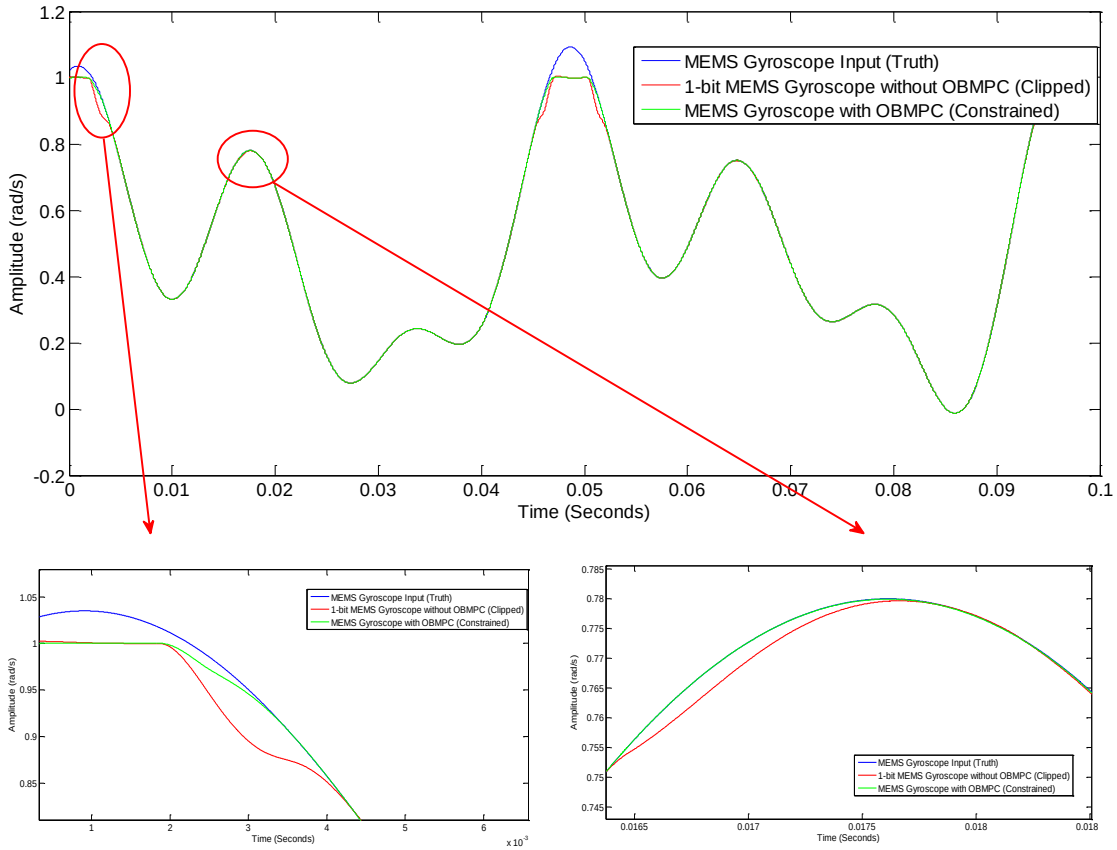

Figure 5.16 Comparisons between the ΔΣ modulator based gyroscope using the OBMPC and the conventional ΔΣ modulator based gyroscope

Figure 5.16 Comparisons between the ΔΣ modulator based gyroscope using the OBMPC and the conventional ΔΣ modulator based gyroscope

Finally, given a random input, adding random noise with relatively high amplitude and low frequency to each of the integrator, the response of the ΔΣ modulator based MEMS gyroscope can be found in Fig.5.16. It can be seen that the OBMPC based MEMS gyroscope tracks the input signal better especially around the quantization level, which proofs the benefits of using the OBMPC controller in the MEMS gyroscope.

5.5 Summary

In this chapter, a 1-bit MEMS gyroscope is discussed. To provide the desired 1-bit data to the OBMPC system, the bi-level ΔΣ modulator becomes an essential part of the sensing component. The ΔΣ modulator can be regarded as an efficient A/D

converter, which incorporates the sensing data into bi-level bit stream. Such $\Delta\sum$ modulator generates very high frequency 1-bit signals, which could be transmitted directly and used for the control system processing.

The challenges of the $\Delta\sum$ modulator based MEMS gyroscope are mainly the randomness of the sensor input and the noise introduced by the mechanical and electrical systems. Hence, it is essential to increase the SNR to improve the control accuracy while maintaining the robustness of the control system of the gyroscope control loop. In this work, we propose to include an OBMPC algorithm in the $\Delta\sum$ modulator based gyroscope. Such structure improves the SNR by minimizing the filtered quantization noise. As a result, constraints applied on the modulator state variables can be included in the controller directly, and an optimized gain can be determined so that the coefficients can be safely scaled. Due to the 1-bit nature of the modulated signal, if the state variable can be decoupled, so that the constraints applied to the state variable are linearly independent, the OBMPC can be implemented with relatively simple circuit under the framework of the 1-bit processing control system. Note that it is not necessary to apply constraints to all the state variables to stabilize the sensing output. Hence if some of the modulator states cannot be decoupled, the constraint can be applied to the last state variable in that branch.

For more general sensing circuits, if the proposed OBMPC controller is not suitable to be implemented, it can still serve as a design guideline for designers (i.e. perform the unconstrained optimization process offline). However, in such implementations, the clipping technique or other stabilization techniques are still required as constraints cannot be directly included in the control loop.

6. OBMPC FOR THE WIRELESS CONTROL SYSTEM AND 1-BIT STATE ESTIMATOR DESIGN

==========

==========

For the fractionated satellite attitude control system, the effects introduced by the WCS need to be considered. Challenges such as network-induced delay, data dropout and quantization error are expected, all of which can cause stability issues to the control system. Thus, in the proposed fractionated satellite attitude control mission, the controller should be designed with considerable efforts to deal with the side effects created by the communication channel, i.e. the ISL.

The purposes of this chapter are twofold. 1) We firstly discuss the robustness of the proposed OBMPC in the WCS. 2) To further improve the performance of the WCS, a state estimation is required. Typical state estimators reconstruct the binary sensing signals into their multi-bit counterpart, where demodulation/decimation on the 1-bit signals is required. However, in doing so, adding the conventional state estimator will compromise the 1-bit feature of the OBMPC system. Therefore, a 1-bit state estimator is designed in order to utilize the benefits of the 1-bit feature of the control system.

6.1 Problem Formulation

The formulations in this thesis assume a master-slave WCS configuration: the controller is centralized on the master satellite while the attitude sensors and actuators are located on the slave satellite. The physical bus system is replaced with the ISL, which forms a WCS. Note that the formulation in this work does not cover WCSs with a peer-to-peer configuration, e.g. the systems studied in (Langbort, et al., 2004).

The control inputs are calculated by the controller on-board the master satellite and sent to the actuators on-board the slave satellite. They are converted by $\Delta\sum$ modulators and the resultant 1-bit signals are sent to the actuators in series. For the slave satellite, the satellite motion can be determined by the $\Delta\sum$ modulator based sensors, e.g. the MEMS gyroscope as discussed in the last chapter. Such 1-bit data are fed back to the controller, which includes the angular position and angular rate for all axes. The interest of this part lays in the robustness of the proposed OBMPC controller under the effect of data loss, disturbances/noise and time delay introduced in the communication process. A state estimator is developed at the controller side to eliminate the effects of the measurement noises and data loss.

The time delay caused by the plant (referred as "Nature delay" or "Plant delay") and the processing time of the controller are considered. Such delays can be modeled in the control system as the onboard computation time at each time step. Also the communication can be time-stamped so that the propagation delay caused by the wireless transmission can be explicitly known. A fixed time delay τ can be used to model the time delays discussed above. In this case, the inputs to the actuators held at their previous values. Small fixed time delays can be modeled in the controller by letting the state variable $\varkappa(k) = x(k+\tau)$. For notional simplicity, we still use $x(k)$ to represent $\varkappa(k)$ in this work, assuming the expected plant delay and the communication delay has been modeled in the system. A state space function for a WCS can be formulated as Eq.6.1:

$$x(k+1) = A\,x(k) + B\mathrm{u}(k) + B_1\omega(k)$$

$$y(k) = Cx(k) + v(k), \tag{6.1}$$

where $\omega(k) \in \mathbb{R}^n$ and $v(k) \in \mathbb{R}^n$ are additive white noises standing for the system noise and the observation noise respectively. Any delay larger than τ is considered to be a data loss. For the following discussion, two basic assumptions are made here.

A 6.1: Both noises $\omega(k)$ and $v(k)$ are Gaussian and have means of zero.

A 6.2: The pair (*A*,*C*) is completely observable.

However, Eq.6.1 cannot accurately model all the time delays that occur in a real world WCS. Even if the clock can be synchronized, large and unexpected delays may still occur and cause deterioration in the control system. Also, in the communication channel with limited bandwidth, the sensor data will be queued in the buffer, which will also cause random time delays. The stability issues caused by the time delay have been developed by many researchers, e.g. (Branicky, et al., 2000). In this work, any unexpected large time delays are regarded as a data loss, and the data loss rate is assumed to be known.

6.2 Data Loss and Time Delay in the OBMPC System

The MPC developed in the WCS applications can be found in many literatures e.g.(Quevedo, et al., 2003), (Hegrenæs, et al., 2005). The OBMPC inherits the benefits of the MPC algorithm for the WCS, in which the prediction data can be used to produce backup information in case of packet loss or a large time delay occurrence. Assuming the plant model is stable and the initial state condition of the satellite is calculated nearly correctly, at time step *k*, with the plant input and output's current and past information, *x(k+i)* can be explicitly known, a clock will be set in the controller to synchronize and index the control process to detect if there is any unexpected data loss or time delay. The predicted value will replace the input data if a data loss or time delay is detected. Such replacement can be achieved by adding a buffer to the controller to store the predicted information during each optimization process. In doing so, the data loss or delay can be treated as a disturbance applied to the system. For example, at time step *k*, the sensor data $x(k|k)$ are sent to the controller and received with negligible error. A predicted state feedback $x(k+i|k)$ in the prediction horizon will be calculated and saved in the buffer. If at time step *k+i*, the packet is lost, the predicted data $x(k+i|k)$ can be taken from the buffer and serve as the feedback signal to maintain the convergence process. Such a buffered control system is similar to the state predictor proposed in (Chan and Ozguner, 1994). The stability issues of such WCS with future data buffering have been discussed in many literatures e.g. (Sha, et al., 2002; Tang and de Silva, 2006). Similarly, data with large

delays can be regarded as data loss, and substituted by the predicted data even if they eventually arrived at the receiver. Therefore, large time delays will be treated as data loss in this work and will not be discussed as a separate issue.

Except for the explicit use of the predicted data, the OBMPC is also less sensitive to the data loss due to the nature of the 1-bit processing control system. As the control signals are oversampled, each 1-bit data carries only partial information due to the OSR, but can be processed in sequence. Hence the significance of data loss is much less than conventional multi-bit D/A conversion methods (see one of our previous works (Wu and Bai, 2010) for more details). In order to emphasize the bi-level quantization nature of the problem, here the author assumes a n channel state feedback acquired from the sensing element is defined as $X(k) \in \mathbb{X}^n$, where $\mathbb{X}$ = {-1,1}. In principle it is only necessary to transmit one bit for each communication channel as the control input information per time step to maintain control progress (more bits are required to address multiple information, e.g. 3 angular position feedbacks and 3 angular velocity feedbacks and so on). As already discussed, to achieve good resolution, a high OSR is typically chosen for the OBMPC system. Such high frequency 1-bit data will be processed in sequence without demodulation/decimation. Hence, in the case of a single bit loss, the equivalent demodulated value (i.e. the average of a series of over sampled 1-bit data) will not be affected significantly.

6.3 State Estimation for 1-Bit Processing Control System

The state feedbacks in the proposed attitude mission can be directly acquired from the sensing elements (e.g. gyroscope, accelerometer, etc.). Therefore the state observer is not required. However, full state feedback does not directly address the issue of the steady state error, especially when considering the disturbances and delays introduced by the wireless communication. The augmented model is proposed in chapter 4 to address the effect of the constant disturbance so that the disturbance model is not necessarily included in the observer to avoid the observer bias. Hence, the state

estimator discussed in this chapter is mainly focus on the regulation purposes rather than disturbance rejection and reference tracking. Also, the design proposed this chapter can be referred as an example of designing the state estimator for the 1-bit processing based control system in a more general case when the full state feedback is not feasible.

6.3.1 State observer

Essentially, the state variable $\boldsymbol{x(k)}$ is estimated via an observer of the form:

$$\hat{x}(k+1) = A\hat{x}(k) + Bu(k) + K_{ob}\big(y(k) - C\hat{x}(k)\big), \tag{6.2}$$

where $\boldsymbol{\hat{x}(k)}$ is the estimated state feedback, $\mathbf{K_{ob}}$ is the observer gain which is designed to converge the state error. This algorithm is able to detect differences between the actual state variable value $\boldsymbol{x}(\mathbf{k})$ and the estimated value $\boldsymbol{\hat{x}(k)}$ and change the estimated value to better fit the environmental noises. With the information of $\boldsymbol{\hat{x}(k)}$ replacing $\boldsymbol{x(k)}$, given the notational context in chapter 4, the optimal solution for the unconstrained MPC can be found as:

$$U(k) = K_y R_s(k) - K_{mpc}\hat{x}(k), \tag{6.3}$$

where $K_y = \overbrace{[I_m\ o_m\ o_m\ o_m]}^{N_c}\Phi^{-1}\Psi$ and $K_{mpc} = -\overbrace{[I_m\ o_m\ o_m\ o_m]}^{N_c}\Phi^{-1}\Omega$. Note that the closed-loop observer error equation is

$$e(k+1) = (A - K_{ob}C)e(k). \tag{6.4}$$

The augmented form of state variable can be then written as

$$\begin{bmatrix} e(k+1) \\ x(k+1) \end{bmatrix} = \begin{bmatrix} A - K_{ob}C & o_{n\times n} \\ -BK_{mpc} & A - BK_{mpc} \end{bmatrix}\begin{bmatrix} e(k) \\ x(k) \end{bmatrix} + \begin{bmatrix} o_{n\times m} \\ BK_y \end{bmatrix} r(k) \tag{6.5}$$

where $o_{n\times n}$ is a $n \times n$ zero matrix and $o_{n\times m}$ is a $n \times m$ zero matrix. The characteristic equation of the closed-loop state-space system is determined by

$$\det(\lambda I - (A - K_{ob}C))\ \det(\lambda I - \big(A - BK_{mpc}\big))=0. \tag{6.6}$$

It can be seen that the design of the predictive control law and the observer can be carried out independently (or separately). Despite this, when the two components are combined together, the Eigenvalues remain unchanged.

Amongst various state estimators, the Kalman filter is the most popular choice because it is simple to implement as well as its capability of maintaining the stability of the system at the design stage. By combining error-containing sensor measurement and the theoretical prediction of the dynamic model of the system, the Kalman filter can provide a good state estimation for the controller. Many literatures have explained the fundamental theory of the Kalman Filter and its use in many applications, e.g. (Lee and Ricker, 1994; Welch and Bishop, 2006; Grewal and Andrews, 2008).

If the constraints exist, then the Moving Horizon Estimation (MHE) can be used in state estimation. Similar to the MPC algorithm, the MHE technique is based on a QP problem which utilizes a moving window containing a fixed number of observed measurements. The MHE can be simplified into the Kalman filter under some conditions. In this work, the MHE method shall be firstly discussed and the Kalman filter will then be discussed as a special case.

6.3.2 Customized moving horizon estimator for the OBMPC

6.3.2.1 Moving horizon estimator and 1-bit processing

Despite of the similarity of the MPC, the MHE is a less popular approach because of the wide success of the EKF. Unlike the EKF, MHE requires solving QP solvers iteratively, which induces computational expense to the estimator. Similar to the early stage of the MPC development, most MHE applications only apply to systems with moderate/slow system dynamics (i.e. Process control).

Similar to the MPC algorithm, the MHE also have the advantage of dealing with hard constraints. Despite being less popular than the MPC, the MHE is still suggested as a practical method to incorporate inequality constraints in estimation for many applications, e.g. (Robertson, et al., 1996). Also the MHE is proven to be a powerful tool to deal with the quantization noise, data loss and time delay introduced in the WCS, e.g. (Rao, et al., 2001; Luo, et al., 2008; Xue, et al., 2012).

In the proposed satellite mission, the state variables $x(k)$ (i.e. angles, angular velocities) can be directly measured using the sensing devices on the slave satellites. The sensing component (e.g. MEMS gyroscope) is embedded in a $\Delta\sum$ modulator

based control loop, which modulates $x(k)$ into 1-bit signals. Normally, the quantized signal is oversampled by the modulator and a low pass filter will be used to decimate the oversampled signal. The Kalman filter technique or the MHE are employed to perform state estimation using the restructured signal e.g. (Goodwin, et al., 2004; Luo, et al., 2008; Wang, et al., 2008; Liu, et al., 2013).

Unlike the above approaches, in this work, we develop a state estimator under the context of 1-bit processing. For the OBMPC system, the implementation of a simple and fast response controller relies on the 1-bit state feedback. Therefore, the interest of this section is to design the state estimator under the context of 1-bit processing so that it complies with the fast sampled control loop, while retaining the characteristic of the 1-bit state feedback. To formulate the estimation problem, the sensing data are assumed to be acquired in 1-bit format and the filtered quantization noise $e(k)$ is relatively small such that will not destabilize the control system. The sensing measurement $x(k)$ on each channel is weighted through a loop filter H_s and a bi-level quantizer $q_\Delta(.) \in \{\Delta, -\Delta\}$. The resultant 1-bit data $\tilde{x}(k)$ will be processed in the estimator directly without decimation. The estimated state feedback $\hat{x}(k)$ needs to be weighted by a $\Delta\sum$ modulator to acquire its quantized counterpart $q\left(H_e\hat{x}(k)\right)$ so that it can be used to perform the online optimization in the OBMPC controller. For the 1-bit MHE design discussed in the next subsection, the same $\Delta\sum$ modulator is used to modulate $\hat{x}(k)$ so that $H_e = H_s$. The control structure with state estimation is shown in Fig.6.2

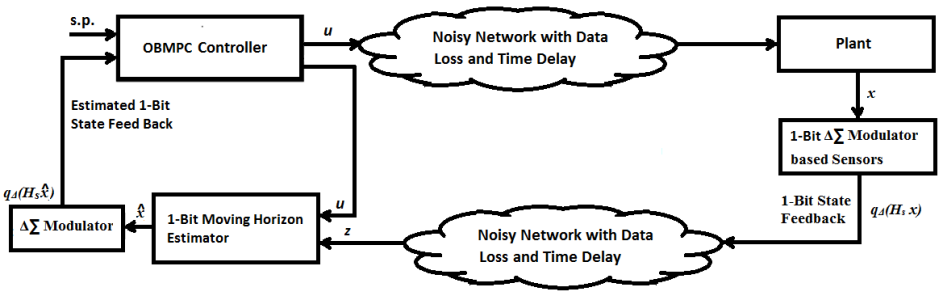

Figure 6.1 OBMPC based WCS with 1-Bit Moving Horizon Estimator

The purposes of such a proposal are twofold. Firstly, the decimation filter can be

avoided as the 1-bit signal can be processed directly. This potentially simplifies the circuit complexity of the state estimator, and removes noises and delays introduced by the decimation filter. Secondly, as both the state feedback and the state estimation are eventually quantized signals, the state estimator can comply with the framework of the 1-bit processing, and therefore achieve a simple (multiplier free) implementation structure, so that a fast response state estimator can be achieved to comply with the oversampled control system. Moreover, as each of the 1-bit state feedback will be treated individually, the state update will be more frequent than the conventional state estimation, and therefore provide better state estimation results.

The main drawback, however, is that such a 1-bit state estimator design will lose the ability to minimize the quantization noise (the 1-bit data will be processed directly so that the quantization noises will remain in the estimator). In this work, we assume the quantization noise can be minimized at the sensing end as discussed in the previous chapter. The proposed estimator will mainly deal with the measurement noises and data loss/packet loss during the communication process.

6.3.2.2 Customized 1-bit moving horizon estimator

In addition to A 6.1 and A 6.2, the following assumptions are needed to discuss the theory of the 1-bit MHE.

A 6.3: The matrix pair (A, C) is an observable pair through the receding horizon *N*.

A 6.4: The quadratic problem is asymptotically stable.

Consider a sensor feedback that is transmitted through the lossy communication network. Define:

$$\gamma_{loss}(k) \triangleq \begin{cases} 0, & \textit{if the packet drop does not occur at time step } k \\ 1, & \textit{if the packet drop occurs at time step } k \end{cases}$$

as an independent and identically distributed Bernoulli white sequence with distribution *Prob* $(\gamma_{loss}(k) = 1)$=*p* and *Prob* $(\gamma_{loss}(k) = 0)$=*1-p*, where $0 \leq p \leq 1$. To simplify the problem, here we combine the data loss in both uplink and down link

together and model them with $\gamma(k)$. Hence the system presented in Eq.6.1 can be described as Eq.6.7 and Eq.6.8:

$$x(k+1) = A\,x(k) + Bu(k) + w(k) \tag{6.7}$$

$$\mathrm{z}_r(k) = C_\gamma(k) q_\Delta\big(H_s(z)x(k) + v(k)\big) + (1 - \gamma_{loss}(k))\mathrm{z}_r(k-1), \tag{6.8}$$

where $\mathrm{z}_r(k)$ is the data received by the state estimator with the stochastic parameter $\gamma(k)$. $C_\gamma(k) = \gamma_{loss}(k)C$. $\hat{x}(k)$ is the estimated state variable. The system can be discussed under the framework of the stochastic system, where the state of the system is determined probabilistically. Given a batch of actual arrival information in a finite horizon window from *k-N* to *k*, a moving horizon estimator based on the 1-bit sensing data is proposed here to solve the state estimation. Define vectors:

$$\mathrm{Z}_{\mathrm{k-N}}^{\mathrm{k}} = [\mathrm{z}_r(\mathrm{k-N}), \mathrm{z}_r(\mathrm{k-N+1}), \ldots \mathrm{z}_r(\mathrm{k})]^{\mathrm{T}};$$

$$\mathrm{Z}_{\mathrm{k-N-1}}^{\mathrm{k-1}} = [\,\mathrm{z}_r(\mathrm{k-N-1}), \mathrm{z}_r(\mathrm{k-N}), \ldots\, \mathrm{z}_r(\mathrm{k-1})]^{\mathrm{T}} \quad ;$$

$$U_{k-N}^{k-1} = [\,u(k-N), u(k-N+1), \ldots\, u(k-1)]^T;$$

$$\Gamma_k = diag[\gamma_{loss}(k-N)I, \gamma_{loss}(k-N+1)I, \ldots, \gamma_{loss}(k)I];$$

$$V_{k-N}^{k} = [\,v(k-N), v(k-N+1), \ldots\, v(k)]^T;$$

$$W_{k-N}^{k} = [\,w(k-N), w(k-N+1), \ldots\, w(k)]^T.$$

According to Eq.6.1 and Eq.6.8, the state estimation vector $\bar{X}_{k-N}^{k}$ and the received data pack Z_{k-N}^{k} within the receding horizon *N* can be described as

$$\bar{X}_{\mathrm{k-N}}^{\mathrm{k}} = F_s\hat{x}(k-N|k) + \vartheta_s U_{k-N}^{k} + (1-\Gamma_k)\mathrm{Z}_{\mathrm{k-N-1}}^{\mathrm{k-1}} \tag{6.9}$$

$$Z_{\mathrm{k-N}}^{\mathrm{k}} = F_s q_\Delta(H_s(z)x(k-N) + v(k-N)) + \vartheta_s U_{k-N}^{k} + (1-\Gamma_k)Z_{\mathrm{k-N-1}}^{\mathrm{k-1}} + \epsilon_e W_{k-N}^{k} \tag{6.10}$$

where

$$F_s(k) = \begin{bmatrix} C_\gamma(k-N) \\ C_\gamma(k-N+1)A \\ C_\gamma(k-N+2)A^2 \\ \vdots \\ C_\gamma(k)A^N \end{bmatrix};$$

$$\vartheta_s(k) = \begin{bmatrix} 0 & 0 & 0 & \cdots & 0 \\ C_\gamma(k-N+1)B & 0 & 0 & \cdots & 0 \\ C_\gamma(k-N+2)AB & C_\gamma(k-N+2)B & 0 & \ddots & \vdots \\ \vdots & \vdots & \vdots & \ddots & 0 \\ C_\gamma(k)A^{N-1}B & C_\gamma(k)A^{N-2}B & C_\gamma(k)A^{N-1}B & \cdots & C_\gamma(k)B \end{bmatrix};$$

$$\epsilon_s(k) = \begin{bmatrix} 0 & 0 & 0 & \cdots & 0 \\ C_\gamma(k-N+1)\gamma(k) & 0 & 0 & \cdots & 0 \\ C_\gamma(k-N+2)A\gamma(k) & C_\gamma(k-N+2)\gamma(k) & 0 & \ddots & \vdots \\ \vdots & \vdots & \vdots & \ddots & 0 \\ C_\gamma(k)A^{N-1}\gamma(k) & C_\gamma(k)A^{N-2}\gamma(k) & C_\gamma(k)A^{N-1}\gamma(k) & \cdots & C_\gamma(k)\gamma(k) \end{bmatrix}.$$

The cost function for the 1-bit MHE can be then described as

$$\min_{\hat{x}^*(k-N|k)} J(k) = \mathrm{E}\left\{ min_{\hat{x}(k-N|k)} \left\{ \sum_{i=k-N}^{k} \left(||z(i) - \bar{x}(i|k)||^2_{\hat{P}_s} + ||\hat{x}(k-N|k) - \bar{x}(k-N|k-1)||^2_{\hat{Q}_s} \right) \right\} \right\} \quad (6.11)$$

where $\mathrm{z}_r(i|k) = C_\gamma(i) q_\Delta\big(H_s(z)x(i) + v(i)\big) + \big(1 - \gamma_{loss}(i)\big)\mathrm{z}_r(i-1);$

$$\bar{x}(i|k) = Aq_\Delta(H_s\hat{x}(i-1|k)) + Bu(i-1);$$

$$\bar{x}(k-N|k-1) = Aq_\Delta(H_s\hat{x}(k-N-1|k-1)) + Bu(k-N-1);$$

$\hat{P}_s \in \mathbb{S}_+^n$ and $\hat{Q}_s \in \mathbb{S}_+^n$ are weighting matrices, which stand for the confidence of the prediction $x(k-N|k)$ and the state estimation $\hat{x}(i|k)$ respectively. $\bar{x}(i|k)$ is the *priori* state estimation based on the *posteriori* state estimation at time step *k-1*. The quantizer output is a set of bi-level signal where $\hat{x}(i|k) \in \mathbb{X} = \{x : x \in (\Delta, -\Delta)\}$.

Theorem 6.1: For an unconstrained close-loop OBMPC control system with a stable control law $U(k) = -K_{MPC} q_\Delta\big(H_S\hat{x}^*(k|k)\big)$, given weighting matrices $\hat{P}_s \in \mathbb{S}_+^n$ and $\hat{Q}_s \in \mathbb{S}_+^n$, the optimization state estimation $\hat{x}^*(k-N|k)$ can be uniquely solved as:

$$\hat{x}^*(k-N|k) = q_\Delta(H_e\{\left(\hat{Q}_s I + \hat{P}_s F_s(k)^T F_s(k)\right)^{-1} (\hat{Q}_s(A - BK_{MPC}) q_\Delta\big(H_e\hat{x}^*(k-$$

$$N-1|k-1)\big)+\hat{P}_s F_s(k)^T F_s(k) q_\Delta(H_s x(k-N)+v(k-N))+\hat{Q}_s w(k-N-1)-$$

$$\hat{P}_s F_s(k)^T \epsilon_s(k) W_{k-N}^k)\}) \qquad (6.12)$$

Proof:

Directly solve the cost function Eq.6.11:

$$\nabla_{\hat{x}(k-N|k)} J\big(\hat{x}^*(k-N|k)\big)=2\hat{Q}_s(\hat{x}^*(k-N|k)-\bar{x}(k-N|k-1))$$

$$-2\hat{P}_s F_s(k)^T(Z_{k-N}^k-F_s(k)\hat{x}^*(k-N|k)-\vartheta_s(k)U_{k-N}^k-(1-\Gamma_k)Z_{k-N-1}^{k-1})=0. \quad (6.13)$$

Therefore

$$\hat{x}^*(k-N|k)=\big(\hat{Q}_s I+\hat{P}_s {F_s}^T(k)F_s(k)\big)^{-1}\{\hat{Q}_s\bar{x}(k-N|k-1)-\hat{P}_s F_s(k)^T[Z_{k-N}^k-$$

$$(1-\Gamma_k)Z_{k-N-1}^{k-1}-\vartheta_s(k)U_{k-N}^k]\}; \quad (6.14)$$

According to Eq.6.14, we obtain:

$$Z_{\mathrm{k-N}}^{\mathrm{k}}-(1-L)Z_{\mathrm{k-N-1}}^{\mathrm{k-1}}-\vartheta_s(k)U_{k-N}^k=F_s(k)q_\Delta(H_s x(k-N)+v(k-N))+$$

$$\epsilon_s(k)\mathrm{W}_{\mathrm{k-N}}^{\mathrm{k}}. (6.15)$$

The state estimation can then be derived as:

$$\hat{x}^*(k-N|k)=\big(\hat{Q}_s I+\hat{P}_s F_s(k)^T F_s(k)\big)^{-1}\{\hat{Q}_s\bar{x}(k-N|k-1)-$$

$$\hat{P}_s F_s(k)^T F_s(k) q_\Delta(H_s x(k-N)+v(k-N))-\hat{P}_s F_s(k)^T\epsilon_s(k)W_{k-N}^k\}. \qquad (6.16)$$

Given a control law $U(k)=-K_{MPC}q_\Delta(H_s\hat{x}^*(k|k))$, if the quantization noise is small enough to be ignored, a *priori* state estimation of a stable 1-bit processing control system can then be derived as Eq.6.17.

$$\bar{x}(k-N|k-1)=(A-BK_{MPC})q_\Delta(H_e\hat{x}^*(k-N-1|k-1))+w(k-N-1). \quad (6.17)$$

Substitute Eq.6.17 into Eq.6.16. Hence Eq.6.12 can be obtained, which completes the proof. □

As shown Eq. 6.12, the state optimization $\hat{x}^*(k-N|k)$ can be obtained based on the *a posteriori* state estimation $q_\Delta\big(H_S\hat{x}^*(k-N-1|k-1)\big)$ and the quantized state

feedback $q_\Delta(H_s x(k-N)+v(k-N))$. Hence, by pre-calculating the parameters in Eq.6.12, the state estimator can be implemented under the framework of the 1-bit processing to comply with the fast sampled OBMPC controller.

Moreover, due to the fact that γ(k) is a stochastic parameter, it is necessary to analyze the expectation of the estimation error generated by the estimator.

6.3.3 Mean analysis

Define the estimation error at time *k-N* as $e_{k-N} \triangleq x(k-N)-\hat{x}^*(k-N|k)$, re-arrange Eq.6.12, we have:

$$\left(\hat{Q}I+\hat{P}F_s(k)^T F_s(k)\right)\left(\hat{x}^*(k-N|k)-q_\Delta(H_S x(k-N)+v(k-N))\right)=$$

$$\hat{Q}\left(q_\Delta\left(H_S\hat{x}^*(k-N|k-1)\right)-q_\Delta\left(H_s x(k-\mathrm{N}-1)\right)\right)+\hat{Q}_s w(k-N-1)-$$

$$\hat{P}_s F_s(k)^T \epsilon_s(k) W_{k-N}^k. \qquad (6.18)$$

For notational simplicity, define $E_{\hat{x}^*}=E\{q_\Delta(H_S\hat{x}^*(k-N|k))\}$, $E_w=E\{w(k)\}$, $E_x=E\{q_\Delta(H_S x(k-N))+v(k-N)\}$, $E_{K_{E\_pri}}=\mathrm{E}\{K_{E\_pri}\}$, $E_{e_{k-N}}=\mathrm{E}\{e_{k-N}\}$, $E_{\Phi^{-1}}=E\{\hat{Q}_s I+\hat{P}_s F_s(k)^T F_s(k)\}$, $E_\Omega=E\{\hat{P}_s F_s(k)^T\}$ and $E_{\epsilon_s}=E\{\epsilon_s(k)\}$.

If the observation noise term $v(i)$ is not deterministic (i.e. not significant enough to change the sign of the received state feedback), then the received state feedback coincides with the output of the ΔΣ modulator based measurement unit. Assume the quantization noise has zero mean, hence

$$E_x=E\{x(k-N)\}; \qquad (6.19)$$

$$E_{\hat{x}^*}=E\{\hat{x}^*(k-N|k)\}.$$

Based on the independence and stationary assumptions, the expected value for the state estimation can be written as:

$$E_{\hat{x}^*(k-\mathrm{N})}=E_{x(k-N)}-E_{\Phi^{-1}}\hat{Q}_s\left(E_{x(k-N-1)}-E_{\hat{x}^*(k-N-1)}\right)+E_{\Phi^{-1}}(\hat{Q}_s-E_\Omega E_{\epsilon_s})E_w). \qquad (6.20)$$

Then the expected value of the error can be found as:

$$E_{e_{k-N}} = E_{x(k-N)} - E_{\hat{x}^*(k-\mathrm{N})} = E_{\Phi^{-1}}\widehat{Q}_s E_{e_{k-N-1}} + E_{\Phi^{-1}}\left(\widehat{Q}_s - E_\Omega E_{\epsilon_s}\right)E_w. \quad (6.21)$$

Note that since $\widehat{Q}_s$ and $\widehat{P}_s$ are positively defined matrices, then $E_{\Phi^{-1}}\widehat{Q}_s \leq 1$. Then the state estimator is a stable system which is driven by additive white noise $w(k)$, where $\left\|E_{e_k}\right\|$ will converge to zero if $k \to \infty$.

6.3.4 1-bit estimator using the Kalman filter technique

Similar to the proposed RHE, a Kalman filter can also be used to implement the 1-bit state estimation. One can define $\mathrm{Q_{Kal}}$ and $\mathrm{R_{Kal}}$ respectively as the covariance of the process noise and the measurement noise. During the estimation process, the first step is to obtain the state estimation through an *a priori* estimate of the state and the error covariance of the current time step, based on information from the previous time step. Given a quantized *a posteriori* state estimation $q_\Delta\left(H_e\hat{x}(k-1)\right)$ at time step k-1, the *a priori* state estimate and estimate covariance can be found as

$$\hat{x}(k)^- = A(q_\Delta\left(H_e\hat{x}(k-1)\right) + Bu(k-1)$$

$$P_{Kal}\,(k)^- = AP_{Kal}\,(k-1)A^T + Q_{Kal}\,, \quad (6.22)$$

where $q_\Delta\left(H_e\hat{x}(k-1)\right)$ is the quantized state estimation of the previous time step. Then the Kalman gain can be updated as:

$$K_{Kal}(k) = P_{Kal}\,(k)^- {H_o}^T\left(H_o P_{Kal}\,(k)^- {H_o}^T + R_{Kal}\right)^{-1}, \quad (6.23)$$

where H_o is the observation matrix. Note that in Eq.6.23, H_o is modelled as identity as the state feedback is measurable in the proposed space mission. At the next time step, *a posteriori* estimation of the state and the error covariance are found by

$$\hat{x}(k) = \hat{x}(k)^- + K_{Kal}(k)(z(k) - H_o\hat{x}(k)^-)$$

$$P_{Kal}\,(k) = (1 - K_{Kal}(k)H_o)P_{Kal}\,(k)^-. \quad (6.24)$$

The estimated state variable $\hat{x}(k)$ is weighted in a $\Delta\sum$ modulator, then the quantized state variable can be presented as $q_\Delta\left(H_e\hat{x}(k)\right)$. The error covariance can then be found by substituting $\mathrm{K_{Kal}(k)}$ into

$$P_{Kal}(k) = P_{Kal}(k)^{-} - P_{Kal}(k)^{-}H_o{}^{T}\left(H_oP_{Kal}(k)^{-}H_o{}^{T} + R_{Kal}\right)^{-1}H_oP_{Kal}(k)^{-}. \tag{6.25}$$

Similar to the RHE case, the mean analysis can also be used to justify the use of the Kalman filter in the 1-bit processing system. Again given a stable closed-loop control law $U = -K_{mpc}\,x(k)$, simply minus $\hat{x}(k)$ with $x(k)$, we have

$$\hat{x}(k) - x(k) = (A - BK_{mpc})(q_\Delta\left(H_e\hat{x}(k-1)\right) - q_\Delta\left(H_ex(k-1)\right)) + K_{Kal}(k)H_o\Big(\left(A - BK_{mpc}\right)q_\Delta\left(H_ex(k-1)\right) - \left(A - BK_{mpc}\right)q_\Delta\left(H_e\hat{x}(k-1)\right)\Big). \tag{6.26}$$

Re-arrange Eq. 6.26, we have:

$$\hat{x}(k) - x(k) = \left(A - BK_{mpc}\right)(I - K_{Kal}(k)H_o)(q_\Delta\left(H_e\hat{x}(k-1)\right) - q_\Delta\left(H_ex(k-1)\right)). \tag{6.27}$$

Adopting again the mean analysis gives us that

$$E_{\hat{x}(k)} - E_{x(k)} = \left(A - BK_{mpc}\right)(I - K_{Kal}(k)H_o)(E_{\hat{x}(k-1)} - E_{x(k-1)}). \tag{6.28}$$

Then the expected value for the error can be derived as

$$\left\|E_{e(k)}\right\| = \left|\left(A - BK_{mpc}\right)(I - K_{Kal}(k)H_o)\right|\left\|\mathrm{E}_{e(\mathrm{k}-1)}\right\| \ . \tag{6.29}$$

Then if $K_{Kal}(k)$ is designed to be stable, then $\left\|E_{e(k)}\right\|$ will converge to zero if $\mathrm{t} \to \infty$. It is worth noting that, with known values of Q_{Kal} and R_{Kal}, the iterative solution of the covariance of the state vector estimation and the Kalman gain is not required in real time. Therefore, it is feasible to design the 1-bit Kalman filter under the framework of 1-bit processing control system.

6.4 Summary

In this chapter, we first discussed the OBMPC controller in a wirelessly control

system (WCS). The benefits of the OBMPC controller toward the WCS mainly include two aspects. Firstly, as a predictive control algorithm, a predicted data can be used if a data loss or a large time delay is detected. Although such predictions rarely coincide with the actual data, they still provide a reasonable estimation while retaining the operation of the control system. Secondly, as a 1-bit processing based control system, the control system is less sensitive to the noises and delays due to the oversampled modulation techniques.

However, the communication channels are still noisy and a 1-bit state estimator is required to improve the state feedback. A 1-bit processing based state estimator has been designed to improve such WCS architecture. Unlike the conventional state estimator methods, in the proposed OBMPC system, it is unnecessary to demodulate the 1-bit sensing signal to perform digital processing. The quantized data in the proposed 1-bit processing system can be processed directly by taking the advantages of signal processing techniques. If the loop filters of the $\Delta\sum$ modulator are well designed so that the filtered quantization noise power is retained within a small range, then the quantized sensing feedbacks can be treated as independent state feedback. Due to the nature of the 1-bit PDM, the modulated data can be demodulated by simply averaging a certain period of data group, i.e. according to the OSR. For example, if the sampling time is T_s, and the OSR is set to 200, then any 200 bits can be regarded as a single analogue measurement. From this point of view, the 1-bit data can be directly used in most filter techniques as the expectation of the resulted 1-bit state estimation over a certain period will be equivalent to the conventional state estimation results. Also, due to the 1-bit nature of the feedback data, the proposed estimator can be designed under the framework of the 1-bit processing control system, and therefore achieve a fast response, multiplier free structure. A 1-bit moving horizon estimator has been developed in this chapter as an example of the state estimator design. The design of the 1-bit Kalman filter is also discussed as a special case of the MHE. The simulation results will be discussed in the next chapter.

7. FRACTIONATED SATELLITE CONTROL SYSTEM IMPLEMENTATION, MATLAB SIMULATION AND HARDWARE IMPLEMENTATION

==========

==========

7.1 Mission Modeling

The OBMPC is designed for a fractionated satellite project in which two 2-unit CubeSats will be developed. One CubeSat serves as a master satellite, which carries a primary onboard controller and bus subsystems. The other one serves as a slave satellite, which carries payload sensors for actual scientific missions. The two CubeSats together form a "fractionated satellite" structure. The slave satellite has its own attitude sensors and actuators. However, the control algorithm runs on the primary onboard controller of the master satellite. The sensing and control signals are passed through a wireless data bus using the ISL. A charge exchange thruster (CXT) is developed as the attitude actuator for the slave satellite at the University of Sydney (Funamoto, et al., 2012). The CXT is only 50 grams in mass, which is specially designed for our nano-satellites.

7.1.1 Slave satellite dynamic model

A rigid-body satellite is used in this application as the slave satellite. It is symmetric about all three axes. Therefore, the equation of motion can be obtained for the attitude of the satellite using the Euler's equation of motion for a rigid body as described in Eq.7.1.

$$T_{ctrl} + T_g + T_d = I\dot{\omega}_{S/N} + \omega_{S/N} \times I\omega_{S/N}\,, \qquad (7.1)$$

where I is the inertia matrix of the satellite, $\omega_{S/N}$ and $\dot{\omega}_{S/N}$ are the angular rate and the angular acceleration of the satellite respectively in reference to the inertial system. T_{ctrl} is the control torque applied to the satellite by the actuator and T_d is the total disturbance. T_g is the linearized gravity gradient disturbance. The $\omega_{S/N} \times I\omega_{S/N}$ component represents a gyroscopic term between angular velocity vectors. The body coordinate system axes being the same as the main inertia axes, therefore, Eq.7.1 can be written in the scalar form:

$$\dot{\omega}_{S/Nx} I_x = \omega_{S/Ny}\omega_{S/Nz}(I_y - I_z) + T_x$$

$$\dot{\omega}_{S/Ny} I_y = \omega_{S/Nx}\omega_{S/Nz}(I_z - I_x) + T_y$$

$$\dot{\omega}_{S/Nz} I_z = \omega_{S/Nx}\omega_{S/Ny}(I_x - I_y) + T_z. \tag{7.2}$$

I_x , I_y and I_z are the inertia of the satellite about the x, y and z-axis; and T_x , T_y and T_z are the total torques about three axes respectively. An angular momentum in the coordinates of the orbital coordinate system can be expressed as

$$\omega_{S/N} = \omega_{S/R} + \overbrace{\begin{pmatrix} 1 & \varphi & -\theta \\ -\varphi & 1 & \emptyset \\ \theta & -\emptyset & 1 \end{pmatrix}}^{A_{DCM}} \begin{pmatrix} 0 \\ -\omega_o \\ 0 \end{pmatrix}, \tag{7.3}$$

where $\emptyset, \theta$ and φ are the Euler angles for three channels and A_{DCM} is the approximate result of the direction cosine matrix (DCM) for small angles (Vallado, 2001; Funamoto, et al., 2012). $\omega_{S/R}$ is the angular velocity of the reference attitude system and ω_o is the rotational velocity of the satellite. The quadratic terms can be ignored since they are of a low order. By denoting each axis in $\omega_{S/R}$ as $\omega_x, \omega_y, \omega_z$ respectively and by substituting Eq.7.3 into Eq.7.2, the linearized equation of motion can then be expressed as Eq.7.4:

$$\dot{\omega}_x = -\sigma_1\omega_o^2\varphi + (1-\sigma_1)\omega_o\omega_z + \frac{T_x}{I_x}$$

$$\dot{\omega}_y = \frac{T_y}{I_y}$$

$$\dot{\omega}_z = \sigma_3\omega_o^2\varphi - (1+\sigma_3)\omega_o\omega_x + \frac{T_z}{I_z}, \tag{7.4}$$

where $\sigma_1 = \frac{I_y - I_z}{I_x}$; $\sigma_2 = \frac{I_z - I_x}{I_y}$; $\sigma_3 = \frac{I_x - I_y}{I_z}$. Before continuing to build the state space model, we use Psiaki's idea (Vallado, 2001) to implement the linearized gravity gradient disturbance.

$$T_g = 3I\omega_o^2 \begin{pmatrix} -\sigma_1\emptyset \\ \sigma_2\theta \\ 0 \end{pmatrix}, \tag{7.5}$$

From Eq. 7.3 to Eq.7.4, the linear satellite dynamic model can be derived:

$$\dot{x} = Ax + \begin{bmatrix} 0_{3,3} \\ I^{-1} \end{bmatrix} T_{ctrl}, \tag{7.6}$$

where:

$$A = \begin{bmatrix} 0 & 0 & 0 & 1 & 0 & 0 \\ 0 & 0 & 0 & 0 & 1 & 0 \\ 0 & 0 & 0 & 0 & 0 & 1 \\ -4\omega_o^2\sigma_1 & 0 & 0 & 0 & 0 & \omega_o(1-\sigma_1) \\ 0 & 3\omega_o^2\sigma_2 & 0 & 0 & 0 & 0 \\ 0 & 0 & \omega_o^2\sigma_3 & -\omega_o(1+\sigma_3) & 0 & 0 \end{bmatrix};$$

The state vector is given as $x = (\emptyset\ \theta\ \varphi\ \omega_x\ \omega_y\ \omega_z)^T$. The inputs to the model have units in $[Nm]$.

7.1.2 Constraints on control torque

The control torque's saturation plays an important role in the attitude control process of fractionated satellites missions. Due to the constraints applied on actuators, the control process then becomes a non-linear control problem. As shown in Table 7.1, the maximum thrust for CXT in this case is limited to $86\mu N$ at the current stage when using Argon gas (Funamoto, et al., 2012).

Table 7.1 Thrust produced by the most recent CXT

Gas	Mass flow rate [sccm]	Applied voltage	Power Use [W]	Thrust[μN]
Hydrogen	7	12.5	2.7	18
Argon	<1	15	0.4	86

In this simulation, we consider the attitude control of a 2U CubeSat (20cm×10cm×10cm) by using two CXTs on each axis, where the maximum torque for the longer side is approximately 1.72×10^{-5}Nm. In the following simulation, 1×10^{-5}Nm is taken as the hard constraint for the control torque of the roll channel and yaw channel, and 0.5×10^{-5}Nm for the pitch channel.

7.1.3 Environmental models

1) Solar pressure:

The solar pressure will instantly jump to the highest value once the satellite comes out of the shadow of the earth and as soon as the satellite will reach the earth shadow again it will also vanish nearly instantly. This would be the worst case scenario for the controller. The force of the solar pressure is calculated with the following formula from (Vallado, 2001; Funamoto, et al., 2012):

$$F_{Solar} = p_S c_R A_{sat} \tag{7.7}$$

where p_S is the solar pressure, A_{sat} is the solar illuminated cross section area of the satellite and c_R = 2 is the reflection coefficient. Then the moment of solar disturbance can then be presented as

$$T_{Solar} = \begin{cases} F_{Solar} d_{Solar} \sin\beta & 90^o \le \beta \le 270^o \\ 0 & else \end{cases}, \tag{7.8}$$

where β is the angle of the latitude of the satellite, d_{Solar} is the torsion arm. The torque generated through the solar pressure normally just affects the attitude in the y-axis. However, if we have bigger attitude changes, with respect to the reference coordinate system, the x-axis of the satellite might also be affected. The z-axis is unaffected as long as the center of gravity is near the z-axis.

2) Aerodynamic drag

The acceleration due to aerodynamic drag can be estimated as

$$F_{aero} = -\frac{1}{2} c_D A_{sat} \rho v_{rel}^2$$

$$T_{aero} = F_{aero} \times d_{aero}\,, \tag{7.9}$$

where c_D is the coefficient of drag; ρ is the density of the air and v_{rel} is the relative velocity of the air and d_{aero} is the torsion arm of aerodynamic drag. In this work, we assume both disturbances are constant in the simulation.

7.2 System Architecture and Control System Design

An augmented model is proposed for the fractionated satellite attitude control mission. Consider a discretized linear satellite dynamic model

$$x_m(k+1) = A_m x_m(k) + B_m u(k)$$

$$y_m(k) = C_m x_m(k). \tag{7.10}$$

The state vector is given with $x = (\emptyset\ \theta\ \varphi\ \omega_x\ \omega_y\ \omega_z)^T$, which are fully observable. The inputs to the model are actuator torques (in [Nm]) for three axes. The model can be further translated into the δ-form by defining $A_\delta = \frac{A_m - I_m}{T}$, $B_\delta = B_m/T$, $C_\delta = C_m$, then Eq.7.10 can be rewritten as

$$x(k+1) = A_\delta x(k) + B_\delta u(k)$$

$$y(k) = C_\delta x(k). \tag{7.11}$$

One can further rewrite Eq.7.11 into the augmented model:

$$\begin{bmatrix} \Delta x_\delta(k+1) \\ y_\delta(k+1) \end{bmatrix} = \begin{bmatrix} A_\delta & 0_\delta{}^T \\ C_\delta A_\delta & I_{q\times q} \end{bmatrix} \begin{bmatrix} \Delta x_\delta(k) \\ y_\delta(k) \end{bmatrix} + \begin{bmatrix} B_\delta \\ C_\delta B_\delta \end{bmatrix} \Delta u(k)$$

$$y(k) = [0_\delta \quad I_{q\times q}] \begin{bmatrix} \Delta x_\delta(k) \\ y_\delta(k) \end{bmatrix}. \tag{7.12}$$

In addition to the benefits stated in Chapter 4, the augmented model also appears to be advantageous in WCS as it retains most of the properties of the dynamic system, while requiring fewer bits to specify the control signal (Vallado, 2001; Quevedo, et al., 2003). Integrators are required on the actuator side to obtain the control input. A new state variable vector is chosen to be $x = [\Delta x_m{}^T\ \mathrm{y_m}]^T$. For notational simplicity,

Eq.7.12 can be denoted as:

$$x(k+1) = Ax(k) + B\Delta u(k)$$

$$y(k) = Cx(k). \tag{7.13}$$

The OBMPC algorithm is used for the attitude control of the proposed mission. From the master to the slave satellite, the augmented control input is given as the increase of the control torque. They are modulated by $\Delta\sum$ Modulation, and the resultant 1-bit data are queued in a buffer and transmitted to the decentralized actuators in series. To avoid gyroscopic effects, only one axis is controlled at one time. All the other input previous channels are held at status while one desired actuation control in progress.

The attitudes of the slave satellite are sensed by the $\Delta\sum$ Modulator based MEMS gyroscope, and encoded into 1-bit data, and then transmitted back to the controller in 1-bit format as state feedback. Such 1-bit state feedback has information including the angular position and angular rate for all axes. A state estimator can be used at the controller side to decrease the noises generated during the communication process. The control system structure can then be denoted as Fig.7.1

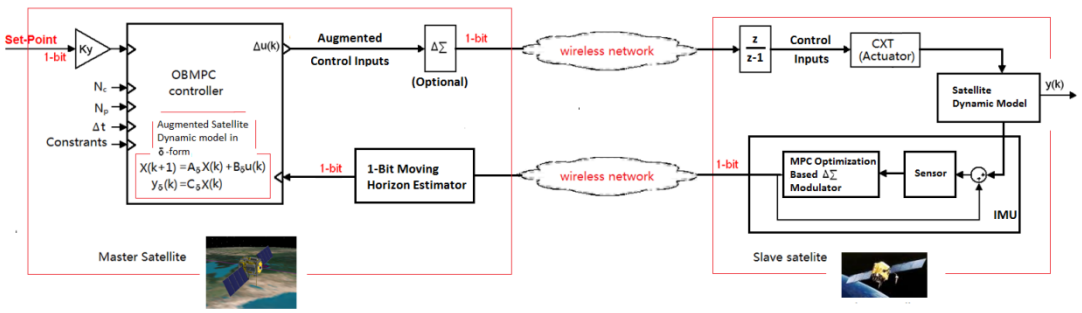

Figure 7.1 Fractionated satellite attitude control with OBMPC and 1-bit state estimator.

In Fig.7.1, the optimized control decision is solved online by the OBMPC controller using the attitude information. The control signals generated by the OBMPC controller are modulated and transmitted in the format of the augmented signals. Integrations are needed at the slave satellite end. The satellite's motion is measured by the $\Delta\sum$ Modulator based gyroscope as discussed in Chapter 5 and transmitted back to

the master satellite via the ISL. The sensor fusion technique will not be discussed in this work but is left as further work for researchers who are interested in the 1-bit processing control system.

To deal with the measurement noise, data loss or unexpected large time delay, a 1-bit moving horizon estimator is used for the state estimation. The output of the estimator will retain the characteristics of the 1-bit data and therefore enable the implementation of the OBMPC controller. Alternatively, the 1-bit MHE can be degraded into a 1-bit Kalman Filter by setting the prediction horizon as 1, and using the noise covariance as the tuning parameters during the design process.

7.3 Matlab Simulation

The structural data of a slave satellite is shown in Table 7.2.

Table 7.2 The slave satellite parameters

Orbit	Height(km)	320
	Time of Circulation(s)	1.6h
	Inclination(°)	79
	Velocity(m/s)	7572.3
	Rotational Velocity(1/s)	1.09×10^{-3}
Satellite Dynamic Model	Size(cm)	20×10*10
	Mass(kg)	2kg
	Moment of Inertia x-axis (kg*m^2)	5.98×10^{-3}
	Moment of Inertia y-axis (kg*m^2)	6.00×10^{-3}
	Moment of Inertia z-axis (kg*m^2)	9.64×10^{-3}

Based on Eq. 7.6, the continuous state-space model can be derived as

$$\dot{x}(t) = Ax(t) + Bu(t),$$

$$y(t) = Cx(t) \tag{7.14}$$

where:

$$A = \begin{bmatrix} 0 & 0 & 0 & 1 & 0 & 0 \\ 0 & 0 & 0 & 0 & 1 & 0 \\ 0 & 0 & 0 & 0 & 0 & 1 \\ -4.64\times10^{-6} & 0 & 0 & 0 & 0 & 1.28\times10^{-3} \\ 0 & 6.62\times10^{-7} & 0 & 0 & 0 & 0 \\ 0 & 0 & 0 & -1.08\times10^{-3} & 0 & 0 \end{bmatrix};$$

$$B = \begin{bmatrix} 0 & 0 & 0 \\ 0 & 0 & 0 \\ 0 & 0 & 0 \\ 1.46 \times 10^3 & 0 & 0 \\ 0 & 1.46 \times 10^3 & 0 \\ 0 & 0 & 1.22 \times 10^3 \end{bmatrix}; C = \begin{bmatrix} 0 & 0 & 0 & 0 & 0 & 0 \\ 0 & 0 & 0 & 0 & 0 & 0 \\ 0 & 0 & 0 & 0 & 0 & 0 \\ 0 & 0 & 0 & 1 & 0 & 0 \\ 0 & 0 & 0 & 0 & 1 & 0 \\ 0 & 0 & 0 & 0 & 0 & 1 \end{bmatrix}.$$

An OBMPC is designed and implemented on-board the master satellite to control the slave satellite. The initial attitude is assumed to be known and set as the reference for the attitude control. For three axes attitude control and stabilization, it is recommended that each time only one axis is controlled. The master satellite carries out control system processing for the slave satellite directly upon the 1-bit signals, and then encodes and transmits the control signal as 1-bit signals to the slave satellite to drive the actuators directly. Firstly, we shall examine the OBMPC in the proposed mission without the effect of data loss and random time delay. The state estimator is not used in the control loop for this analysis.

In the simulation, only the roll angle is controlled and the other two axes are set to zeros. The sampling time requirement is 10 seconds for the proposed mission. The OBMPC controller is considered with the *OSR* set to 200, so that the sampling time is 0.05s. Set N_p=4, N_c=4 and the weighting matrix R_w=0.5×10^7. P and Q are chosen to satisfy the Lyapunov equation $A^TPA+Q=P$. The set point for the roll angle is set to 1 degree. A conventional MPC controller is also simulated as a benchmark for the OBMPC based on the same sampling rate and tuning parameters.

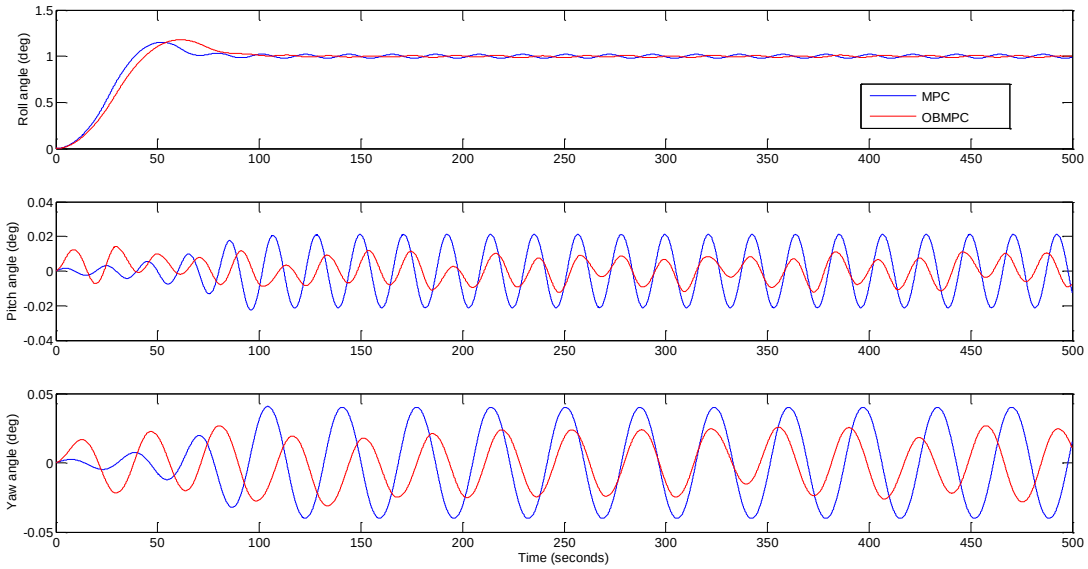

(a) Control result comparison

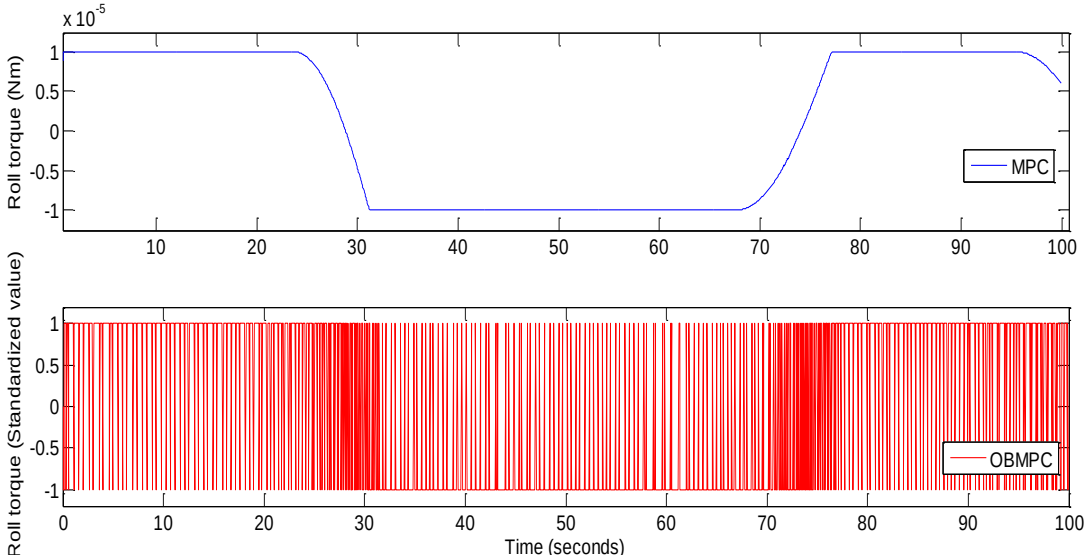

(b) Control torque comparison

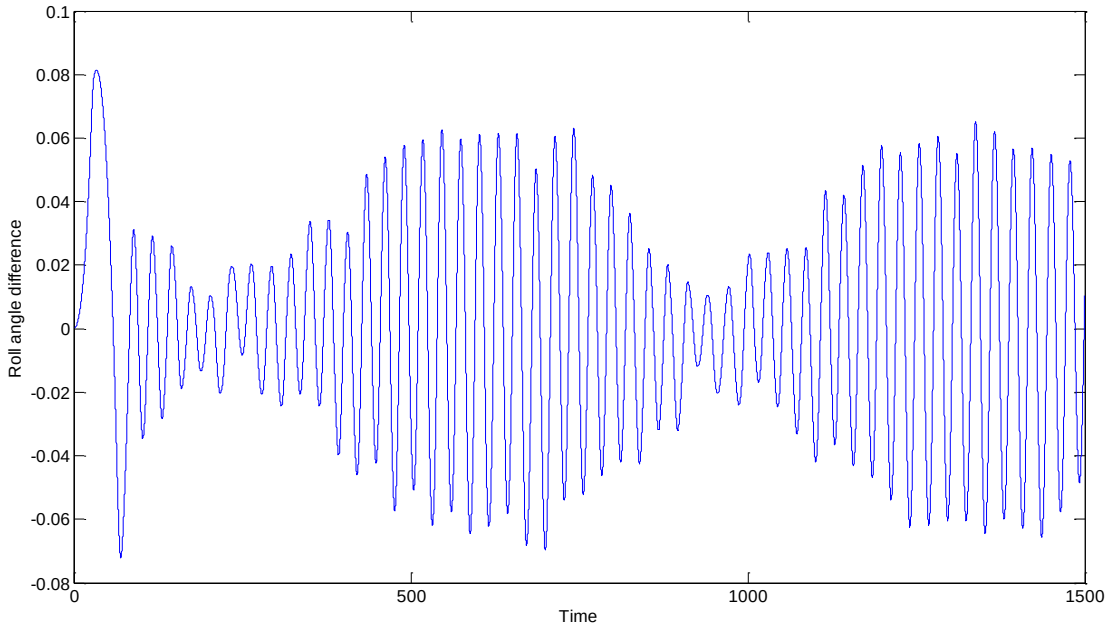

(c) Attitude difference between OBMPC and MPC

Figure 7.2 OBMPC *vs* MPC control simulation

In Fig.7.2(a), we can see that for the controlled roll angle axis, both controllers track the command and reach stable status in about 100 seconds. The difference between the stable values after 100 seconds is within 2%. The oscillations after 100 seconds are mainly caused by the gyroscopic effect. As suggested in Fig.7.2(b) and (c), the 1-bit signals are able to drive the satellite accurately.

For the benchmark controller, the OSR is actually not required. Hence, the OSR is removed and the sampling time of the control benchmark is changed to 10 seconds in the next simulation. N_p and N_c remain the same as the previous simulation. Other parameters including the sampling time of the OBMPC have been set to be the same as the previous simulation. It is shown in Fig.7.3 (a) and (b) that the proposed OBMPC provides similar control performance as the benchmark controller, but the control trajectory is smoother.

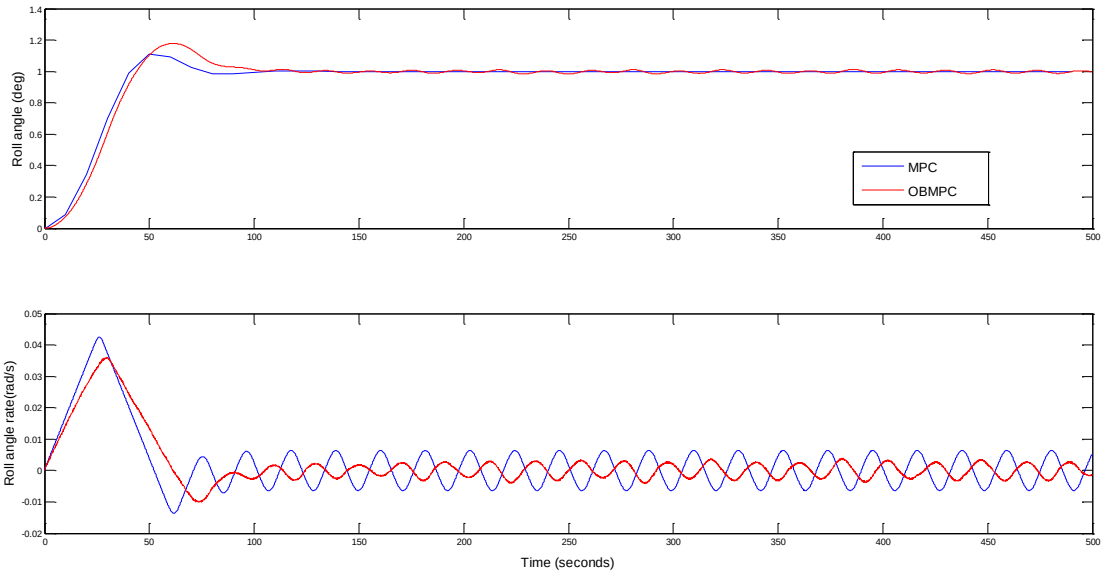

(a) comparison in terms of angular position and angular rate

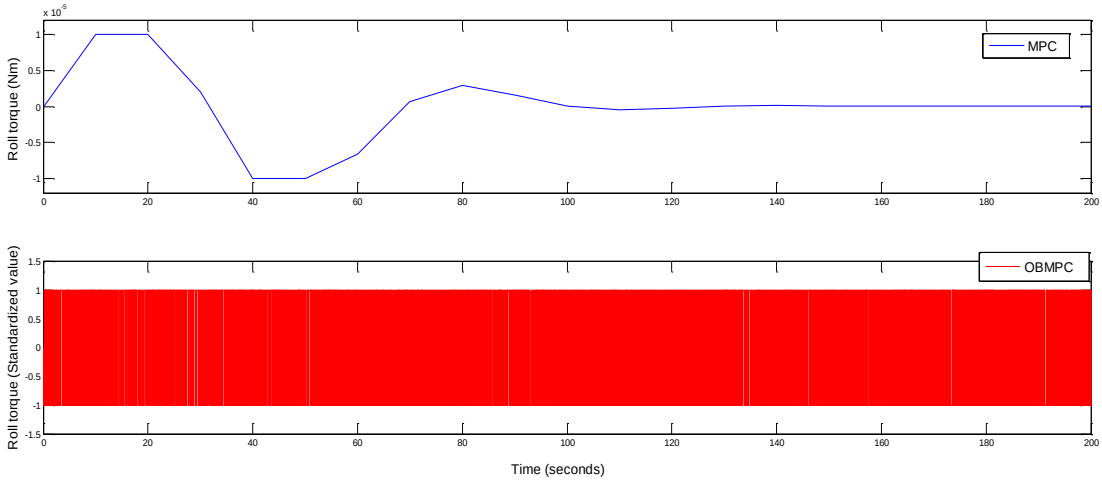

(b) Control torque comparison

Figure 7.3 Oversampled OBMPC vs MPC simulation

To further study the performance of the OBMPC in the WCS, the effects of the wireless communication are included in the system. In the following simulation, the wireless link can be modelled via a known fixed time-delay (i.e. the on-board computation time can be well estimated and the communication can be time-stamped so that the propagation delay during the communication can be explicitly known). Any unexpected time delay is regarded as data loss. The data loss rate is known based on experience models. In this case, the inputs to the actuators are held at their previous values. Also, random instant noises may occur during the communication, which may cause numerical flips (e.g. from 1 to 0) in the 1-bit data sequence. The

data loss and noisy data together form the communication noises, which are also implemented in the simulation. Firstly, two groups of random data losses are added into the OBMPC and the benchmark controller with no estimator in use. In both the OBMPC and its benchmark, the predicted control data is stored in the buffer and used as sub-optimal value if the data dropout occurs. The BER is set to be the same for both control loops where BER=10^{-3} (Although the BER of the ISL in the proposed mission is around 10^{-7}, the value was increased so that its influence on the result is notable within a small time period). The conventional MPC is using 16 bits binary signals to present the analogue signal.

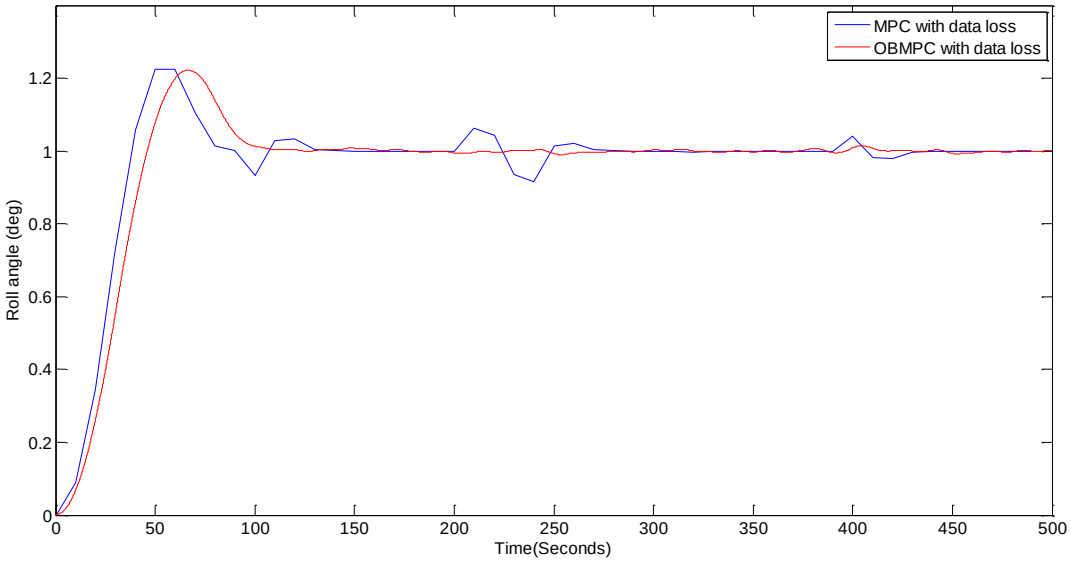

Figure 7.4 Oversampled OBMPC vs MPC with time delay and data loss

In the OBMPC, each data loss only presents a single bit error under the OSR. On the other hand, the conventional MPC will suffer the loss of the entire state feedback, i.e. the effect of the data loss in 1-bit processing control system will be diluted by the OSR, and evenly distributed in the highly sampled control feedbacks. From Fig.7.4, it is observed that the OBMPC control tracks the control trajectory accurately whereas its benchmark showed two notable V shape variation curve. Therefore the effect of data loss is less significant for OBMPC than conventional MPC.

Then we further integrate a 1-bit state estimator into the OBMPC system. As discussed in Chapter 6, it is possible to directly include to RHE to process the 1-bit

data without decimation, and provide the state estimation to the controller to perform control action. The main objective is to test the feasibility of implementing the 1-bit state estimator in the OBMPC system. Here, a RHE is designed to deal with the measurement noise, data loss and time delay. The BER remains the same so that $\gamma = 0.001$. A similar methodology can also be used to design a Kalman filter as discussed in chapter 6. The horizon is set to $N_e = 4$. No constraint is applied to the estimator. The simulation result is shown in Fig.7.5:

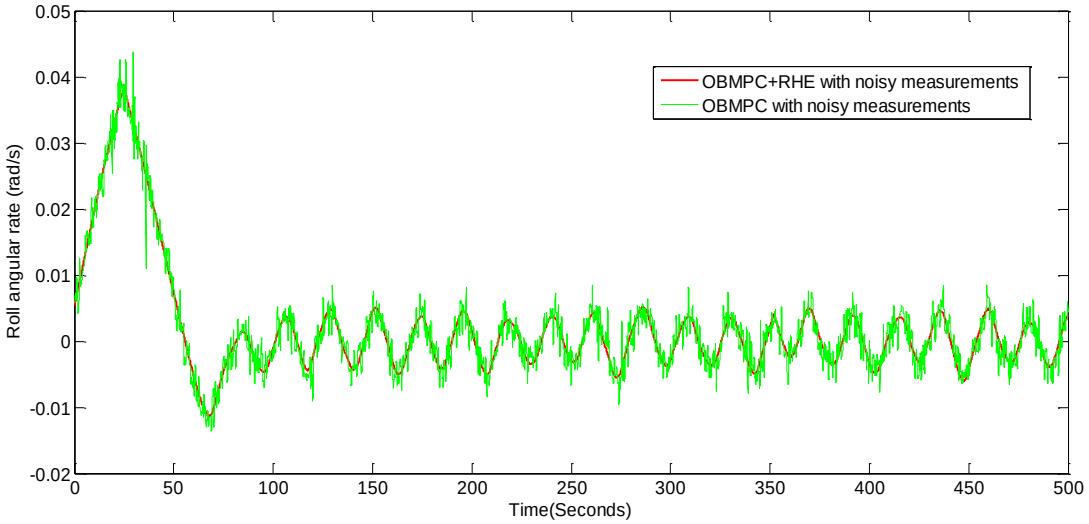

Figure 7.5 State estimation using the 1-bit RHE

Based on the RHE, the control trajectory is shown in Fig.7.6. A reference OBMPC (truth) is used as shown in dashed black.

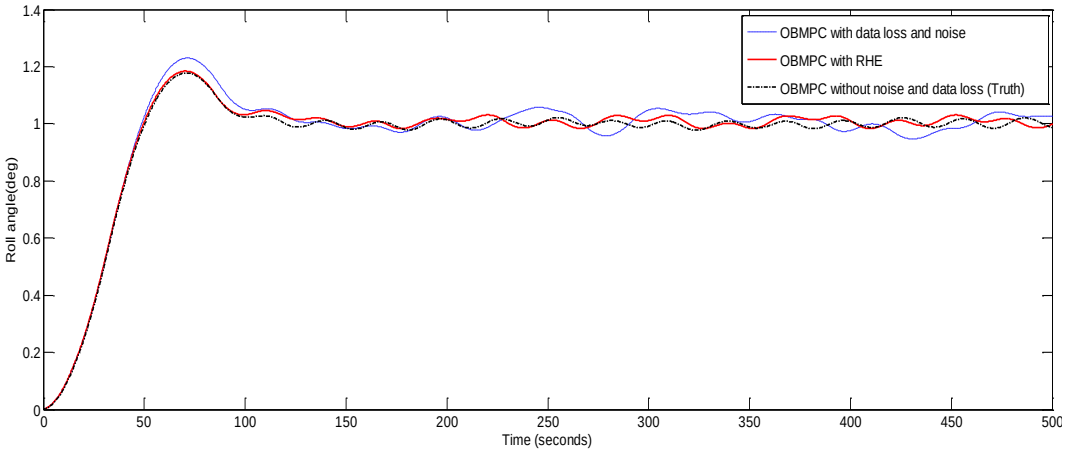

Figure 7.6 1-bit RHE for Oversampled OBMPC with time delay and data loss

It is observed in Fig.7.6 that the 1-bit RHE tracks its benchmark well despite of the noisy measurement and the noises introduced in the control loop, which proves that

the 1-bit RHE is as functional as usual RHE methods. Hence, it is feasible to include the state estimators in the control loop.

Based on the simulation results provided above, conclusions can be drawn that the OBMPC controller is feasible for MIMO satellite attitude control systems, and can provide better results under the OSR when compared to the conventional MPC benchmark. To further verify the onboard resource consumption issues in terms of speed, power and area, the above simulations are implemented in a field-programmable gate array (FPGA) board.

7.4 Hardware Implementation

7.4.1 Arithmetic Blocks

The arithmetic blocks used to implement the OBMPC are relatively simple. As discussed in the previous chapters, the state feedback in the OBMPC is restricted to the quantization level set $\mathbb{X} = \{\Delta, -\Delta\}$ and the optimal solution is uniquely defined as a piecewise affine function over $\mathbb{X}^n$. In other words, the control input at each time step can be mapped with respect to the 1-bit state feedback and the pre-calculated multi-bit controller coefficient. If the quantization levels can be chosen as values of 2's power, then there are only three arithmetic operations that are needed to complete all the calculations in the OBMPC: conditional-negate (CN), add and shift. (The quantization levels need to be carefully chosen to satisfy the stability issues discussed in Chapter 4. It is normally restricted in a specified range between stability requirement and SNR requirement. Practically, one can use the closest value of 2's power which is just larger than the maximum modulator input, e.g. control input/output saturation, as the quantization level). Among these operations, the CN and shift operations can substitute for the conventional multipliers: the CN operation is used to change the sign of the coefficients and the shift operation is used to scale the coefficients to the quantization level. Normally, right shift operations are applied as the quantization level is larger than the modulator input. The negative sign is

included in the coefficients for negative feedbacks so that the subtract operation is avoided. A comparison between a CN-shift operation and a conventional multiply-and-accumulation (MAC) arithmetic block implementation has been as presented in Table 7.3. Such MAC uses two data types: a 6-bit mantissa and a 5-bit exponent for coefficients and a 27-bit signed fixed point form for state variables. The results are obtained by realizing these operations with a VLSI process which is the UMC 0.13μm, 8-layer copper process. The power consumptions of these designs are also estimated in Synopsys Power Compiler (Cumplido-Parra, et al., 2001).

Table 7.3 Comparisons between arithmetic operations

	Conventional		1-Bit Processing		
	Multiply	MAC	CN	Add	Shift
Area(μm^2)	21351.1	25369.1	1229.8	4800.4	3337.6
Frequency(*MHZ*)	621.2	440.7	2597.4	2143.6	2520.8
Power(*mW*)	5.0805	5.7825	0.1838	0.7263	0.4820

It can be seen from Table.7.3 that the area and power consumption of arithmetic operations used for the proposed structure are significantly smaller than the conventional one. It is worth noting that for longer bit length, the "1-bit" shows even more privilege than the conventional ones as the area and power consumption increase significantly with the increase of bit length while CN and Shift operations remain almost the same. So by eliminating the multipliers, in theory the OBMPC can achieve better performance in terms of area, speed and power. Such a proposition will be verified in the next section.

7.4.2 Direct implementation

The FPGA implementation made in this thesis is for design verification purpose only. Hence, a simple direct implementation is discussed in this section. For conventional MPC implementation, some improvements have been made to optimize matrix multiplication based on the work proposed in (Cumplido-Parra, et al., 2001). The

FPGA resource occupation and the power consumption are estimated by Xilinx power estimator (XPE) for both the MPC and the OBMPC. 1-bit signals are embedded into the OBMPC by second order $\Delta\sum$ modulators on both control inputs and feedbacks. The $\Delta\sum$ modulators for the control inputs act as A/D converters which are located off chip while the ones for the feedbacks are integrated in the MEMS to incorporate the sensors on the slave satellites. The coefficients are pre-calculated and hard wired on-chip. The global optimal solution and the modified Lagrange multiplier stated in Eq. 4.21 and Eq. 4.27 are processed and stored in registers. At each time step, the state feedback $x(k)$ is acquired from sensors as controller inputs and the controller outputs are calculated and written to the output port of the chip. All the calculations operate on two's complement numbers. The sign bit identifies a value as positive or negative, where 1 means a negative value and 0 means a positive value.

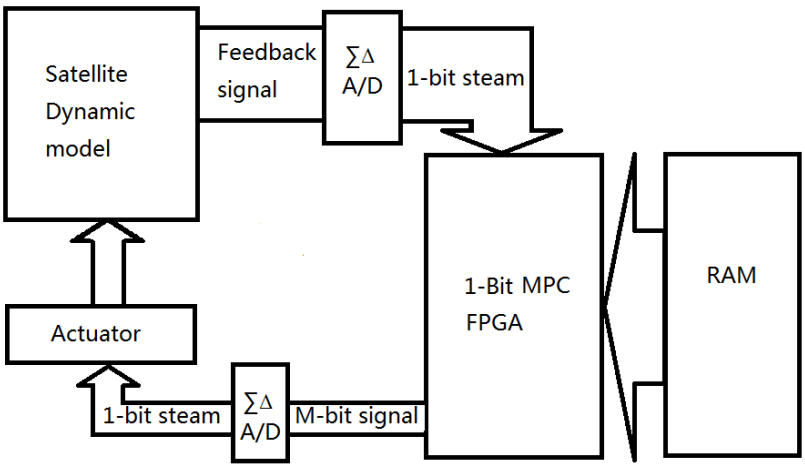

Figure 7.7 The FPGA implementation for satellite attitude control mission.

The proposed OBMPC hardware implementation can follow the steps stated below:

1. Acquire the 1-bit feedback signal and calculate the global optimal solution using Eq.4.21. Since there are only two states for a modulated $\Delta\sum$ signal, the global optimal solution can be solved by simple bit shifts and sign switching operations as suggested in Lemma 4.1, e.g. only conditional-negates (CN) and bit shifters are required to process the multiplication between the 1-bit signal and parameters.

2. Compare the global optimal solution with all the constraints. If there is no violation, send the solution to the actuator and go back to step (1).
3. Otherwise, calculate the modified Lagrange multiplier $\bar{\lambda}$ using Eq. 4.27. The operation remains between 1-bit feedback signals and parameters. Repeat the step until the Lagrange multiplier converges to zero (or small enough), which means the solution is optimal enough (Normal finite loop can be set to converge the Lagrange multiplier).
4. Solve Eq.4.27 with $\bar{\lambda}$, and send the resulting actuation signal to the actuator then go back to step 1

A flow chart of the simulation configuration is shown in Fig.7.7.

Matrix operations in Eq.4.21 and the iteration process in Eq.4.28 are resource expensive for FPGA implementations. Since Ω, ϕ and G are constant matrices, matrix inversions can be pre-calculated offline to balance performance and resource utilization. Only input optimization with respect to state feedback needs to be processed in real time. Xilinx Vertex5 330t is used as the simulation device for both implementations.

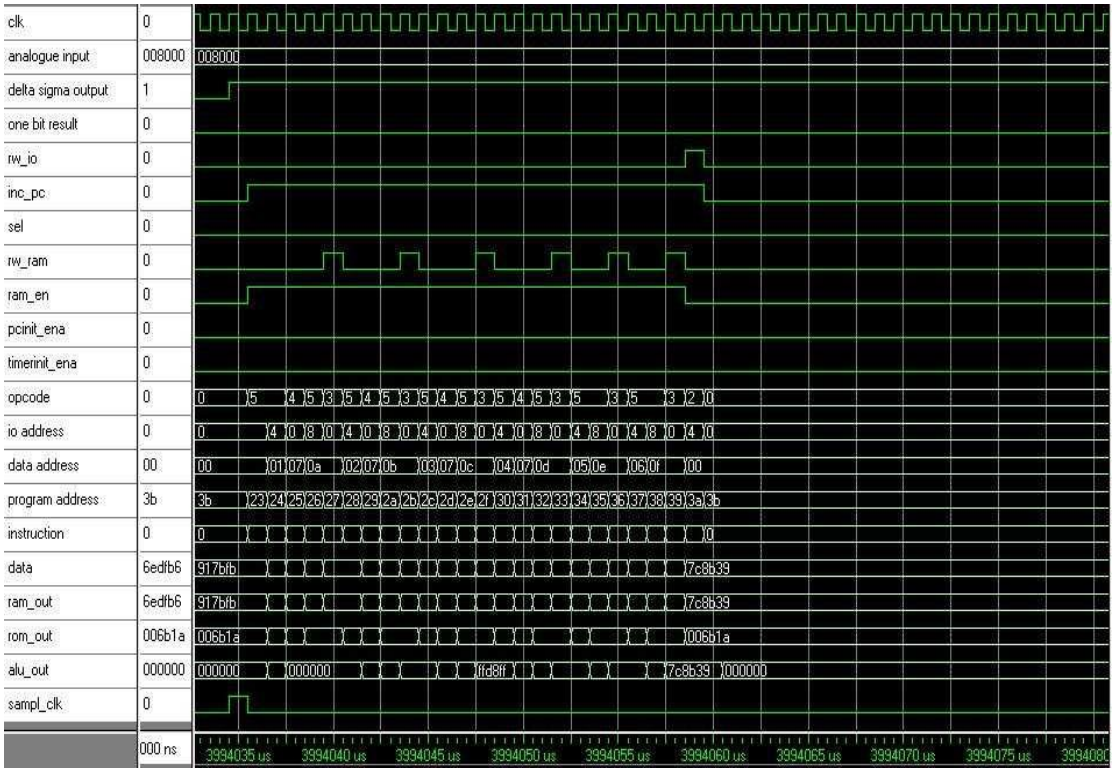

Figure 7.8 Simulation in Progress

The design summary is listed in Table 7.4.

Table 7.4 Direct implementation design summary

	MPC			OBMPC		
Slice Logic Utilization	Used	Available	Utilization	Used	Available	Utilization
Number of Slice Registers	3,361	207,360	1%	2,112	207,360	1%
Number of Slice LUTs	81,462	207,360	39%	17,462	207,360	8%
Number of occupied Slices	26,841	51,840	51%	6,684	51,840	12%
Number of fully used LUT-FF pairs	3,268	17,850	18%	1,724	17,850	9%
Number of BUFG/BUFGCTRLs	1	32	3%	1	32	3%
Number of DSP48E1s	192	192	100%	0	192	0%

As presented in Table.7.4, the OBMPC controller has much lower circuit complexity. The occupied slices are less than half and the Slice Lookup Tables (LUTs) are about 2/3 less in comparison to its benchmark, and the later one also used up all the DSPs in the device. The power consumption for both implementations is compared in Table.7.5

Table 7.5 (a) Detailed power consumption for the OBMPC and the MPC

Ambient Temp: 0 °C		OBMPC			MPC		
Supply Summary		Total	Dynamic	Quiescent	Total	Dynamic	Quiescent
Source	Voltage	Current(A)	Current (A)	Current(A)	Current(A)	Current(A)	Current(A)
Vccint	1.000	1.161	0.017	1.144	1.193	0.049	0.145
Vccaux	2.500	0.353	0.000	0.353	0.353	0.000	0.353
Vcco25	2.500	0.012	0.000	0.012	0.012	0.000	0.012

(b) Power consumption comparison between MPC and Oversampled OBMPC

	Frequency	Supply Power (W)		
		Total	Dynamic	Quiescent
OBMPC(Oversampled)	1MHz	2.074	0.017	2.057
MPC	5kHz	2.106	0.049	2.057

The clock for OBMPC is set to 200 times higher than the MPC controller to show the power comparison under the effect of OSR. It can be seen from Table.7.5 that with OSR, the dynamic power consumption for the proposed OBMPC controller (17mW) is much smaller than MPC controller (49mW). Hence, even under the effect of OSR, the OBMPC still shows notable power efficiency over the conventional MPC.

7.5 Summary

In this chapter, a fractionated attitude control system has been developed and simulated. Firstly, the dynamic model of the slave satellite (the control objective) has been modeled, along with the constraints applied on the actuator. An environmental model has then been introduced. The parameters of the mission modeling are based on a 2-unit CubeSat satellite structure designed for the QB50 space mission.

Secondly, the control system structure has been introduced. The controller is located on the master satellite while the actuator is fractionated in the space and wirelessly controlled via the ISL. The 1-bit sensing component discussed in Chapter 5 has been used to provide 1-bit state feedback to the controller. Also a 1-bit state RHE has been used to deal with the data loss and the large time delays introduced by the ISL. The Matlab simulation results have proven the feasibility of the OBMPC controller of the proposed space mission, as well as the efficiency of the proposed 1-bit RHE.

To further prove the efficiency of the OBMPC controller, a direct implementation has been conducted based on the Xilinx vertex5 330t FPGA board. Comparison has been made between an oversampled (with the OSR=200) OBMPC controller and a conventional MPC controller. The design summary verified that the OBMPC controller has much lower circuit complexity in term of the occupied slices (less than 1/2 of its benchmark) and the Slice LUTs (about 2/3 less comparing to its benchmark). The implementation of the conventional MPC also used up all the DSPs in the device. Power consumption for both implementations have been compared. The dynamic power consumption of the proposed oversampled OBMPC structure (17mW) is much smaller than MPC structure (49mW). The simulation results show that circuit complexity of the OBMPC structure is much simpler than that of the conventional one. Also even under the effect of OSR, the OBMPC structure still shows notable power efficiency over the conventional MPC structure.

8. CONCLUSIONS

==========

8.1 Main Contributions
8.2 Limitations and Further Work

==========

8.1 Main Contribution

8.1.1 Design of an OBMPC framework

The OBMPC controller design has been discussed in this work. The 1-bit processing control system is based on the bi-level $\Delta\sum$ modulation. The resultant 1-bit data is in PDM nature which includes all the useful information but also includes quantization noises. As a nonlinear component, the behaviour of the $\Delta\sum$ modulation can be modelled by linearizing the quantization noise into additive white noise. To maintain the robustness of the controller, such noise needs to be sufficiently shaped to decrease the noise within the bandwidth of interest. A build-in noise shaping filter is applied to address this problem, but this may also require a high OSR to achieve the desired precision.

If high OSR is engaged, the fast sampled control system may trigger various problems to the control loop. Firstly, the high sampling rate normally means long word length, which means it is impractical for implementation. Secondly, the use of small time intervals may be a challenge to the controller, especially for the embedded control systems where the on-board resources are limited. This means the controller needs to be carefully customized to suit the needs of the 1-bit processing control system. The discussion of the 1-bit processing based PID control system has been conducted in Chapter 3, along with a numerical simulation utilizing a small satellite model.

Similar to the 1-bit processing control system discussed in Chapter 3, we first addressed the numerical issues generated by the high sampling rate, i.e. the OSR. High sampling rate may result in long word lengths for both coefficients and variables

within the controller, which will compromise the accuracy of the controller considering that limited bits are allowed for almost all the digital controllers. In the OBMPC controller, a δ-transform is proposed to replace the conventional *z* transform to overcome such numerical issues by performing a simple linear transformation. The design of the OBMPC structure is built on the 1-bit processing control system. Due to the online optimization nature, direct implementation of the MPC algorithm is not suitable for most embedded control systems, especially the ones with high sampling rates and/or limited onboard resources. The core idea of the OBMPC algorithm is to take the advantage of the explicit relation between the multi-bit coefficients and 1-bit controller state feedbacks. All the operations in the embedded controller can be achieved by simply using conditional-negate (CN), add and shift operations. Therefore, the control loop can be implemented with a multiplier free approach. As multiplications are the major power consumer for the onboard controller, the OBMPC structure can be very efficient in term of power and circuit complexity. The system is in digital control nature, affected by quantization noise introduced by $\Delta\sum$ modulators.

To achieve such multiplier free structure, the explicit relationships between the 1-bit state feedbacks and the multi-bit coefficients shall be derived subject to:

1) unconstrained systems;
2) constrained system with convex constraint sets;
3) constrained system with non-convex constraint sets.

It has been proven that all the above three system can be implemented under the OBMPC scheme. It is worth noting that other than the demonstrated method developed in Chapter 4, many other fast MPC schemes can be implemented by the OBMPC structure directly or with minor modifications.

8.1.2 Stability analysis for the OBMPC algorithm and design criteria

The stability analyses for the OBMPC algorithm and design criteria are included in

this work. The stability issues for the ΔΣ modulation based control system are difficult to analyze, especially for high order ΔΣ modulators due to the non-linearity nature of the quantizer and the integrators in the structure. In Chapter 4, we first discussed the problem using the stable MPC controller as well as the stable ΔΣ modulator method for the stable OBMPC system design based on the assumptions that high OSR is provided and that the quantization noise is well filtered by the in loop filters of the ΔΣ modulator. In this case, designing a stable ΔΣ modulator is very important. The stability analysis involved designing the quantization level, followed by some stability criteria collected for stable ΔΣ modulator design. Also, general stability analyses for the MPC algorithm has also been briefly introduced in this section. If the OSR is not sufficiently high, that is, when the quantization noise is not small enough to be ignored, it can be proven that the signal-plus-white-noise structure as suggested in Chapter 3 is also suitable for the OBMPC algorithm, and therefore a stable close-loop control system can be designed. Moreover, a sufficient condition can be found to determine the positively invariant set of the OBMPC system with the control horizon $N_c = 1$.

8.1.3 Design of the 1-bit MEMS gyroscope sensor

Chapter 5 discussed a 1-bit ΔΣ modulator based MEMS gyroscope for the OBMPC system. It serves as the sensing component and modulates the control signal into the 1-bit format. In fact, embedding the ΔΣ modulator with the MEMS gyroscopes turned out to be a successful application due to the circuit simplicity and the benefits of incorporating the sensing component in a feedback control loop. If one treats the sensing mode of the gyroscope dynamics as a second order transfer function, then designing a bi-level ΔΣ modulator based MEMS gyroscope (i.e. a 1-bit MEMS gyroscope) falls into the framework of the 1-bit processing control system as discussed previously.

To further improve the 1-bit MEMS gyroscope, the MPC algorithm can be used to minimize the quantization noise introduced by the ΔΣ modulator. A direct

implementation of the OBMPC structure to the MEMS gyroscope has then been studied. In comparison to the work achieved in (Cumplido-Parra, et al., 2001; Quevedo and Goodwin, 2005), the proposed method can include the constraints to the quantizer inputs, which serve as a clipping technique to stabilize the $\Delta\sum$ modulator if quantizer overloading occurs.

8.1.4 Design of the 1-bit Moving Horizon Estimator

A 1-bit processing based moving horizon estimator has been proposed in this work as an example of implementing the state estimator in the 1-bit processing based control systems. For the proposed space mission, the control system is maintained by the communication via the ISL. Due to the harsh space environment, a state estimator is required to deal with the noises and data loss during the communication process. Typically, the quantized data is demodulated at the state estimator to reconstruct the multi-bit signal in order to perform an estimation of the future state and the covariance of noise. Such demodulation would once again require digital signal processing, which removes the benefit of simple, direct implementation of the 1-bit processing control system.

In the proposed OBMPC system, it is unnecessary to demodulate the 1-bit sensing signals to perform digital processing like other approaches. The modulated signals can be treated as independent measurement information with shaped quantization noise and can be processed directly by most signal processing techniques. From this point of view, the 1-bit data can be directly used in most types of Kalman filter or other sensor state estimation techniques. To prove this conclusion, a 1-bit processing based moving horizon estimator has been proposed in Chapter 6 as the state estimator for the OBMPC system. Therefore in the proposed OBMPC technique, one can avoid the use of complex A/D convertors in the control loop and retain the benefits of the simple 1-bit format state feedback.

8.1.5 Feasibility study and hardware implementation for the OBMPC in a fractionate satellite attitude control mission

To verify the OBMPC controller and validate the claimed power efficiency for the proposed fractionate satellite attitude control mission, simulation and hardware implementation are developed in this work.

For the proposed OBMPC controller, the author has firstly verified it in a motor control system in Chapter 4 to prove the feasibility of the algorithm. Then in Chapter 7, the control system is designed to perform attitude control for a nano-satellite in a fractionated satellite mission to validate the proposed OBMPC control algorithm. Simulations have been made to compare the OBMPC. The simulation results of both the OBMPC and the traditional MPC are compared in Matlab. The efficiency of the OBMPC is also compared in terms of power and area with the conventional MPC using FPGA implementations.

8.2 Limitations and Further Work

8.2.1 1-bit data fusion techniques

In this work, the author assumed that the acquired sensory data is accurate before being modulated by $\Delta\sum$ modulators. However, noises generated by the gyroscope such as gyroscope bias, bias instability (which is a major concern in MEMS gyroscopes), gyroscope scale factor error and nonorthogonality, are not considered in this work. Also, to acquire more dependable sensory data, disparate sources could be necessary for some desired propositions. Typically, a sensor fusion center is required. The quantized data is collected and demodulated at the sensor fusion center to perform an estimation of future states and the covariance of noise. Given the 1-bit processing concept developed throughout the thesis, one can design a 1-bit sensor fusion technique which processes the 1-bit data directly without demodulation. For the sake of brevity, the design of a data fusion center is reserved for the further work. The authors hope the design of the 1-bit state estimator presented in Chapter 6 can

induce more valuable contributions, i.e.1-bit control system based sensor fusion techniques, to improve the 1-bit processing control systems.

8.2.2 Direct communication using the 1- bit data.

New space network system developments, e.g. the development of Interplanetary Internet (e.g. InterPlaNet) protocol will certainly improve the control results of the fractionate satellite attitude control missions. Also, new development of the communication techniques, e.g. optical communication for satellites (Quevedo and Goodwin, 2005), will also improve the communication results. As the 1-bit processing control systems are usually highly sampled, if the communication channels can be well established, where the BER is reasonably small, one can send the 1-bit data directly via the ISL without extra modulation techniques. For example, as proposed in (Wissinger, 1995), an all optical binary $\Delta\sum$ modulator is used. It provides faster A/D conversion and induces less noise in the modulation loop. More importantly, it uses the electro-optical modulator (EOM) which provides optical outputs. If the range of such optical modulators can be extended to the operational range of a fractionated satellite mission, then the data can be directly transmitted to the control object. Such communication will base on only the physical layer and the communication protocol can be greatly simplified.

8.2.3 Implementation of high efficiency OBMPC controllers

In this work, to verify the power efficiency of the OBMPC control, a direct implementation method is adopted. To further improve the feasibility of the OBMPC control for the proposed mission, high efficiency OBMPC control system processor (CSP) can be developed to adopt the embedded controller for a proposed satellite mission. Moreover, it is necessary to guarantee that all the variety of functions can be processed under the sampling time interval to maintain the real-time performance. Therefore, a dual processor or a pipelining structure can be adopted to satisfy the required computational power. Moreover, as an implementation method, the OBMPC can be combined with many other techniques such as model reduction methods, fast

online QP solvers and hybrid control schemes.

REFERENCES.

Adams, R. W. (1984). "Companded predictive delta modulation: a low-cost conversion technique for digital recording." Journal of the Audio Engineering Society 32(9): 659-672.

Afanasiev, K. and Hinze, M. (2001). "Adaptive control of a wake flow using proper orthogonal decomposition." Lecture Notes in Pure and Applied Mathematics: 317-332.

Agudelo, O. M., Baes, M., Espinosa, J. J., Diehl, M. and De Moor, B. (2009). "Positive polynomial constraints for POD-based model predictive controllers." Automatic Control, IEEE Transactions on 54(5): 988-999.

Alessandri, A., Baglietto, M. and Battistelli, G. (2003). "Receding-horizon estimation for discrete-time linear systems." Automatic Control, IEEE Transactions on 48(3): 473-478.

Alessio, A. and Bemporad, A. (2009). A survey on explicit model predictive control. Nonlinear model predictive control, Springer: 345-369.

Antonello, R. and Oboe, R. (2012). "Exploring the potential of MEMS gyroscopes: successfully using sensors in typical industrial motion control applications." Industrial Electronics Magazine, IEEE 6(1): 14-24.

Antoulas, A. (2005). "An overview of approximation methods for large-scale dynamical systems." Annual reviews in Control 29(2): 181-190.

Antoulas, A., Sorensen, D. and Gugercin, S. (2001). "A survey of model reduction methods for large-scale systems." Contemporary mathematics 280: 193-220.

Ardalan, S. and Paulos, J. (1987). "An analysis of nonlinear behavior in delta-sigma modulators." Circuits and Systems, IEEE Transactions on 34(6): 593-603.

Atwell, J. A., Borggaard, J. T. and King, B. B. (2001). "Reduced order controllers for Burgers' equation with a nonlinear observer." Applied Mathematics And Computer Science 11(6): 1311-1330.

Axehill, D. and Hansson, A. (2008). A dual gradient projection quadratic programming algorithm tailored for model predictive control. Decision and Control, 2008. CDC 2008. 47th IEEE Conference on, IEEE.

Aziz, P. M. and Sorensen, H. V. (1996). "An overview of sigma-delta converters." Signal Processing Magazine, IEEE 13(1): 61-84.

Bai, X. and Wu, X. (2011). Customized Processor Architecture for Model Predictive Control in Magnetic Actuated Small Satellites. Advanced Electrical and Electronics Engineering, Springer: 71-79.

Bai, X. and Wu, X. (2013). "1-Bit Processing Based Model Predictive Control for Fractionated Satellite Missions." Acta Astronautica.

Baird, R. T. and Fiez, T. S. (1994). "Stability analysis of high-order delta-sigma modulation for ADC's." Circuits and Systems II: Analog and Digital Signal Processing, IEEE Transactions on 41(1): 59-62.

Barnhart, D. J., Vladimirova, T. and Sweeting, M. N. (2007). "Very-small-satellite design for distributed space missions." Journal of Spacecraft and Rockets 44(6): 1294-1306.

Bemporad, A. and Filippi, C. (2003). "Suboptimal explicit receding horizon control via approximate multiparametric quadratic programming." Journal of optimization theory and applications 117(1): 9-38.

Bemporad, A. and Morari, M. (1999). Robust model predictive control: A survey. Robustness in identification and control, Springer: 207-226.

Bemporad, A., Morari, M., Dua, V. and Pistikopoulos, E. N. (2002). "The explicit linear quadratic regulator for constrained systems." Automatica 38(1): 3-20.

Bemporad, A. and Patrinos, P. (2012). Simple and certifiable quadratic programming algorithms for embedded linear model predictive control, IFAC.

Best, M. J. (1996). An algorithm for the solution of the parametric quadratic programming problem, Springer.

Bhattacharya, R. and Balas, G. J. (2004). "Anytime control algorithm: Model reduction approach." Journal of Guidance, Control, and Dynamics 27(5): 767-776.

Bitmead, R., Gevers, M. and Wertz, V. Adaptive optimal control: the thinking man's GPC, 1990, Prentice-Hall, New York.

Bourdopoulos, G. I., Anastassopoulos, V., Pnevmatikakis, A., & Deliyannis, T. L. (2003). Delta-Sigma Modulators Modeling, Design and Applications, Imperial College Press.

Boyd, S. and Vandenberghe, L. (2009). Convex optimization, Cambridge university press.

Branicky, M. S., Phillips, S. M. and Zhang, W. (2000). Stability of networked control systems: Explicit analysis of delay. American Control Conference, 2000. Proceedings of the 2000, IEEE.

Brooks, T. L., Robertson, D. H., Kelly, D. F., Del Muro, A. and Harston, S. W. (1997). "A cascaded sigma-delta pipeline A/D converter with 1.25 MHz signal bandwidth and 89 dB SNR." Solid-State Circuits, IEEE Journal of 32(12): 1896-1906.

Brown, O. and Eremenko, P. (2006). Fractionated space architectures: a vision for responsive space, DTIC Document.

Brown, O., Eremenko, P. and Hamilton, B. (2002). "The value proposition for fractionated space architectures." Sciences 99(1): 2538-2545.

Bui-Thanh, T., Willcox, K., Ghattas, O. and van Bloemen Waanders, B. (2007). "Goal-oriented, model-constrained optimization for reduction of large-scale systems." Journal of Computational Physics 224(2): 880-896.

Burns, R., McLaughlin, C. A., Leitner, J. and Martin, M. (2000). TechSat 21: formation design, control, and simulation. Aerospace conference proceedings, 2000 IEEE, IEEE.

Chan, H. and Ozguner, U. (1994). Control of interconnected systems over a communication network with queues. Decision and Control, 1994., Proceedings of the 33rd IEEE Conference on, IEEE.

Chao, K.-H., Nadeem, S., Lee, W. L. and Sodini, C. G. (1990). "A higher order topology for interpolative modulators for oversampling A/D converters." Circuits and Systems, IEEE Transactions on 37(3): 309-318.

Chen, C. and Shaw, L. (1982). "On receding horizon feedback control." Automatica 18(3): 349-352.

Chen, H. and Allgöwer, F. (1998). "A quasi-infinite horizon nonlinear model predictive control scheme with guaranteed stability." Automatica 34(10): 1205-1217.

Chisci, L., Lombardi, A. and Mosca, E. (1996). "Dual-receding horizon control of constrained discrete time systems." European Journal of Control 2(4): 278-285.

Cohen, A., Daubechies, I. and Vial, P. (1993). "Wavelets on the interval and fast wavelet transforms." Applied and Computational Harmonic Analysis 1(1): 54-81.

Cohen, K., Siegel, S., Seidel, J. and McLaughlin, T. (2006). "Reduced order modeling for closed-loop control of three dimensional wakes." AIAA Paper 3356.

Colson, B., Marcotte, P. and Savard, G. (2005). "Bilevel programming: A survey." 4OR 3(2): 87-107.

Cortés, P., Kazmierkowski, M. P., Kennel, R. M., Quevedo, D. E. and Rodríguez, J. (2008). "Predictive control in power electronics and drives." Industrial Electronics, IEEE Transactions on 55(12): 4312-4324.

Cortes, P., Wilson, A., Kouro, S., Rodriguez, J. and Abu-Rub, H. (2010). "Model predictive control of

multilevel cascaded H-bridge inverters." Industrial Electronics, IEEE Transactions on 57(8): 2691-2699.

Cumplido-Parra, R. A., Jones, S. R., Goodall, R. M. and Bateman, S. (2001). High performance control system processor. System Design Automation, Springer: 140-151.

DARPA (2007). Broad Agency Announcement of System F6.

Datta, A., Ho, M.-T. and Bhattacharyya, S. P. (2000). Structure and synthesis of PID controllers, Springer.

De Rooij, N., Gautsch, S., Briand, D., Marxer, C., Mileti, G., Noell, W., Shea, H., Staufer, U. and Van Der Schoot, B. (2009). Mems for space. Solid-State Sensors, Actuators and Microsystems Conference, 2009. TRANSDUCERS 2009. International, IEEE.

Delchamps, D. F. (1990). "Stabilizing a linear system with quantized state feedback." Automatic Control, IEEE Transactions on 35(8): 916-924.

Den Camp, O., Verheijen, O., Huisman, L. and Backx, A. (2008). "Application of proper orthogonal decomposition to reduce detailed CFD models of glass furnaces and forehearths." Glass Technology-European Journal of Glass Science and Technology Part A 49(3): 119-125.

Dong, Y., Kraft, M., Hedenstierna, N. and Redman-White, W. (2008). "Microgyroscope control system using a high-order band-pass continuous-time sigma-delta modulator." Sensors and Actuators A: Physical 145: 299-305.

Dong, Y., Kraft, M. and Redman-White, W. (2007). "Higher order noise-shaping filters for high-performance micromachined accelerometers." Instrumentation and Measurement, IEEE Transactions on 56(5): 1666-1674.

Dong, Y., Kraft, M. and Redman-White, W. (2007). "Micromachined vibratory gyroscopes controlled by a high-order bandpass sigma-delta modulator." Sensors Journal, IEEE 7(1): 59-69.

Dorf, R. C. (1995). Modern control systems, Addison-Wesley Longman Publishing Co., Inc.

Dunn, C., & Sandler, M. (1994, March). "Use of clipping in Sigma-Delta modulators." In Oversampling Techniques and Sigma-Delta Modulation, IEE Colloquium on: 8-1.IET.

Ebert, W. (2001). "Optimal filtered predictive control–a delta operator approach." Systems & control letters 42(1): 69-80.

Einicke, G. A. (2012). "Smoothing, Filtering and Prediction-Estimating the past, present and future." New York: InTech.

Fagnani, F., and Zampieri, S. (2003). "Stability analysis and synthesis for scalar linear systems with a quantized feedback." Automatic Control, IEEE Transactions on 48(9): 1569-1584.

Ferreau, H. J., Bock, H. G. and Diehl, M. (2008). "An online active set strategy to overcome the limitations of explicit MPC." International Journal of Robust and Nonlinear Control 18(8): 816-830.

Feuer, A. and Goodwin, G. C. (1996). Sampling in digital signal processing and control, Birkhauser Boston Inc.

Garcia, C. E., Prett, D. M. and Morari, M. (1989). "Model predictive control: theory and practice—a survey." Automatica 25(3): 335-348.

Genuit, B., Lu, L. and Heemels, W. (2012). "Approximation of explicit model predictive control using regular piecewise affine functions: an input-tostate stability approach." Control Theory & Applications, IET 6(8): 1015-1028.

Gibbens, P. W. and B. Medagoda, E. D. (2011). "Efficient model predictive control algorithm for aircraft." Journal of guidance, control, and dynamics 34(6): 1909-1915.

Gill, E., Steckling, M. and Butz, P. (2001). Gemini: A milestone towards autonomous formation flying.

ESA Workshop on On-Board Autonomy, October.
Goodall, R. M. (1990). "The delay operator z-1-inappropriate for use in recursive digital filters?" Transactions of the Institute of Measurement and Control 12(5): 246-250.
Goodall, R. M. and Donoghue, B. (1993). "Very high sample rate digital filters using the δ operator." IEE Proceedings G (Circuits, Devices and Systems) 140(3): 199-206.
Goodwin, G. C.,, Leal, R. L., Mayne, D. and Middleton, R. (1986). "Rapprochement between continuous and discrete model reference adaptive control." Automatica 22(2): 199-207.
Goodwin, G. C., Haimovich, H., Quevedo, D. E. and Welsh, J. S. (2004). "A moving horizon approach to networked control system design." Automatic Control, IEEE Transactions on 49(9): 1427-1445.
Gore, A. and Chakrabartty, S. (2010). "A Min–Max Optimization Framework for Designing Learners: Theory and Hardware." Circuits and Systems I: Regular Papers, IEEE Transactions on 57(3): 604-617.
Grancharova, A. and Johansen, T. (2008). Explicit solution of regulation control problems for nonlinear systems with quantized inputs. Proceedings of the International Conference on Automatics and Informatics, Sofia, Bulgaria, pp. I-15–I-18.
Grancharova, A. and Johansen, T. A. (2009). Explicit approximate model predictive control of constrained nonlinear systems with quantized input. Nonlinear Model Predictive Control, Springer: 371-380.
Grancharova, A. and Johansen, T. A. (2011). "Design and comparison of explicit model predictive controllers for an electropneumatic clutch actuator using on/off valves." Mechatronics, IEEE/ASME Transactions on 16(4): 665-673.
Greco, L., Fontanelli, D. and Bicchi, A. (2007). Almost sure stability of anytime controllers via stochastic scheduling. Decision and Control, 2007 46th IEEE Conference on, IEEE.
Grewal, H. S. and Andrews, A. P. (2008). Kalman Filtering: Theory and Practice Using MATLAB. New Jersey, Wiley.
Gugercin, S. and Antoulas, A. C. (2004). "A survey of model reduction by balanced truncation and some new results." International Journal of Control 77(8): 748-766.
Hahn, J. and Edgar, T. F. (2002). "An improved method for nonlinear model reduction using balancing of empirical gramians." Computers & chemical engineering 26(10): 1379-1397.
Hegrenæs, Ø., Gravdahl, J. T. and Tøndel, P. (2005). "Spacecraft attitude control using explicit model predictive control." Automatica 41(12): 2107-2114.
Hein, S. and Zakhor, A. (1991). On the stability of interpolative sigma delta modulators. Circuits and Systems, 1991., IEEE International Sympoisum on, IEEE.
Hein, S. and Zakhor, A. (1993). On the stability of sigma delta modulators. IEEE TRANSACTLONS ON SIGNAL PROCESSING, VOL. 41. NO. 7. JULY 1993, Citeseer.
Henriksson, D. and Åkesson, J. (2004). Flexible implementation of model predictive control using sub-optimal solutions, Univ.
Henriksson, D., Cervin, A., Akesson, J. and Arzen, K.-E. (2002). On dynamic real-time scheduling of model predictive controllers. Decision and Control, 2002, Proceedings of the 41st IEEE Conference on, IEEE.
Hildreth, C. (1957). "A quadratic programming procedure." Naval research logistics quarterly 4(1): 79-85.
Hovland, S. and Gravdahl, J. T. (2008). Complexity reduction in explicit MPC through model reduction. Proceedings of the IFAC World Congress, Seoul, Korea.
Hovland, S., Gravdahl, J. T. and Willcox, K. E. (2008). "Explicit model predictive control for

large-scale systems via model reduction." Journal of guidance, control, and dynamics 31(4): 918-926.

Hovland, S., Willcox, K. and Gravdahl, J. (2006). MPC for large-scale systems via model reduction and multiparametric quadratic programming. Decision and Control, 2006 45th IEEE Conference on, IEEE.

Janssen, E. and Van Roermund, A. (2011). Basics of Sigma-Delta Modulation. Look-Ahead Based Sigma-Delta Modulation, Springer: 5-28.

Luo, J., Chai, L. and Jiang, P. (2008). Moving horizon state estimation for nonlinear systems using quantized data from wireless sensor networks. Control Conference, 2008. CCC 2008. 27th Chinese, IEEE.

Jiang, X., Seeger, J. I., Kraft, M. and Boser, B. E. (2000). A monolithic surface micromachined Z-axis gyroscope with digital output. VLSI Circuits, 2000. Digest of Technical Papers. 2000 Symposium on, IEEE.

Funamoto, J., Khachan, J., Wu, X, Israel, A. and Vermay, R. (2012). Electric (ion) propulsion devices for satellites of any size: The Charge Exchange Thruster (CXT). 11th Australia Space Science Conference Proceedings, Canberra.

Johansen, T. A. and Grancharova, A. (2003). "Approximate explicit constrained linear model predictive control via orthogonal search tree." Automatic Control, IEEE Transactions on 48(5): 810-815.

Johns, D. and Lewis, D. (1991). "IIR filtering on sigma-delta modulated signals." Electronics letters 27(4): 307-308.

Johns, D. A.,and Lewis, D. M. (1993). "Design and analysis of delta-sigma based IIR filters." Circuits and Systems II: Analog and Digital Signal Processing 40(4): 233-240.

Jones, C. and Morari, M. (2009). Approximate explicit MPC using bilevel optimization. European control conference.

Jones, C. N. and Morari, M. (2010). "Polytopic approximation of explicit model predictive controllers." Automatic Control, IEEE Transactions on 55(11): 2542-2553.

Keerthi, S. a. and Gilbert, E. G. (1988). "Optimal infinite-horizon feedback laws for a general class of constrained discrete-time systems: Stability and moving-horizon approximations." Journal of optimization theory and applications 57(2): 265-293.

Kershaw, S., Summerfield, S., Sandler, M. and Anderson, M. (1996). Realisation and implementation of a sigma-delta bitstream FIR filter. Circuits, Devices and Systems, IEE Proceedings-, IET.

Kouro, S., Cortés, P., Vargas, R., Ammann, U. and Rodríguez, J. (2009). "Model predictive control—A simple and powerful method to control power converters." Industrial Electronics, IEEE Transactions on 56(6): 1826-1838.

Kraft, M. and Ding, H. (2009). Sigma-delta modulator based control systems for MEMS gyroscopes. Nano/Micro Engineered and Molecular Systems, 2009. NEMS 2009. 4th IEEE International Conference on, IEEE.

Kuhn, H. W. and Tucker, A. W. (1951). Nonlinear programming. Proceedings of the second Berkeley symposium on mathematical statistics and probability, California.

Kvasnica, M., Löfberg, J. and Fikar, M. (2011). "Stabilizing polynomial approximation of explicit MPC." Automatica 47(10): 2292-2297.

Lamburn, D. J., Gibbens, P. W. and Dumble, S. J. (2014). "Efficient constrained model predictive control." European Journal of Control **20**(6): 301-311.

Langbort, C., Chandra, R. S. and D'Andrea, R. (2004). "Distributed control design for systems interconnected over an arbitrary graph." Automatic Control, IEEE Transactions on 49(9): 1502-1519.

Lauritsen, M. and Rostgaard, M. (1997). Delta-operator predictive control. Decision and Control, 1997., Proceedings of the 36th IEEE Conference on, IEEE.

Lee, J. H. and Ricker, N. L. (1994). Extended Kalman Filter Based Nonlinear Model Predictive Control. Industrial & Engineering Chemistry Research: 1530-1541.

Liu, A., Yu, L., Zhang, W.-A. and Chen, M. Z. (2013). "Moving Horizon Estimation for Networked Systems With Quantized Measurements and Packet Dropouts." Circuits and Systems I: Regular Papers, IEEE Transactions on 60(7): 1823-1834.

Manum, H. and Skogestad, S. (2010). Bilevel programming for analysis of reduced models for use in model predictive control. International Conference February.

Mathieu, C. and Weigel, A. (2005). Assessing the flexibility provided by fractionated spacecraft. Proc. of AIAA Space 2005 Conference, Long Beach, CA, USA.

Mathieu, C. and Weigel, A. (2006). Assessing the fractionated spacecraft concept, Massachusetts Institute of Technology, Engineering Systems Division, Technology and Policy Program.

Mayne, D. Q. and Michalska, H. (1990). "Receding horizon control of nonlinear systems." Automatic Control, IEEE Transactions on 35(7): 814-824.

Mayne, D. Q., Raković, S. (2003). "Model predictive control of constrained piecewise affine discrete-time systems." International Journal of Robust and Nonlinear Control 13(3-4): 261–279.

Mayne, D. Q., Rawlings, J. B., Rao, C. V., & Scokaert, P. O. (2000). "Constrained model predictive control: Stability and optimality." Automatica 36(6): 789–814.

Medagoda, E. D. and Gibbens, P. W. (2010). Efficient predictive flight control. Control Automation and Systems (ICCAS), 2010 International Conference on, IEEE.

Medagoda, E. D. and Gibbens, P. W. (2014). "Multiple Horizon Model Predictive Flight Control." Journal of Guidance, Control, and Dynamics **37**(3): 946-951.

Mehrotra, S. (1992). "On the implementation of a primal-dual interior point method." SIAM Journal on optimization 2(4): 575-601.

Michalska, H. and Mayne, D. Q. (1993). "Robust receding horizon control of constrained nonlinear systems." Automatic Control, IEEE Transactions on 38(11): 1623-1633.

Middleton, R. H. and Goodwin, G. C. (1986). "Improved finite word length characteristics in digital control using delta operators." Automatic Control, IEEE Transactions on 31(11): 1015-1021.

Middleton, R. H. and Goodwin, G. C. (1990). Digital control and estimation: a unified approach, Prentice Hall Professional Technical Reference.

Miller, M. R. and Petrie, C. S. (2003). "A multibit sigma-delta ADC for multimode receivers." Solid-State Circuits, IEEE Journal of 38(3): 475-482.

Moore, B. (1981). "Principal component analysis in linear systems: Controllability, observability, and model reduction." Automatic Control, IEEE Transactions on 26(1): 17-32.

Morari, M. and H Lee, J. (1999). "Model predictive control: past, present and future." Computers & Chemical Engineering 23(4): 667-682.

Moussavi, S. M., & Leung, B. H. (1994). "High-order single-stage single-bit oversampling A/D converter stabilized with local feedback loops." Circuits and Systems II: Analog and Digital Signal Processing, IEEE Transactions on, 41(1): 19-25.

Msechu, E. J., Roumeliotis, S. I., Ribeiro, A. and Giannakis, G. B. (2007). Distributed iteratively quantized Kalman filtering for wireless sensor networks. Signals, Systems and Computers, 2007. ACSSC 2007. Conference Record of the Forty-First Asilomar Conference on, IEEE.

Müller, C., Quevedo, D. E. and Goodwin, G. C. (2011). "How Good is Quantized Model Predictive

Control With Horizon One." IEEE Trans. on Automatic control 56(11).
Muske, K. R. and Rawlings, J. B. (1993). "Model predictive control with linear models." AIChE Journal 39(2): 262-287.
Muske, K. R., Rawlings, J. B. and Lee, J. H. (1993). Receding horizon recursive state estimation. American Control Conference, 1993, IEEE.
Narciso, D. and Pistikopoulos, E. (2008). "A combined Balanced Truncation and multi-parametric programming approach for Linear Model Predictive Control." Computer Aided Chemical Engineering 25: 405-410.
Nesterov, Y. (1983). A method of solving a convex programming problem with convergence rate O (1/k2). Soviet Mathematics Doklady.
Norsworthy, S. R., Schreier, R., and Temes, G. C. (Eds.) (1996). Delta-sigma data converters: theory, design, and simulation. New York, IEEE press.
Pannocchia, G., Rawlings, J. B. and Wright, S. J. (2007). "Fast, large-scale model predictive control by partial enumeration." Automatica 43(5): 852-860.
Parra, R. A. C. (2001). On the design and implementation of a control system processor, Loughborough University.
Patrinos, P. and Bemporad, A. (2012). An accelerated dual gradient-projection algorithm for linear model predictive control. Decision and Control (CDC), 2012 IEEE 51st Annual Conference on, IEEE.
Patrinos, P., Sopasakis, P. and Sarimveis, H. (2011). "A global piecewise smooth Newton method for fast large-scale model predictive control." Automatica 47(9): 2016-2022.
Pernebo, L. and Silverman, L. (1982). "Model reduction via balanced state space representations." Automatic Control, IEEE Transactions on 27(2): 382-387.
Petkov, V. P. and Boser, B. E. (2005). "A fourth-order ΣΔ interface for micromachined inertial sensors." Solid-State Circuits, IEEE Journal of 40(8): 1602-1609.
Petkov, V. P. and Boser, B. E. (2006). "High-order electromechanical ΣΔ modulation in micromachined inertial sensors." Circuits and Systems I: Regular Papers, IEEE Transactions on 53(5): 1016-1022.
Picasso, B., Pancanti, S., Bemporad, A., & Bicchi, A (2003). Receding–horizon control of LTI systems with quantized inputs. In Analysis and Design of Hybrid Systems: A Proceedings Volume from the IFAC Conference, St. Malo, Brittany, France.
Prosalentis, E. A. and Tombras, G. S. (2007). "A 2-bit adaptive delta modulation system with improved performance." EURASIP Journal on Applied Signal Processing 2007(1): 3-3.
Qin, S. J. and Badgwell, T. A. (1997). An overview of industrial model predictive control technology. AIChE Symposium Series, New York, NY: American Institute of Chemical Engineers, 1971-c2002.
Qin, S. J. and Badgwell, T. A. (2000). An overview of nonlinear model predictive control applications. Nonlinear model predictive control, Springer: 369-392.
Qin, S. J. and Badgwell, T. A. (2003). "A survey of industrial model predictive control technology." Control engineering practice 11(7): 733-764.
Quevedo, D. E., Goodwin, G.C. and De Don á, J. (2004). "Finite constraint set receding horizon quadratic control." International Journal of Robust and Nonlinear Control 14(4): 355–377.
Quevedo, D. E. and Gupta, V. (2013). "Sequence-based Anytime Control."
Quevedo, D. E. and Goodwin, G. C. (2005). "Multistep optimal analog-to-digital conversion." Circuits and Systems I: Regular Papers, IEEE Transactions on 52(3): 503-515.
Quevedo, D. E., Goodwin, G. C. and De Dona, J. A. (2004). "Finite constraint set receding horizon quadratic control." International journal of robust and nonlinear control 14(4): 355-377.

Quevedo, D. E., Goodwin, G. C. and Welsh, J. S. (2003). Minimizing down-link traffic in networked control systems via optimal control techniques. Decision and Control, 2003. Proceedings. 42nd IEEE Conference on, IEEE.

Raman, J., Cretu, E., Rombouts, P. and Weyten, L. (2009). "A closed-loop digitally controlled MEMS gyroscope with unconstrained sigma-delta force-feedback." Sensors Journal, IEEE 9(3): 297-305.

Rao, C. V., Rawlings, J. B. and Lee, J. H. (2001). "Constrained linear state estimation—a moving horizon approach." Automatica 37(10): 1619-1628.

Rao, C. V., Wright, S. J. and Rawlings, J. B. (1998). "Application of interior-point methods to model predictive control." Journal of optimization theory and applications 99(3): 723-757.

Ravindran, S. (2000). "A reduced ‐ order approach for optimal control of fluids using proper orthogonal decomposition." International journal for numerical methods in fluids 34(5): 425-448.

Rawlings, J. B. and Muske, K. R. (1993). "The stability of constrained receding horizon control." Automatic Control, IEEE Transactions on 38(10): 1512-1516.

Reefman, D. and Janssen, E. (2004). "One-bit audio: an overview." Journal of the Audio Engineering Society 52(3): 166-189.

Richalet, J. (1993). "Industrial applications of model based predictive control." Automatica 29(5): 1251-1274.

Richter, S., Jones, C. N. and Morari, M. (2009). Real-time input-constrained MPC using fast gradient methods. Decision and Control, 2009 held jointly with the 2009 28th Chinese Control Conference. CDC/CCC 2009. Proceedings of the 48th IEEE Conference on, IEEE.

Robertson, D. G., Lee, J. H. and Rawlings, J. B. (1996). "A moving horizon ‐ based approach for least ‐ squares estimation." AIChE Journal 42(8): 2209-2224.

Sabol, C., Burns, R. and McLaughlin, C. A. (2001). "Satellite formation flying design and evolution." Journal of Spacecraft and Rockets 38(2): 270-278.

Schreier, R. (1993). "An empirical study of high-order single-bit delta-sigma modulators." Circuits and Systems II: Analog and Digital Signal Processing, IEEE Transactions on 40(8): 461-466.

Schreier, R., Goodson, M.V. and Bo Zhang (1997). "An Algorithm for Computing Convex Positively Invariant Sets for Delta–Sigma Modulators." IEEE Trans. on Circuits and Systems I: Fundamental Theory and Applications 44(1): 38-44.

Scokaert, P. O., Rawlings, J. B. and Meadows, E. S. (1997). "Discrete-time stability with perturbations: Application to model predictive control." Automatica 33(3): 463-470.

Sha, L., Liu, X., Lu, Y. and Abdelzaher, T. (2002). Queueing model based network server performance control. Real-Time Systems Symposium, 2002. RTSS 2002. 23rd IEEE, IEEE.

Sklar, B. (2001). Digital communications, Prentice Hall PTR New Jersey.

Slotine, J.-J. E. and Li, W. (1991). Applied nonlinear control, Prentice-Hall Englewood Cliffs, NJ.

Smith, T., Nys, O., Chevroulet, M., DeCoulon, Y. and Degrauwe, M. (1994). A 15 b electromechanical sigma-delta converter for acceleration measurements. Solid-State Circuits Conference, 1994. Digest of Technical Papers. 41st ISSCC., 1994 IEEE International, IEEE.

Spjøtvold, J., Kerrigan, E. C., Jones, C. N., Johansen, T. A. and Tøndel, P. (2004). Conjectures on an algorithm for convex parametric quadratic programs, Citeseer.

Steiner, P. and Yang, W. (1997). "A framework for analysis of high-order sigma-delta modulators." Circuits and Systems II: Analog and Digital Signal Processing, IEEE Transactions on 44(1): 1-10.

Stewart, B. and Pfann, E. (1998). "Adaptive DSP Sigma Delta Algorithms and Architectures for Digital Communications."

Sun, J., Kolmanovsky, I. V., Ghaemi, R. and Chen, S. (2007). "A stable block model predictive control with variable implementation horizon." Automatica 43(11): 1945-1953.

Tang, P. L. and de Silva, C. W. (2006). "Compensation for transmission delays in an ethernet-based control network using variable-horizon predictive control." Control Systems Technology, IEEE Transactions on 14(4): 707-718.

Theodoropoulos, C. (2011). Optimisation and linear control of large scale nonlinear systems: a review and a suite of model reduction-based techniques. Coping with Complexity: Model Reduction and Data Analysis, Springer: 37-61.

Tøndel, P. and Johansen, T. A. (2002). Complexity reduction in explicit linear model predictive control. Proc. 15th IFAC world congress, Spain.

Tøndel, P., Johansen, T. A. and Bemporad, A. (2003). "An algorithm for multi-parametric quadratic programming and explicit MPC solutions." Automatica 39(3): 489-497.

Tøndel, P., Johansen, T. A. and Bemporad, A. (2003). "Evaluation of piecewise affine control via binary search tree." Automatica 39(5): 945-950.

Troster, G., Dreßler, H.-J., Golberg, H.-J., Schardein, W., Zocher, E., Wedel, A., Schoppe, K. and Arndt, J. (1993). "An interpolative bandpass converter on a 1.2-µm BiCMOS analog/digital array." Solid-State Circuits, IEEE Journal of 28(4): 471-477.

Vallado, D. A. (2001). Fundamentals of Astrodynamics and Applications, Springer.

Wang, H. (1993). On the stability of third-order sigma-delta modulation. Circuits and Systems, 1993., ISCAS'93, 1993 IEEE International Symposium on, IEEE.

Wang, L. (2009). Model Predictive Control System Design and Implementation Using MATLAB®, Springer.

Wang, Y. and Boyd, S. (2010). "Fast model predictive control using online optimization." Control Systems Technology, IEEE Transactions on 18(2): 267-278.

Wang, Y., Ishwar, P. and Saligrama, V. (2008). "One-bit distributed sensing and coding for field estimation in sensor networks." Signal Processing, IEEE Transactions on 56(9): 4433-4445.

Welch, G. and Bishop, G. (2006). An Introduction to Kalman Filter. North Carolina, University of North Carolina at Chapel Hill.

Wissinger, A. B. (1995). Satellite communications system, Google Patents.

Wu, H. (2009). System architecture for mode-matching a MEMS gyroscope, Massachusetts Institute of Technology.

Wu, X. and Bai, X. (2010). A fractional attitude decision and control system design for a virtual satellite. Decision and Control (CDC), 2010 49th IEEE Conference on, IEEE.

Wu, X. and Bai, X. (2010). A Fractionated Attitude Decision and Control System for Virtual Satellite Missions. 49th IEEE Conference of Decision and Control, Hilton Atlanta GA.

Wu, X. and Goodall, R. (2005a). "One-bit processing for digital control." IEE Proceedings-Control Theory and Applications 152(4): 403-410.

Wu, X. and Goodall, R. (2005b). One-bit processing for real-time control, Loughborough University.

Xie, W., Bonis, I. and Theodoropoulos, C. (2011). "Off-line model reduction for on-line linear MPC of nonlinear large-scale distributed systems." Computers & Chemical Engineering 35(5): 750-757.

Xue, B., Li, S. and Zhu, Q. (2012). "Moving horizon state estimation for networked control systems with multiple packet dropouts." Automatic Control, IEEE Transactions on 57(9): 2360-2366.

Yazkurt, U., Dundar, G., Talay, S., Beilleau, N., Aboushady, H. and de Lamarre, L. (2006). Scaling Input Signal Swings of Overloaded Integrators in Resonator-based Sigma-Delta Modulators.

Electronics, Circuits and Systems, 2006. ICECS'06. 13th IEEE International Conference on, IEEE.

Yildirim, E. A. and Wright, S. J. (2002). "Warm-start strategies in interior-point methods for linear programming." SIAM Journal on Optimization 12(3): 782-810.

Young, R. E., Bartusiak, R. D. and Fontaine, R. W. (2002). Evolution of an industrial nonlinear model predictive controller. AICHE SYMPOSIUM SERIES, New York; American Institute of Chemical Engineers; 1998.

Yu, J. (1992). Design and analysis of fixed and adaptive sigma-delta modulators, King's College London (University of London).

Yu, J., Sandler, M. and Hawken, R. (1992). "Adaptive quantisation for one-bit sigma-delta modulation." IEE Proceedings G (Circuits, Devices and Systems) 139(1): 39-44.

Zampieri, F. F. a. S. (2003). "Stability Analysis and Synthesis for Scalar Linear Systems With a Quantized Feedback." IEEE Trans. on Automatic control 48(9).

Zeilinger, M. N., Jones, C. N. and Morari, M. (2011). "Real-time suboptimal model predictive control using a combination of explicit MPC and online optimization." Automatic Control, IEEE Transactions on 56(7): 1524-1534.

Zheng, A. (1999). "Reducing on-line computational demands in model predictive control by approximating QP constraints." Journal of process control 9(4): 279-290.

Zierhofer, C. M. (2000). "Adaptive sigma-delta modulation with one-bit quantization." Circuits and Systems II: Analog and Digital Signal Processing, IEEE Transactions on 47(5): 408-415.

Zorn, C., Brückner, T., Ortmanns, M. and Mathis, W. (2013). "State scaling of continuous-time sigma-delta modulators." Advances in Radio Science 11(10): 119-123.